TÉCNICO LISBOA

Electrodermal Activity Sensor (EDA) with Adaptive Gain Control

António Francisco Rodrigues Banganho

Thesis to obtain the Master of Science Degree in

Electrical and Computer Engineering

Supervisor(s): Prof. Marcelino Bicho dos Santos
Prof. Hugo Humberto Plácido da Silva

Examination Committee

Chairperson: Prof. Francisco André Corrêa Alegria
Supervisor: Prof. Marcelino Bicho dos Santos
Member of the Committee: João Miguel Raposo Sanches

November 2019

Declaration

I declare that this document is an original work of my own authorship and that it fulfills all the requirements of the Code of Conduct and Good Practices of the Universidade de Lisboa.

Dedicated to my mother and father who always gave all for the success of their sons

Acknowledgments

The accomplishment of this master thesis would not have been possible without the support, guidance, encouragement and love of my closest ones, to whom I thank.

To my parents, who always helped to purse my dreams and beliefs without question, and my brother who always helped to manage my stress levels through his always relaxed state of mind and sense of humor.

To Leonor, my second half who supported me and encouragement when we were distant, and without whom life would not be the same, thank you for being beside me for all this time.

To Gonçalo Machado for his mindset outside of the box, Jorge Reis for his naivety, Francisco Martins and António Teixeira for the afternoon basketball matches, and all the other fellow friends from Coimbra thank you for being my second family.

To Mónica Amaral, Mário Bento, and Frederico Mota, thanks for working beside me to fulfil tight schedules and all the laughs and talks.

To Professor João Valente and the neuroscience company BrainAnswer for providing one of the datasets that supported one of the initial parts of this research.

This work was partially funded by Instituto de Teelecomunicações (IT) under grant BIL/Nº54 10-07-2018, and by by Xinhuanet Co. Ltd. under project S-0003-LX-18 XiPhy - Xinhua Net Physiological Computing Scientific Research Cooperation, which are gratefully acknowledged. To all the IT personnel who volunteered to participate in my experiment, thanks for the predisposition and curiosity.

To my supervisors Professor Marcelino Santos and especially Professor Hugo Silva whom is already with me since Coimbra, thank you for believing and for being so present in my academic life.

Finally, but not least, thanks to the professors that marked my academic path, from Instituto Superior de Engenharia de Coimbra, Professor Milton Macedo, Professor Arménio Correia and from the Instituto Superior Técnico, Professor Teresa Almeida.

Resumo

A atividade eletrodérmica (EDA) é um dos sinais fisiológicos passível de ser medido de forma pouco intrusiva, e associado ao sistema nervoso simpático, que regula a resposta de luta ou fuga em humanos. Embora não substitua outros sinais biomédicos, tem sido utilizado com sucesso, por exemplo, no estudo de condições psicofisiológicas como autismo, epilepsia ou síndrome de burnout. Utilizado juntamente com tecnologias comumente encontradas em smartwatches ou bandas de fitness atuais, poderá ser útil para fornecer feedback ininterruptamente sobre o estado emocional e níveis de stress do utilizador. No entanto, ainda existem algumas limitações em relação ao hardware, como por exemplo, sensibilidade a artefactos, variabilidade por efeito de variáveis ambientais e locais de gravação, entre outros. Este trabalho pretende resolver alguns dos problemas existentes em medições EDA, através do desenvolvimento de um novo circuito com controlo de ganho adaptativo, permitindo ter sensibilidade de acordo com a intra-variabilidade encontrada numa população, enquanto mantêm o custo geral baixo. Também estuda elétrodos compostos por materiais não convencionais, como o MEDTEX P130, o material GMLC, ou ainda a possibilidade de usar elétrodos compostos por PLA, produzidos por impressão 3D desktop, bem como locais alternativos para captar o sinal EDA, como a testa. O circuito proposto demostrou resultados comparáveis ao adquirido com um dispositivo de referência, obtendo um coeficiente de correlação de 0.967, e apresentou desempenho melhorado nos casos em que o sensor comparável saturaria. O circuito proposto também inclui um novo frontend pensado para separar as duas componentes, tónica e fásica, que compõem o sinal EDA. Os resultados dos materiais de elétrodos não convencionais mostram que o MEDTEX P130 tem um desempenho comparável ao de um material de referência, com um coeficiente de correlação de 0,789, enquanto os testes realizados na testa não foram conclusivos.

Palavras-chave: Atividade Eletrodérmica (EDA), Electrodes não convencionais, Testa EDA, sensor EDA BITalino, Sistema Tegumentar

Abstract

Electrodermal activity (EDA) is one of the physiological signals that can be measured unintrusively and associated with the sympathetic nervous system, which regulates the fight or flight response in humans. Although not a substitute for other biomedical signals, it has been successfully used, for example, in the study of psychophysiological conditions such as autism, epilepsy or burnout syndrome. Used in conjunction with technologies commonly found in today's smartwatches or fitness bands, it can help provide continuous feedback on the user's emotional state and stress levels. However, there are still some hardware limitations, such as sensitivity to artefacts, variability by effect of environmental variables and recording locations, among others. This paper aims to solve some of the problems with EDA measurements by developing a new circuit with adaptive gain control, allowing to be sensitive according to the intra-variability found in a population, while keeping the overall cost low. It also studies electrodes composed of unconventional materials such as MEDTEX P130, GMLC material, or the possibility of using PLA composite electrodes produced by desktop 3D printing, as well as alternative locations to record EDA signal such as the forehead. The proposed circuit showed comparable results to that obtained with a reference device, obtaining a correlation coefficient of 0.967, and showed improved performance in cases where the comparable sensor would saturate. The proposed circuit also includes a new frontend designed to separate the two components, tonic and phasic, that compose the EDA signal. Results from unconventional electrode materials show that the MEDTEX P130 has comparable performance to that of reference material, with a correlation coefficient of 0.789, while tests performed on the forehead were not conclusive.

Keywords: Electrodermal Activity (EDA), Non-Convencional electrode materials, EDA forehead, BITalino EDA sensor, Integumentary System

Contents

List of Tables

List of Figures

Acronyms

AC Alternate Current.

ANS Autonomic Nervous System.

ASD Autism Spectrum Disorder.

CNS Central Nervous System.

DAC Digital to Analog Converter.

DC Direct Current.

DIY Do it yourself.

EDA Electrodermal Activity.

EDL Electrodermal Level.

EDR Electrodermal Response.

EMF Electromotive Force.

GSR Galvanic Skin Reflex.

MCU Microcontroller Unit.

NS.EDR Non-Specific Electrodermal Response.

p-coeff Pearson Correlation Coefficient.

PWM Pulse Width Modulation.

RC Resistive and Capacitive.

RMSE Root Mean Square Error.

SC Skin Conductance.

SCL Skin Conductance Level.

SNS Sympathetic Nervous System.

SPR Skin Potential Response.

SR Skin Resistance.

SY Skin Admittance.

SYL Skin Admittance Level.

SZ Skin Impedance.

Chapter 1

Introduction

1.1 Scope and Context

Recently there have been significant developments in the area of wearables, low-cost embedded systems and Internet of Things (IoT) for biomedical applications. These technologies provide new opportunities to simplify health assessment processes, as well as to solve problems in unprecedented ways due to their increased observation periodicity and diversity of data collected from the patients.

Electrodermal Activity (EDA) designatesthe continuous electrical variations influenced by the properties of the skin, mainly caused by fluctuations on the impedance that result from regulation of the sweat glands; this activity is partially associated with thermal adaptation, but is also associated with changes in the cognitive state of an individual, reason for which it can be further defined as being an indirect observation of the Sympathetic Nervous System (SNS) [1]. EDA sensing devices have been used for decades, but they often lack the portability, limiting the potential studies and application to the laboratory environment. With the growth of wearable technology and its miniaturisation, an increasing number of wearable EDA devices are now appearing, which enable a near continuous monitorization of an individual emotional state and in his/her daily life. The added value of this technology, in turn, enables the study of the SNS in a less intrusive and more comfortable fashion, having already proven to be an added value modality to complement more established biosignals (e.g. Electroencephalography - EEG), and applicable in the study of psychophysiological conditions such as epilepsy, autism, schizophrenia, depression, stress disorders, and many others [2–4].

However, challenges still exist at multiple levels. One of the challenges comes from the EDA signal, which is composed of two components, the tonic and the phasic. The tonic component is considered as the baseline of the signal and presents slow variations, while the other, the phasic component, presents more rapid varying behaviour that superimposes to the baseline, frequently fluctuating according to a know elicitation of a particular stimulus. Thanks to this superimposition, problems may arise during the analysis since this phasic component superimposes to itself, adding burst responses that occur in a short period, and therefore increasing the difficulty of correctly separating each event. Another challenging characteristic is the masking of each component on the overall signal. While the tonic component

can fluctuate between 0 and 80 μS, the phasic component has a more reduced scale between 0.01μS and 5μS [5]. In retrospect, devices need to be able to detect a high-dynamic range, while ensuring that they have enough resolution to sense the smallest possible variations in phasic component, especially in the presence of ADC with low resolution. A third challenging characteristic of EDA is the limited available measurement locations, which are typically the hand palms or feet soles, due to the fact that these locations do not show direct correspondence to the skin thermoregulation mechanism found in other body locations, and indeed, they showed to be more active in times of high arousal. The problem is the fact that these locations can obstruct the user movements and, therefore, it is not easy to make a direct transition from the lab to a more periodic monitoring of the EDA in real-life use cases. To complement those already challenging properties, the EDA is prone to artefacts that cause difficulties when acquiring data in everyday naturalistic scenarios. There are techniques to solve challenging aspects of the two components, which can be applied in hardware or software. One of them is to separate the two components of the EDA and rebuild the signal afterwards. This can be accomplished through individualized filtering, since both components fall into a specific frequency range.

EDA monitoring devices use several measurement approaches, and the most common ones include simple voltage dividers, Wheatstone bridges or operational amplifiers. These can resort to what is called exosomatic or endosomatic techniques to measure the signal. The difference between them is that in the first there is the application of an external source, Direct Current (DC) or Alternate Current (AC), where the second uses the body potentials, with no external source.

This work addresses the above-mentioned challenges through the development of a low-cost, affordable EDA sensor design with adaptive gain control. Before developing the circuit itself, it is useful to review the integumentary system and understand how can it be electrically modeled, particularly the sweat glands. Of the same importance is to present the current technology, the available devices, their applications, and electrode materials.

1.2 Goals

The goals of the present work consist in proposing a set of improvements to EDA measurement, in particular addressing:

- A review of the integumentary system and how can it be electrically model;
- A review of current EDA applications and their impact on society;
- A review of the state-of-the-art on EDA monitoring technologies and devices;
- A study of non-conventional electrode materials to facilitate EDA measurement in naturalistic scenarios;
- A study of different body locations for EDA measurement and compare with gold standard locations;
- A sensor circuit design capable of extending the measurement dynamic range;

- A experimental evaluation of the proposed circuit with a population of real-world users.

1.3 Contributions

This work has resulted in a number of contributions, of which the following are highlighted:

- A novel EDA sensor design with adaptive gain;
- A supporting software for standardized EDA data acquisition;
- A database with EDA collected from 16 participants in a standardised test environment;
- An evaluation of non-conventional electrode materials for EDA measurement;
- An evaluation of EDA measurement on the forehead;
- An abstract accepted and presented at the 1st International Conference of the Portuguese Physiology Society (Physioma 2019);
- A submitted article to the IEEE Potentials Magazine special issue on ”Medical Technology Breakthroughs, March 2020” [Under Review].

1.4 Thesis Outline

The remainder of this document is structured into five main chapters. Chapter 2 provides an overview of the integumentary system, including an anatomical description of the skin, sweat gland structure and its characteristics. Chapter 3 describes the base concepts used in EDA measurements, essential properties of the skin and sweat glands, as well as the state-of-the-art in terms of devices. Chapter 4 presents the sensing circuit and its main design considerations towards providing an EDA sensor with adaptive gain. Chapter 5 presents the experiments and results obtained during the evaluation of the new EDA sensor design. Additionally, it also presents experiments with EDA signals from the forehead and tests with alternative non-conventional electrode materials. Chapter 6 presents the discussion of the results, future work perspectives, and the main conclusions of this work.

Chapter 2

Integumentary System

To better understand the electrodermal phenomena, how sweat is associated with the EDA and other assumptions, it is crucial to understand the physiological nature of this data source. In particular, how does the human body react in certain conditions, what underlying processes are related to such reactions, how is the skin stratified, and other related aspects. These are fundamental features to consider when designing systems that can effectively measure EDA.

2.1 Skin Structure

From a sensory standpoint, the skin (also known as cutis), houses various nerve cells, which react to touch (mechanoreceptors), pain (nociceptors), and temperature (thermoreceptors). The skin has several roles, namely: prevents the body from drying out, with the help of the sweat glands; enables a controlled emission of body fluid for thermal regulation purposes and offers protection of the vital organs from the external world.

Stratified in multiple layers, depicted in Figure 2.1, each constituent of the skin has different characteristics at different body locations. In the scope of this work, some of these constituents are especially significant because of their relation with the Sympathetic Nervous System (SNS).

The skin is composed of three markedly distinct layers, namely: the epidermis, the dermis and the hypodermis. The epidermis is located at the skin surface and consists of epithelial tissue, which becomes progressively tougher and dryer closer to the surface. The layer underneath, the dermis, consists of tight, fibrous connective tissue. The outermost layer and therefore more stringent is called stratum corneum and is unusually thick on the palmar and plantar sites, which are the locations where the sympathetic regulation of sweat glands is more noticeable.

In comparison with the epidermis, the dermis is significantly thicker [6]. The dermis presents two distinct layers, papillary and reticular layer, which can be differentiated based on the density and arrangement of the collagen fibres. These fibers, present in the dermis, give strength and elasticity to the skin. In the reticular region, we can find the roots of the hair, sebaceous glands, sweat glands, receptors and blood vessels. As for the hypodermis (also known as subcutis), it is composed of loose connective

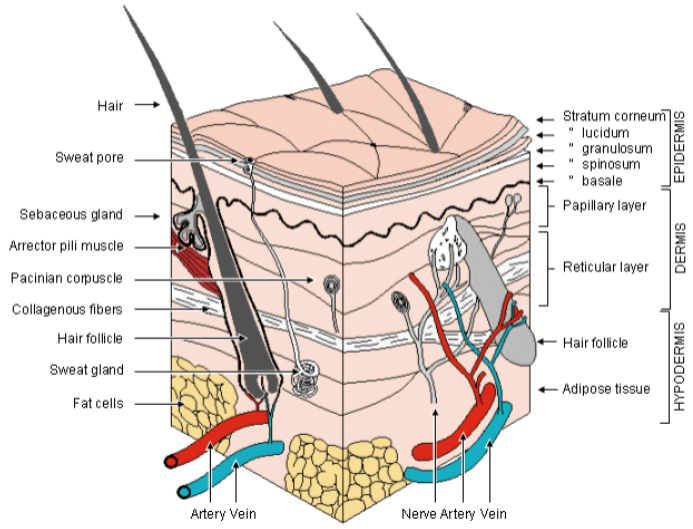

Figure 2.1: Typical skin stratification and constituents [7].

tissue, which covers the muscles and allows for functional mobility of the skin. It can also contain part of the secretory system, sweat glands (appearing as a glomerulus) as well as fatty tissue, and the larger blood vessels that supply the body surface. From these larger vessels, a vascular system composed of smaller ramifications supplies the sweat glands. The skin is also composed of a lymphatic system present at the dermis and hypodermis layers, which are thought to contribute to the overall high electrical conductivity of the inner skin layers

2.2 Distribution and Structure of the Sweat Glands

The human body has between 1.6 - 4 million sweat glands [8], where the locations with a higher density of sweat glands are the hand palms, feet soles and forehead, reason for which EDA measurements are often performed in these regions. The lowest density regions are found on the arms, legs, and trunk.

The density of sweat glands can be expressed per cm^2 of the adult's skin and usually present values approximately characterized as follows: 230 on the hand palms, 620 on the feet soles, 360 on the forehead, and 120 on the thighs [9], although a significant variability is found in the available literature reporting such findings, due to differences in the methodology used to characterize them. Since birth, the number of sweat glands is always the same throughout life, however, not all of these glands are active at a particular period in life, and the number of active glands can significantly vary according to age, gender and ethnic differences. For example, children may exhibit much higher sweat glands density since the inter-gland distance is lower, and deterioration of the skin occurs as the person gets older, reducing the sweat glands density.

All sweat glands in humans are considered exocrine glands since they secrete directly to the skin surface. However, it is possible to characterize two types of sweat glands, namely, eccrine and apocrine glands. The eccrine glands are more abundant, can be found in higher density at the hand palms, feet soles and forehead, and do not present appreciable quantities of any glandular cells cytoplasm in their

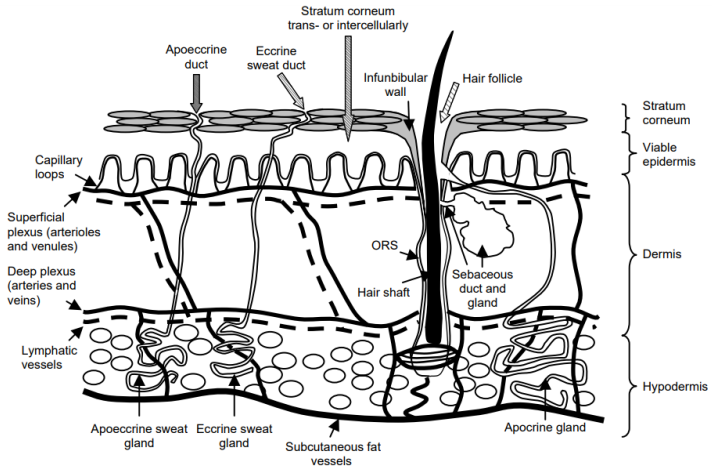

Figure 2.2: Cross sectional view of the sweat glands [14].

secretions. Apocrine sweat glands, which are considered to play a less critical role in sweating, are characterised for having cytoplasm, which has to be replaced. They exhibit an increased density on regions such as the breast areola, axillary, circumanal and genital regions (associated with hair follicles) [10].

Eccrine glands produce a clear, odourless substance, sweat, consisting primarily of water. They are driven by the SNS, primarily through cholinergic fibres whose discharge fluctuates, for the most part, by changes in core body temperature (thermoregulation), although adrenergic fibres play an essential role as well. The glands present on hand palms and feet soles do not show activity correlated with thermoregulation, but display it at times of arousal [11–13].

As shown in Figure 2.2, the eccrine sweat glands are subdivided into the duct and the secretory segment. The latter is found at the hypodermis or the dermis zone, and consist of a tube curled up into a rounded mass with roughly 0.4mm in diameter. It is succeeded by the duct, following a spiral route through the dermis and spiralling through the epidermis. The dermal part of the duct can contain secretory cells, and the duct opens onto the skin surface through a small pore. A more in-depth explanation can be found in [2].

2.3 Physiological Principles of Electrodermal Activity (EDA)

The sweat gland activity takes part in the homeostatic process of thermoregulation, together with other skin organs that are involved in the thermoregulatory function of the Autonomic Nervous System (ANS). As an example, when a human is subjected to severe stress, secretion rates can reach up to 2 litres of sweat per hour, which may translate in a loss of up to $\frac{1}{4}$ of the whole body fluids during a single day [2].

The sympathetic innervation paths are depicted in Figure 2.3; the skin is reached by a large number of efferent vegetative fibres, which include sympathetic fibres, responsible for the arrector pili muscles, and the innervation of the eccrine sweat gland's secretory segment. The postganglionic sympathetic fibres, corresponding to those fibres from the ganglion until the effector organ, leave the sympathetic trunk via the gray communications ramus, in conjunction with all motor and sensory fibres. These fibres

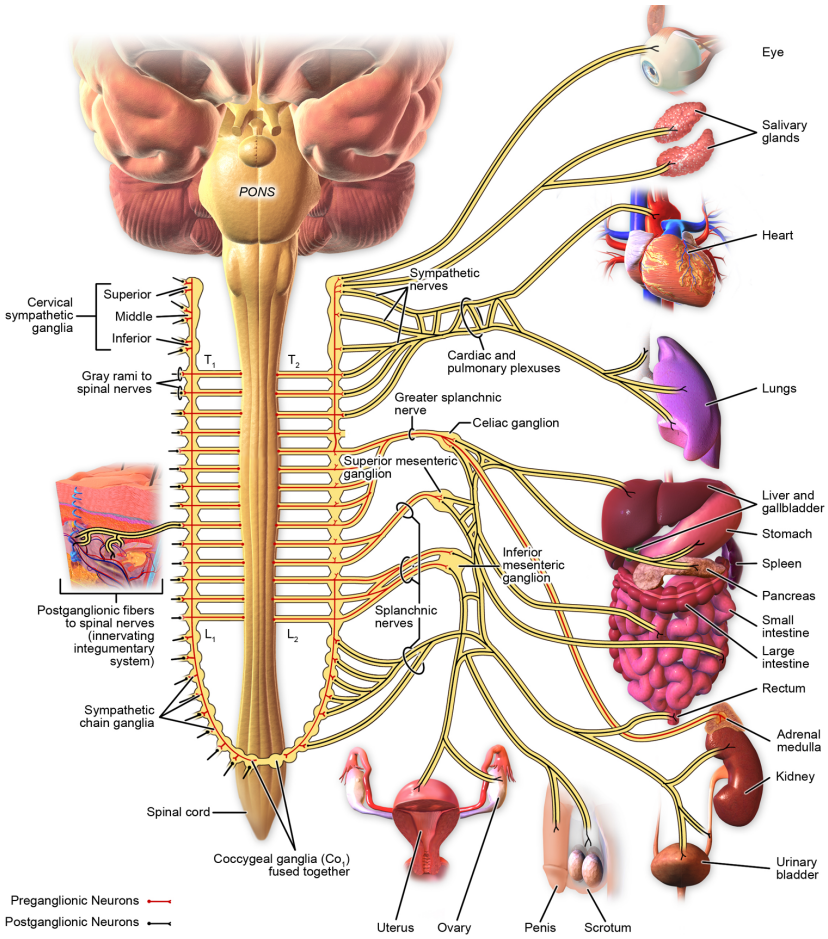

Figure 2.3: Sympathetic innervation pathway [15].

then travel close to the somatosensory fibres for surface sensibility and form characteristic plexuses in the subcutis. The sympathetic spinal nerves, which descend in the anterolateral part of the spinal cord, are switched over in the lateral column and exit the spinal cord through the ventral root simultaneously with the motoric fibres, travelling along the white communicating ramus to the sympathetic trunk.

As for the innervation of the sweat glands, which is of utmost importance to the scope of this work, the secretory part of the sweat gland is supplied by widely ramified sympathetic postganglionic nerve fibres, the nonmyelinated class C fibres [8].

The sympathetic trunk is a highly segmented structure as depicted in Figure 2.4, which shows the area of skin regulated by a specific spinal nerve, also known as a dermatome. Understanding the dermatome areas is essential when endosomatic recordings are the used measurement method, because electrodes placement can influence the accuracy of the reading due to a possible electrical potential difference between two distinct dermatomes.

There are several theories concerning the origin of the electrodermal activity, but in general, the hypothalamus is believed to be the control centre of all vegetative functions. For a more extensive review we direct the reader to [2] and references therein.

It appears that a regional distinction exists, in the form of how the innervation of sweat glands happens; this is one of the reasons why the main recommended locations for measuring EDA are the hand

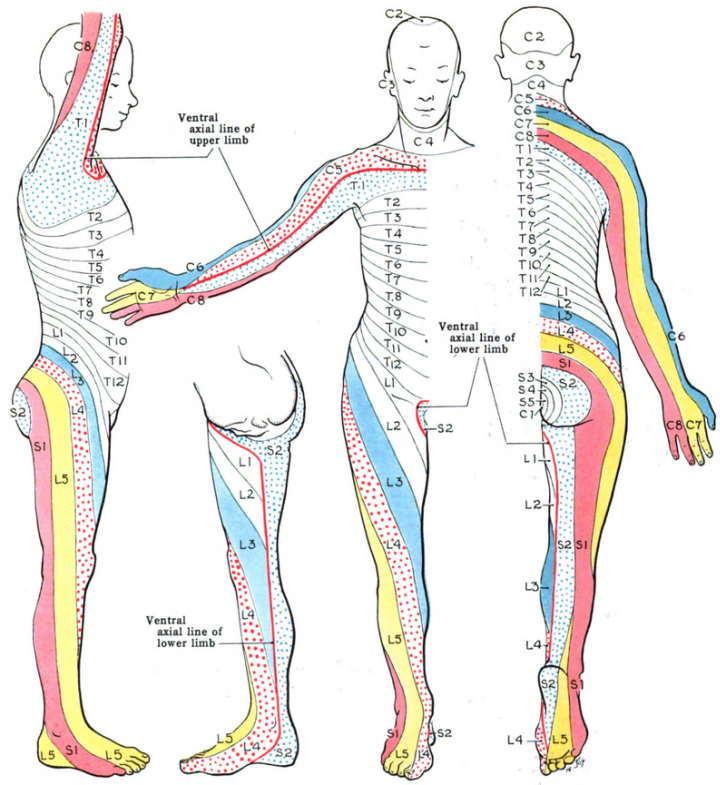

Figure 2.4: Dermatomes areas: C-cervical; T-thoracic; L-lumbar; and S-sacral segments [16].

palms or feet soles. Sweat gland innervation at the face is also referred in the literature [2, 17], and in Section 5.3, we will explore the potential to measure EDA signals from the forehead.

2.4 Sweat and its Characteristics

The secretory segment of the sweat gland is composed of clear and dark secretory cells. Precursor sweat in the gland's secretory segment is regarded to be more hypertonic than blood, therefore implying the existence of an active transport mechanism for sodium chloride from the interstitial fluid into the lumen, which consequently produces an osmotic gradient.

Precursor sweat is mostly composed of sodium, chloride, potassium, possibly bicarbonate and lactic anion, together with small amounts of urea, ions, biogenic amines and vitamins.

The secretion of sweat does not flow continuously through the duct to the skin surface, but rather in a periodic style with pulsations of around 12-21Hz [18] caused by the rhythmic contractions of the myoepithelial, surrounding not only the secretory but also the ductal part of the sweat gland like a helix, which is regarded as the source of the pulse.

The locations distal to the trunk, such as hand palms, feet soles, and ears, are laden in sympathetic adrenergic fibres, which act in a vasoconstrictor manner and show a vigorous tonic activity even under temperature invariant resting conditions. Peripheral vasodilation occurs when inhibiting their activity, while on the other side, the relaxing state of those adrenergic fibres is reduced at the proximal parts of extremities or trunk itself, while its increase leads to vasoconstriction.

Reduced sweating can result in cooled skin areas, despite a high amount of sudomotor impulses from the CNS, in turn, results in local warming of the skin that can increase sweating.

According to [19], it is possible to identify five additional kinds of sweating that result from multisensory stimuli, namely:

- **Emotional sweating**. Increased sweat gland activity occurs as a consequence of psychological and emotional states that appear, for example, in high arousal or under stress. Emotional sweating can be noticed primarily on palmar and plantar sites, in axillary and genital regions, as well as on the forehead. Studies report that there is increased sweating at other body sites during emotional strain induced by arithmetic exercise; the amount of sweating is directly proportional to the number of sweat glands per region, therefore indicating no regional differences in emotional sweating [20]. The likelihood of the explicit reactivity of palmar and plantar sweating being related to psychological stimulation is dependent on the higher sweat gland density on these sites. Thus, the specific manifestations of emotional sweating at the palms and soles remains to be determined;
- **Gustatory sweating**. Appears when sour, highly spicy or salted food is ingested. It is expressed mainly on the face, specifically, on the forehead or the upper lip. Even without gustatory stimuli, this specific sweating can be elicited via chewing or olfactory stimulation;
- **Ubiquitous (or spontaneous) sweating**. Appears on the palmar and plantar sites and is considered as an expression of resting tonus;
- **Reflex sweating**. Appears at sites that are innervated from spinal cord segments distal to the location of particular damage (e.g. paraplegia);
- **Pharmacological produced sweating**. Sweating elicited through injection of substances or iontophoresis with cholinergic substances.

The specific meaning of all these types of sweating was not yet exhaustively explored, and emotional sweating is the type that has seen more extensive research [21].

2.5 Bioelectrical Properties of the Skin

Now that we have a better understanding of the anatomy and inherent properties of the skin, it is possible to characterize electrical equivalent circuits that model the electrodermal system of the skin. These models are approximations, since the skin does not display systematic properties consistently.

2.5.1 Electrophysical Properties of the Skin and Sweat Glands

When an external current is applied to a biological tissue, such as the skin, it acts like an electrical network built of resistors and capacitors [2]. Depending on the ionic concentrations, blood, ductal sweat and interstitial fluid, different conductance levels will be originated, displaying a similar behaviour to that of variable resistors. In contrast, cellular membrane boundaries appear to have more capacitor-like

characteristics, since they possess selective permeability that forms an obstacle for the ions involved in the current flow, presenting back electromotive force (EMF). Such membranes can store electrical energy and can act as polarisation capacitors, becoming electrical potential sources. They are presumed to be located at the sweat gland membranes, at the dermal-epidermal boundary membrane, and in the epidermis. These properties are known as the active sources for electrodermal phenomena [2].

The skin resistance can greatly vary depending on factors like weather, age, gender, the current state of the SNS, and a few others more. The average skin resistance is around 100kΩ but can go as low as 10kΩ and as high as 20MΩ.

Resistive Properties of the Skin and Sweat Glands

The dermis and the hypodermis possess good electrical conductance since they are well supplied with interstitial fluid and blood, but it can oscillate when changes in blood flow occur, e.g., by applying pressure. Also, the epidermal malpighian layer and the stratum intermedium are regarded as relatively conductive structures. The upper layers (corneal zone), being relatively impermeable to water and other solutions, are thought to be accountable for the skin's resistance. The stratum corneum does not contain living membranes and acts like a sponge, absorbing water and solutions from inside or outside the body, which then get released when it needs to hydrate the corneum. With an increase in sweating, corneal hydration will also increase, leading to tonic and phasic changes in skin resistance; in contrast, if it becomes dry, tonic skin resistance increases.

It is generally considered that skin conductance increases with the height of the ductal sweat column, and the slow decline presented in EDL (that appears in the absence of EDRs) may reflect dissipation of sweat in the ducts.

To better understand the resistive properties mentioned above, supposing that the skin is composed only by resistive, and considering each sweat gland as a single resistor with a fixed value that can be switched on or off, we can elaborate an electrical model as shown in Figure 2.5, the model assumes that the resistive properties of the skin/sweat gland system can be characterized as several serial and parallel connected resistors where we have:

- A variable resistor formed by the stratum corneum;
- A fixed resistor formed by the epidermal barrier;
- Resistances of the sweat gland ducts that are switched either into or out of the circuit;
- A fixed relatively low resistor of the lower epidermis, dermis and probably the hypodermis.

Also, horizontal resistance pathways can be assumed in all layers of the skin, but especially in the lower epidermis and in the dermis.

Capacitive Properties of the Skin and Sweat Glands

When applying an external current to the skin, the cellular membranes exhibit their polarisation capacities, storing charge like capacitors. The selective permeability for ions is the basis of these capacitive

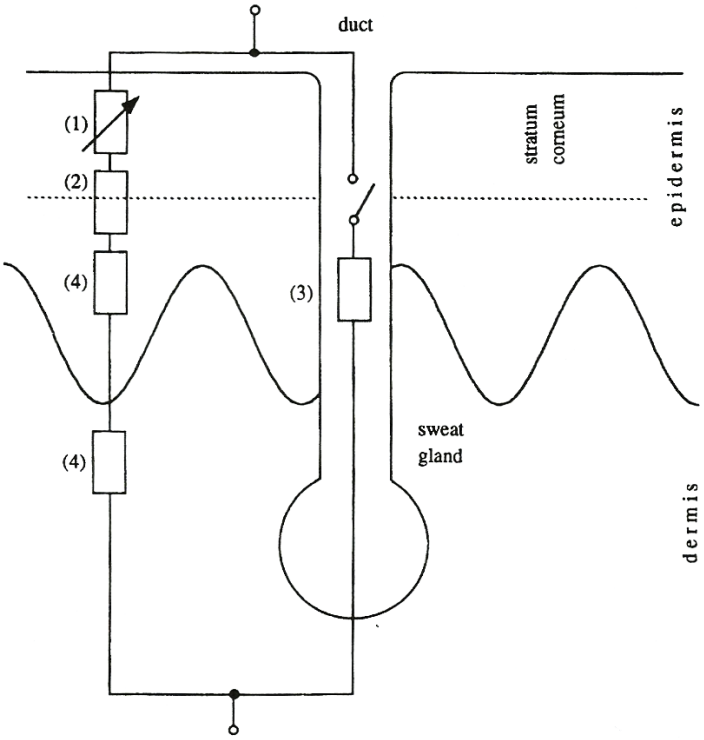

Figure 2.5: Resistive properties of the skin [2].

properties, and therefore the epidermis can be viewed as an RC network when in the presence of external current.

Keratinized epidermal layers are regarded as passive, compared to those of living tissue. Skin also contains active membranes (those of nerve, muscle, and glandular cells). These have a resting charge that becomes reversed when stimulated; they show capacitive properties when an external current is applied and are located, mainly, in the secretory part of the sweat gland. Several studies on the existence of an electrical barrier layer are available, e.g. [2], showing that the depth of the layer is approximately 350μm at the hand palm and 50 μm at the forearm. It was presumed the existence of an active epidermal membrane with a fixed negative charge, making it selectively permeable to cations. Other capacitive properties may come from the membrane polarisation and depolarisation in the blood capillaries, the arrector pili muscles and the myoepithelial surrounding sweat gland (the contribution of the latter is unlikely to affect endosomatic EDA). Membrane-like capacitors with influence in EDA can be found on the stratum germinativum because there is the possibility of epidermal reabsorption processes in the ductal walls [22].

2.5.2 Origins of Active Electrical Properties

In order to investigate the properties of the cellular membrane, endosomatic measurements need to be used, and, as such, skin potential is measured. Unlike exosomatic EDRs, endosomatic SPRs are more complicated since they can appear as monophasic, biphasic or triphasic responses. Because of these responses, various explanations were proposed that combined active membrane properties and

resistive properties of corneal hydration and duct filling.

Edelberg [22, 23], in his model, outlines that a negative intraluminal potential, together with a constant tonic sweat gland activity, results in the appearance of sweat on the malpighian layer. An increase in sweat gland activity or a contraction of the myoepithelial tissue surrounding the duct would result in an outpouring of sweat to the surface. This causes a negative Skin Potential Response (SPR) with long rise time and slow recovery, due to sweat reabsorption in the ductal walls.

Edelberg suggests a short-lasting increase of permeability for cations in the active epidermal membrane as the source of EDRs with fast rise times and quick recovery. Additionally, he explained that the biphasic and triphasic SPRs are made by both positive and negative components, with the first having a short recovery period and the second a slow recovery period. Whether the SPR begins, either with positive or negative is related with the degree of duct filling at the onset of the EDR [22, 24].

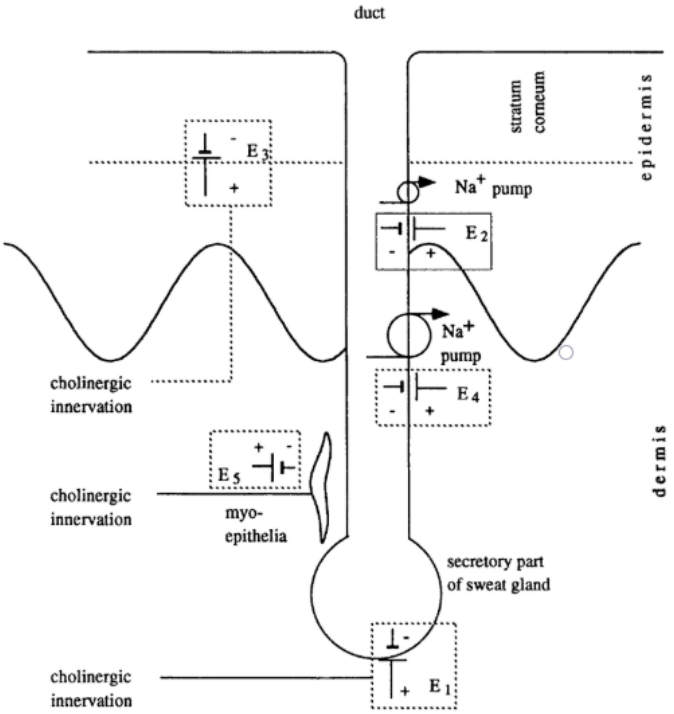

Figure 2.6: Location of the active electrical components of the skin [2]

Figure 2.6, shows the location of the active components in the skin, where:

- E_1 is positioned at the secretory part of the sweat gland;
- E_2 represents the potential source in the epidermal duct at the level of the stratum germinatium;
- E_3 is the membrane potential found at the inner corneal zones;
- E_2 and E_4 are membrane potentials that relate to the sodium reabsorption mechanism;
- Finally, E_5 stems from the myoepithelial.

2.5.3 Models of the Electrodermal System

Models Based Exclusively on Resistive Properties

It is known that the electrodermal system also contains capacitive properties, but the model based on resistive properties alone enables us to have a heuristic value for DC measurement. Figure 2.7 illustrates this model, where:

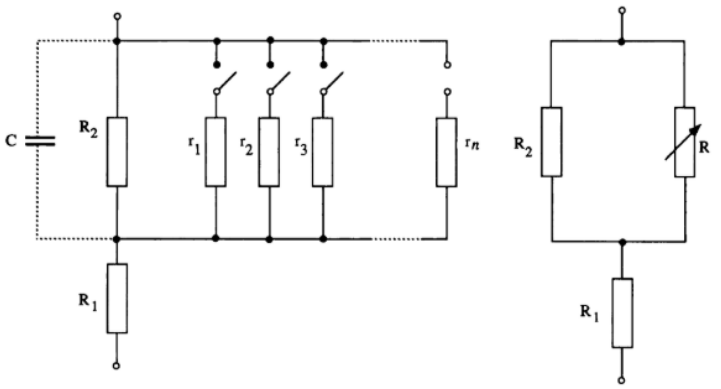

Figure 2.7: A solely resistive model of the skin [2].

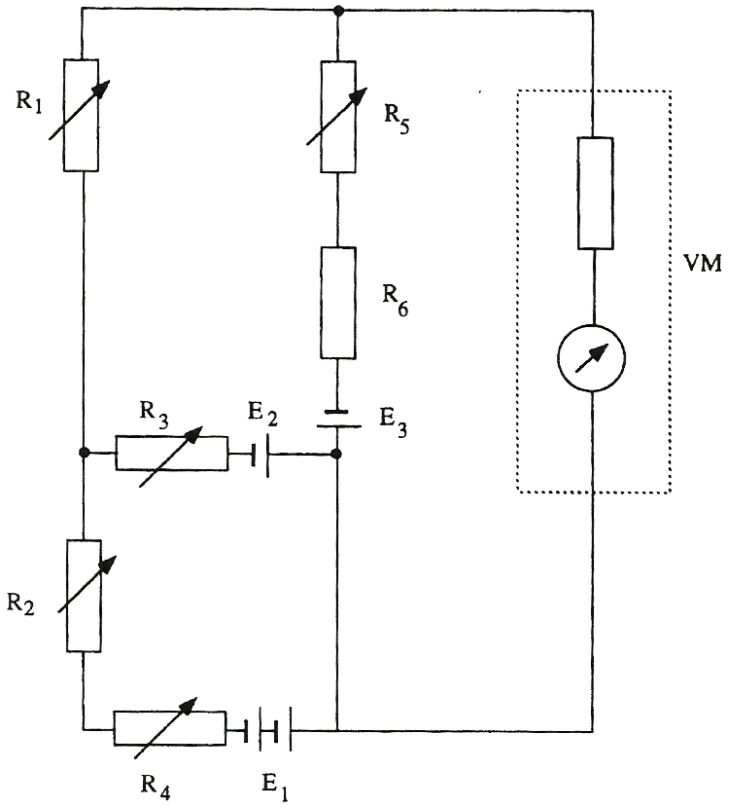

Figure 2.8: Electrical model of the skin proposed by Fowles [25].

- R_1 embodies a series resistance, positioned at the dermis and body core;
- R_2 accounts for the resistive value of the stratum corneum, in parallel with r_1, r_2, r_n (which can be

on or off depending on the sweat gland activity), representing the resistance of the sweat gland ducts.

Models Going Beyond Single Resistive Properties

In this type of models, potential sources or capacitive properties, depending on whether an endosomatic or exosomatic recording is made, are taken into account. Figure 2.8 depicts an example of such models, where:

- E_1 represents a negative lumen potential, originated in the ductal wall at the dermis and determined by the sodium concentration in the lumen;
- R_4 represents the variable resistance of the dermal ductal wall and the variable resistance R_2 represents the dermal section of the duct dependent on the filling level;
- E_2 also represents a negative lumen potential, generated across the epidermal duct wall at the stratum germinativum level, dependent on the concentration of sodium and chloride ions in the lumen. Since the membrane is less selective at this stage, E_2 is likely to be smaller than E_1 during sweat gland activity;
- R_3 has the same purpose as R_4 and R_1 the same as R_2;
- E_3 represents the localized membrane potential, originated at the bottom zone of the stratum corneum, working as a function of the ionic potassium concentration in the interstitial fluid, as well as of the applied electrolyte in the electrode cream; the membrane potential will remain surface negative as long as the external potassium ionic concentration is higher than that of the interstitial fluid, and the values of the R_6 (compact keratinized layer zone) and R_5 (upper layers of the corneum) will vary according to the hydration.

Under complete resting conditions, reabsorption is higher than secretion, so resistances R_1, R_2 and R_3 will maintain high values; on the other hand, potentials E_2 and E_1 will be minimal. Potential E_3 is the most crucial factor for potential measurement and replicates the potassium ionic concentration in the interstitial fluid. Considering a small to moderate sweat secretion, R_2 and R_1 will decrease, leading to a SCR with slow recovery. Also, E_1 will increase as a result of higher sodium ionic concentration in the lumen, producing a slow recovery negative SPR.

Further sweat secretion will decrease even more R_1 and R_2. If the hydrostatic pressure has built high enough that a depolarisation of the epidermal duct membrane occurs, it will elicit a response in the epidermal duct, causing R_3 to decrease, and a small lumen negative potential originates at E_2. This will produce a SCR with short recovery time, and a positive SPR appears because of a shunting effect on E_1. If the ducts are filled to their maximum, only membrane responses will be produced.

In summary, this model presents most of the presumed origins of electrodermal phenomena. Negative SPRs and SCRs with longer recovery times appear according to duct filling. The responses originated at the membrane will be the primary source of SCRs with faster recovery times, of positive SPRs

and perhaps a negative SPRs with short rise time at the beginning of biphasic SPRs or even alone. However, this model still lacks the resistor pathway between the electrodes and the skin, which is not in series with a capacitive element.

The ”poral valve model”, presented by Edelbery [26] has been able to explain a variety of electrodermal phenomena, like the rapid phasic changes, without the supposition of an active reabsorption membrane, which has never been physically demonstrated.

2.6 Background on Electrodermal Activity Measurement

To support the remainder of this work, it is vital to further describe what electrodermal activity is and briefly understand how can it be recorded. The term EDA has been found to appear for the first time in 1966 [27], to describe all the electrical phenomena of the skin, which include all active and passive electrical properties that could be traced back to the skin and all related organs. Electrodermal activity is also known as the galvanic skin reflex (GSR). However, this latter designation is somewhat of an older designation used in the early history of the EDA research, but is no longer encourage since the terminology is misleading [2].

The EDA can be acquired with two different methods, namely, endosomatic or exosomatic. Endosomatic recordings do not use external current and rely only on the potential differences that are present at the skin. Exosomatic recording methods are the ones where direct current (DC) or an alternating current (AC) is applied to the skin. If the method of choice is exosomatic, EDA can be recorded using a constant voltage which, in DC measurement is designated as skin conductance (SC) and in AC measurements designated as skin admittance (SY). However, EDA can also be recorded using a constant current, which, in turn, is designated as skin resistance (SR) when measured in DC, and skin impedance (SZ) when measured in AC.

So far, we know that EDA is a response that an individual has to a stimulus or physiological process (see Section 2.4), which may be traceable or not. For analysis, the EDA waveform is generally divided into two main components: tonic and phasic. Tonic components, also known as electrodermal level (EDL), is a low frequency signal that is typically considered as the baseline of the EDA. Hydration, skin dryness or even autonomic regulation are factors that contribute to the continually changing increase and decrease of the EDL of an individual, the reason for which current research highlights tonic measurements alone are mostly inconclusive. The phasic phenomena, also known as electrodermal response or reaction (EDR), corresponds to the phasic changes, (as shown in Figure 2.9), and expresses the short-term (higher frequency) EDA variations. It exhibits sensitivity to specific emotionally arousing stimulus events, with a nominal latency of around 1-5 seconds after the stimuli, but it is also classified as spontaneous or non-specific when it is not possible to associate with any specific stimuli [28].

Table 2.1 summarises the features that are possible to extract from EDA signal and standard nomenclature used in the literature.

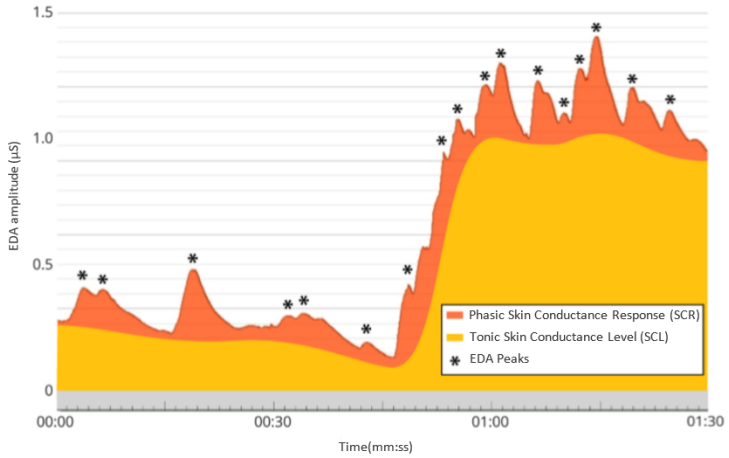

Figure 2.9: Example of a typical EDA signal (adapted from [28]).

Table 2.1: Typical features extracted from electrodermal activity and related signals [29].

Source		**Endosomatic**	**Exosomatic**			
Method		**Voltage Diff.**	**DC**		**AC**	
Measurement	**Description**	**Potential**	**Resistance**	**Conductance**	**Impedance**	**Admittance**
Tonic	Baseline level behavior	SPL	SRL	SCL	SZL	SYL
Phasic	Signal response behavior	SPR	SRR	SCR	SZR	SYR
Non-specific Response	Responses without matching stimulus	NSSPR	NSSRR	NSSCR	NSSZR	NSSYR
Frequency	Phasic response rate	SPR freq.	SRR freq.	SCR freq.	SZR freq.	SYR freq.
Amplitude	Onset-Peak amplitude difference	SPR amp.	SRR amp.	SCR amp.	SZR amp.	SYR amp.
Latency	Time between stimulus and onset	SPR lat.	SRR lat.	SCR lat.	SZR lat.	SYR lat.
Rise Time	Onset-Peak time difference	SPR rise t	SRR rise t	SCR rise t	SZR rise t	SYR rise t
Half Rise Time	Time between onset and 50% amplitude	SPR ris. t/2	SRR ris. t/2	SCR ris. t/2	SZR ris. t/2	SYR ris. t/2
63% Recovery Time	Time between peak and 63% amplitude	SPR rec. t	SRR rec. t	SCR rec. t	SZR rec. t	SYR rec. t
50% Recovery Time	Time between peak and 50% amplitude	SPR rec. t/2	SRR rec. t/2	SCR rec. t/2	SZR rec. t/2	SYR rec. t/2

Chapter 3

State of the Art

In this chapter, we will discuss the base concepts of electrodermal activity measurement. After, we will examine the landscape of commercially-available devices, latest research and applications.

3.1 Current Developments and Devices

Several platforms and devices have already been created and made commercially available to record electrodermal activity. Although cost was a limiting factor until recently, over the past years there has been a rapid increase in low-cost and Do-it-Yourself (DiY) alternatives [30]. Within do-it-yourself platforms, BITalino [31] has been recently released as a scientifically validated low-cost open source hardware and software toolkit for biosignal acquisition, hence being the platform used as the base for the present work [32–34]. MySignals, developed by Libelium's Cooking Hacks [35], is a medical development platform oriented for researchers, and compatible with standard Do it yourself(DIY) hardware, such as the Arduino or Raspberry Pi. On a more end-user approach, the Empatica E4 wristband [36, 37] is a wearable research device that offers real-time physiological data acquisition hardware and software for in-depth analysis and visualisation. GSR 2, developed by Thought Technology [38], is a small, hand-held and self-contained EDA monitoring device for home biofeedback. Also, from Thought Technology, the eVu-TPS sensor [39], is a portable sensor that enables heart rate and EDA data acquisition outside the clinic environment using mobile devices[1]. From BIOPAC Systems, the EDA100C Electrodermal Activity Amplifier [41], is an EDA amplifier focused on research applications, and the BioNomadix Transmitter [42], also combines a wireless photoplethysmograph and EDA sensor to enable simultaneous recording of blood volume pulse and electrodermal activity. The Shimmer3 GSR [43], is a realtime EDA biofeedback device, which offers the possibility of adding other sensors (e.g. Shimmer photoplethysmogram). Lastly, The MindMedia Skin Conductance Sensor [44] is another commercially available option.

Most of the devices mentioned above, record the EDA signal in zones that represent an obstruction to movement or comfort of the wearer, which is a limiting aspect when conducting long-term measurements. Furthermore, the use of pre-gelled electrodes is generally mandatory or recommended. Few

[1] Thought Technology also offers a simple EDA sensor, the SA9309M [40]

Table 3.1: Characteristics of available systems.

Device	Electrode Position	Electrode Type	Measurement Range	Bandwith
BITalino	not restricted	Ag/AgCl	0-25μS	0-2.8Hz
MySignals	medial & distal phalanx	Ag/AgCl with velcro	0-20μS	–
Empatica E4	bottom wrist	Ag/AgCl with ABS core	0,01–100μS	–
GSR 2	medial & distal phalanx	Ag-AgCl	1k-3MΩ	–
eVu-TPS	medial & distal phalanx	–	0-30μS	–
EDA100C	not restricted	Ag-AgCl	0 to 200μS	–
BioNomadix	not restricted	Ag/AgCl with velcro	0-50μS	0-3Hz
Shimmer3	medial & distal phalanx	snap connector Ag/AgCl electrodes	0.2-125μS	0-15.9Hz
MindMedia EDA	medial & distal phalanx	Ag/AgCl with velcro	0.1-1000μS	–

authors like Poh in [45, 46] or Pope & Halter in [47] attempted to solve this problem, designing a wristband that does measurements on the wrist area. Other worth mention works, are from Picard & Scheirer [48], which developed a glove called Galvactivator that maps the skin conductivity onto a LED. Another sensing glove was presented by Lee et al. [49], using conducting fabric and an embedded system. The iCalm sensor [50], characterised for being low-cost, low-power and a wireless platform which can be integrated into a wristband or sock. Lastly, we also highlight the work presented by Sousa et al. [51], in which a glove capable of measuring PPG and EDA data is presented.

On a more consumer-oriented segment, we existing work includes The Pip [52] or even the Moodmetric ring [53], which combines biosignal sensors, such as EDA, with machine learning algorithms to extrapolate an index value of the user stress levels. The former goes as far as delivering exercises to reduce user stress levels.

However, current commercialised devices are too focused in a given application, with limited or no access to raw data, as well as being expensive. As for research oriented devices, they are expensive as well, and low-cost alternatives lack the resolution/sensitivity capacity in EDA measurements.

Numerous articles show that EDA sensors are an added-value tool for applications such as stress management, but also other physiological conditions such as epilepsy, autism, and few other more. On the epilepsy side, the company Empatica provides a consumer-oriented device, called Embrace,which has provided convincing results comparatively to EEG, in the detection of seizures, which is particularly interesting especially considering that we want to monitor the patient around the clock.near-continuous patient monitoring is a desired feature. The company claims to be able to detect seizures with a sensitivity between 92-100%, while the false alarm rate is 0.48 to 2.02 per day. They recently released another FDA approved device, the Embrace 2, that is expected to have an even better performance [54]. In another work, EDA signals have shown a strong correlation with extended post-ictal generalised EEG suppression in cases of Sudden Unexpected Death in Epilepsy (SUDEP) [55].

On the Autism Spectrum Disorder (ASD), an extensive review of devices that integrate EDA measurement is provided by Taj-Eldin. In his work [3], most of the devices focused in this field as an aid to give feedback to the patient and caregiver about the emotional state of the user.

Other applications range from studying stress levels [4, 56] or even for marketing purposes where the influence of audiovisual content on the viewers is studied [57].

Table 3.1 presents a summary of the main characteristics found in the previously mentioned devices.

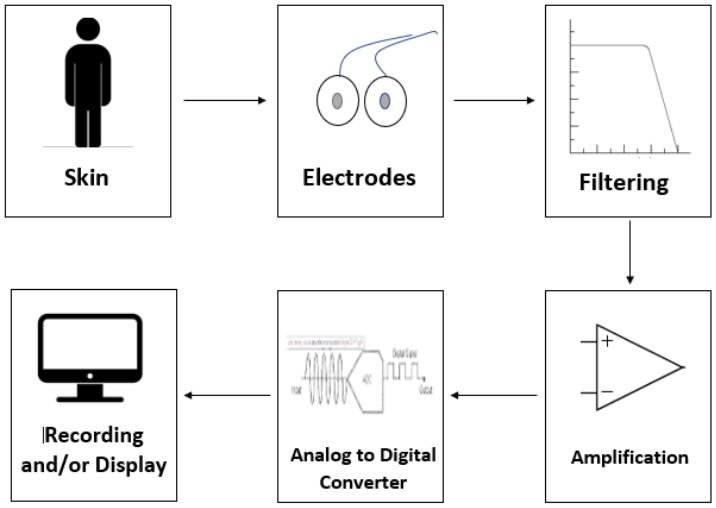

Figure 3.1: Basic workflow for EDA data acquisition.

The block diagram, presented in Figure 3.1, describes the underlying architecture that most of these devices have in common.

The workflow of an EDA measurement system has different variations, depending on the method used (as further detailed in Section 3.2, but in the most basic form, EDA measurement requires a location at the skin of the user where the conductivity or impedance will be measured, electrodes to interface the sensor with the skin, amplification, filtering (in order to mitigate artefacts or other unwanted signals), an analogue-to-digital converter, and, finally, a way to record and/or display data.

3.2 Common Circuits for Electrodermal Activity Measurement

3.2.1 Voltage Dividers

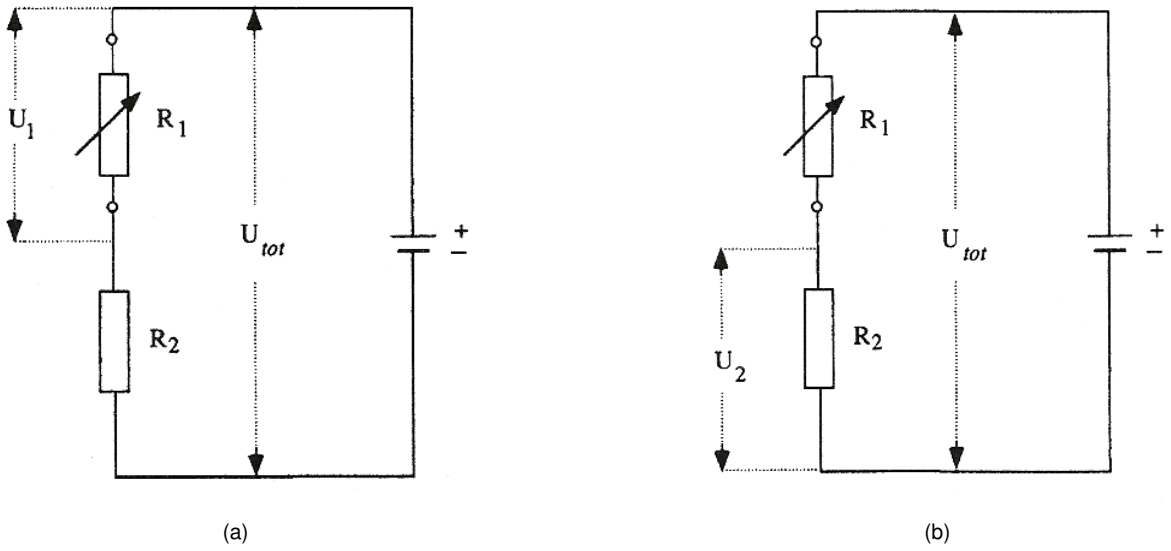

Figure 3.2: Voltage divider for EDA measurement [2].

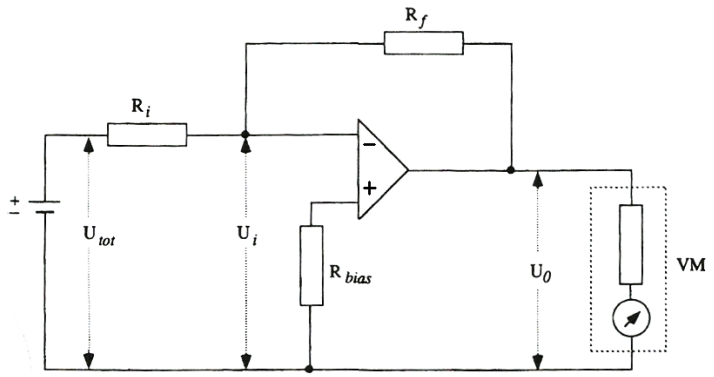

Figure 3.3: EDA measurement using an operational amplifier [2].

In order to measure EDA using voltage dividers, two electrodes are attached to the skin in the target location, connected in series with a system reference resistor, and a voltage source is applied with a constant voltage. There are two different methods of measurement, represented in Figure 3.2, these being:

- The *quasi-constant current method*, Figure 3.2 a), where there is a reference resistor, R_2, and a variable skin resistor, R_1, in series. Using a voltage divider on R_1, we get U_1, the voltage across the skin.

$$U_1 = U_{tot}\frac{R_1}{R_1 + R_2} \tag{3.1}$$

$$I_{tot} = \frac{U_{tot}}{R_{tot}} = \frac{U_{tot}}{R_1 + R_2} \tag{3.2}$$

- The *quasi-constant voltage method*, Figure 3.2 b), where the principle used is the same as the above, but now, we apply the voltage divider to the reference resistor.

$$U_2 = U_{tot}\frac{R_2}{R_1 + R_2} \tag{3.3}$$

Looking at Equation 3.2, if R_2 is much smaller than R_1, I_{tot} will no longer be constant. When R_1 decreases, the current increases and vice versa. We can further conclude that the voltage measured across R_2 is almost totally proportional to variations in the reciprocal of R_1, conductance G_1.

Overall, higher signal amplification is needed for the *quasi-constant voltage method*. It is important to remember that the instrumentation used to measure the phenomena in question has internal resistances and, in case of an amplifier, attention to the input resistance must be given. In summary, when measuring voltages, the resistance and input impedance must be as high as possible (high impedance amplification).

3.2.2 Operational Amplifiers

This method was introduced to avoid possible measurement errors caused by the two previous methods, namely due to the fact that a constant current or voltage is difficult to ensure. Figure 3.3 shows a method that uses active circuitry built upon one operational amplifier. Analysing the circuit, we obtain an output voltage of the inverting amplifier:

$$U_o = -\frac{R_f}{R_i} U_{tot} \tag{3.4}$$

Knowing that the voltage U_i (Figure 3.3) is 0, two different methods of measurement are possible:

- The *constant current method* uses R_f as the skin feedback resistor; the current flowing through R_i, if this is considered as the skin is determined as follows:

$$I = \frac{U_{tot} - U_o}{R_i + R_f} \tag{3.5}$$

  Using U_o, previously presented in Equation 3.4, on Equation 3.5, we have:

$$I = \frac{U_{tot}((R_i + R_f)/R_i)}{R_i + R_f} = \frac{U_{tot}}{R_i} \tag{3.6}$$

  The output voltage will be proportional to the skin resistance R_f following Equation 3.4.

- The *constant voltage method* uses the subject skin as the R_i of the system. The voltage U_o will be proportional to the reciprocal of the skin resistance R_i, but with inverted polarity.

Measurements of the output voltage can be done at a relatively low-impedance level. The reference resistor R_{bias} is used to compensate the impact of bias currents on the amplifier offset.

Nowadays, a relatively distortion-free high amplification of biomedical signals can be obtained. However, there are some constraints in coupling, amplification and filtering of the EDA. In contrast to other biomedical signals, in exosomatic recordings, an electrical separation must exist from all amplifiers inputs to the input of the EDA coupler, otherwise, it may reduce the EDA signal. In the case of amplification, problems are originated by the fact that the EDA signals have a wide range, since many possible differences in EDLs result in a wide dynamic range. On the other hand, fluctuations appearing as EDRs are relatively small. To achieve a high resolution of EDRs, the separation of two components may be useful, in order to amplify them separately with different gain coefficients. The typical problems are related with the fact that only a small part of the EDL is of interest and therefore is generally amplified as well when designing instrumentation with enough sensitivity to measure EDRs.

3.2.3 Electrodermal Responses Separation with s Wheatstone Bridge

Electrodermal responses typically exhibit low amplitude, when compared to the total range of measurements when admitting the EDL also. To address this problem, a simple Wheatstone bridge can be implemented, as shown in the following figure.

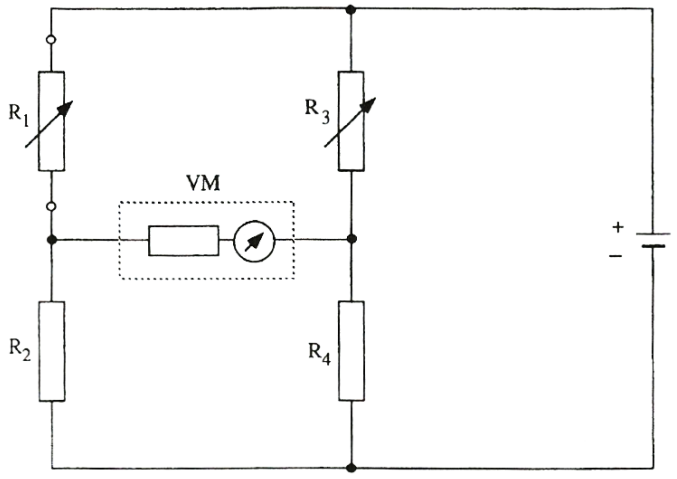

Figure 3.4: EDA measurement using a Wheatstone bridge [2].

In Figure 3.4, R_1 represents the subject's skin resistance, R_3 is a potentiometer to calibrate and correct EDL drift, and R_2 and R_4 are fixed resistors. The potential difference between the central point of both voltage dividers is read with a meter VM. When an EDR happens, the balance between these two points will be disturbed, producing a variation in the output voltage. Amplification is generally needed to increase the sensitivity of the measurement circuit to the EDR.

A more current method to suppress the baseline component of EDA is the use on an AC-coupled amplifier (removes the DC offset). The measurement range is lower in contrast with the possible range of level variations and, consequently, a higher amplification and resolution of the EDR can be achieved. A 6 second time constant is considered long enough to accurately measure EDRs while maintaining a reasonably stable baseline [2]. This time constant plays a significant role in the evaluation of the rise and recovery times of the EDR. Experts refer that at least 3 seconds are recommended in case of exosomatic recordings, time constants over 6 seconds to avoid distortion of the EDR amplification and time constants of 15 seconds or higher for endosomatic recordings [58].

3.3 Measurement Devices

3.3.1 Endosomatic Measurement

As mentioned in a previous Chapter 2.6, endosomatic EDA measurement does not need an external voltage applied to the skin. As for recording sites, it is recommended to use an active site and an inactive site. Comparable interindividual and intraindividual skin potential recordings are better obtained if the corneum is extensively abraded, but this is no longer current practise since it represents an additional inconvenience for the subject and cannot be translated to an environment outside of the laboratory. In this type of measurement, an amplifier with a proper input impedance is required (i.e. $> 1M\Omega$), which most amplifiers currently provide. However, a problem may arise when conducting SP recording, especially when it is not possible to decrease the amplifier gain for SPL recording, which may require up

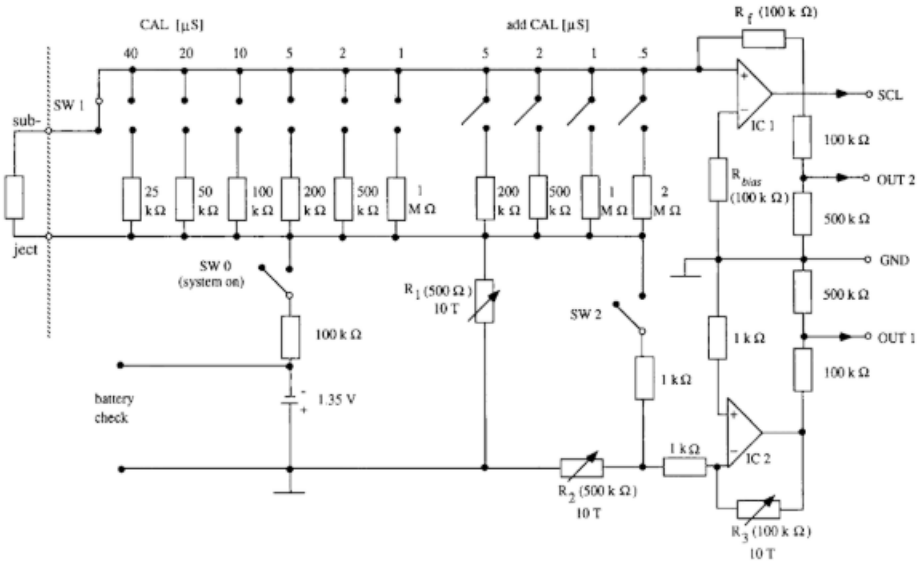

Figure 3.5: Active skin conductance coupler [2].

to 500mV/division.

Another thing that we must consider is using a backing-off circuit, because the SPRs are of smaller size compared to the overall SP signal; this can be implemented by adding the potential of equal value but with a contrary signal to the SPL, enabling the SPR to be amplified at a much higher gain. In case the SPL component does not need to be measured, we can resort to an AC-coupled amplifier with a high time constant to prevent distortion of the signal. Polarisation in AC-coupled amplifiers is non-existent, but due to the small bandwidth of around 0 to 3Hz, the signal is mutually superimposed by possible electrode drifts, expressing the importance of using bias potential free electrodes. The temperature may also influence SP recordings; temperature differences between the two recording sites can cause up to 2mV error and, additionally, an increase in the electrode temperature may cause errors of up to 450μV/°C.

3.3.2 DC Exosomatic Measurement

Exosomatic DC measurement of the EDA is the most frequently used method because of the trade-off between advantages and disadvantages, as well as the easier standardisation that appears with it. Since skin conductance is viewed as the appropriate unit for EDA, constant current recording fell out of use, but the properties that come from using such approach can be appropriate in some fields [58].

A circuit for a skin conductance coupler that enables DC recording of SCL and SCR with high resolution, using a constant voltage source, is presented in Figure 3.5.

This circuit is designed to be connected to a 1.35V mercury cell battery, having the ability to be calibrated using known loads via switch SW_1; it also includes a manually operated backing-off system via SW_2. The voltage applied to the subject should be no more than 0.8V across a single site. This is a recommendation by Eldelberg [59] since he observed that the voltage/current curves are linear below that threshold.

As for constant current recording, the current density should be limited to 10μA/cm^2 because, if exceeded, SRL and SRR decrease abruptly, and even sweat glands may suffer damage. To regulate the current density, one needs to know the contact area of the electrode and, since the shape is generally circular, the correlation between current and area is as follow:

$$I = 2\pi d^2 \tag{3.7}$$

where d will be the electrode diameter.

Since a constant current is needed, and it depends on the area of contact, attention must be given to it. On the other hand, when doing measurements with constant voltage, such restriction is no longer applied. So if measurements are performed with constant current, the size of the electrode area must be specified, in order to enable the correct calculation of the specific resistance and allow a comparison with other results. Nonetheless, there is still no consensus regarding this aspect, with some researchers claiming that the contact area is negligible [60].

3.3.3 AC Exosomatic Measurement

This measurement approach, unfortunately, is not very well studied, but some advantages of using it can be inferred from literature. Firstly Montagu and Coles [61] showed that the smallest amount of polarisation occurs at a 5Hz sampling rate but, if a high AC frequency were applied, the polarisation capacities of the skin would become too low. Overall, and based on previous research, an AC frequency between 5 and 100 Hz is recommended [62]. As such, AC exosomatic measurements have an excellent performance eliminating the effect of polarisation, and, therefore, can be used in alternative to a DC source, as long a rectification of the signal takes place.

A device for AC measurement of EDA described by Boucsein [2] is presented in Figure 3.6 and, as Salter [63] highlights, this method is standard in medical applications, in order to prevent nonlinearities that result from uncontrolled current densities when a sufficient constant voltage is enforced. Impedance and phase angle is obtained, and these values can be transformed into reactance and resistance or susceptance and conductance.

Figure 3.6 shows a block diagram of a phase voltmeter for AC measurement, where a sine wave voltage is generated by an oscillator with a frequency between 1Hz and 1kHz, and then converted by a voltage-to-current converter into a constant current, with peak value between 0 and 10μA, which is delivered to the subject. To obtain the phase angle and impedance values, the voltage from the skin site is pre-amplified and measured in two different ways.

To measure phase angle, the signal must be multiplied in a phase-sensitive detector with the oscillator signal that was phase-shifted, acting as a zero-offset for the phase signal. Finally, the output needs to be rectified and low-pass filtered with the same frequency limit as the impedance signal. As for the impedance, a voltage amplifier is used, with a sensitivity of 1mV to 10V in steps of decades; a rectified signal and low-pass filter with 0.1 or 1Hz frequency is applied, and after subtracting an offset we have the impedance. In this particular circuit [2], the two outputs are then digitised using two channels of a

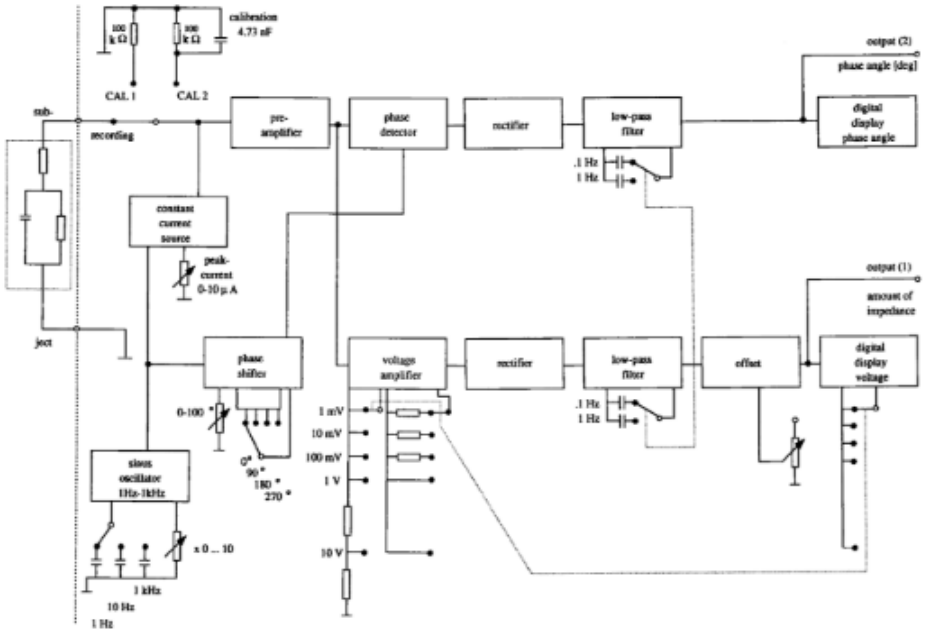

Figure 3.6: AC recording circuit example [2].

12 bit A/D converter with 16Hz, achieving a resolution of 0.1Ω/bit for the impedance, and 0.008^o/bit for phase angle. The ohmic resistance and the reactance at a specific frequency can be calculated from the impedance and phase angle at a specific angle.

Schaefer and Boucsein [64] recommended using the phase angle as a measurement for the EDR amplitude, which has the advantage of being independent of the method used, either using constant alternating voltage or constant alternating current, makes the EDR amplitude comparable without post-processing, and enables changes in phase angle to be treated equally as traditional phasic EDA measurements.

Pulsed DC may be considered as a sine wave AC recording and used as such, since, as Faber presents in [2], there is an intraindividual correlation of around r=0.93 between SCLs obtained with 10Hz sinusoidal signal and a pulsed DC, with a 10 millisecond pulse and an interval of 250 millisecond duration.

Although DC measurement is the recommended measurement technique, we should not disregard AC measurements since the latter present a few advantages over DC measurement. We should also mention that the previous recommendation to use DC has the objective of homogenizing all the measurements conducted in different studies, in an attempt to enable comparison between them and therefore increasing the amount of valid, transmittable, and comparable data that is of utmost importance for data analytics layers. It is important to highlight that does not mean that DC is better than AC and vice-versa, just that it is simpler than AC with the technology available. From studies such as [65], we can summarise the advantages and disadvantages of AC over DC recording. The most significant advantage of using AC is the fact that electrode polarisation is no longer a problem in this type of measurement, which is one of the concerns that we could experience during a DC measurement. AC measurements also en-

able the analysis of skin susceptance, which is related with the amount of current that goes through the membranes (that are considered to behave like capacitors). Therefore, AC can measure the contribution of the resistive as well as capacitive properties of the skin. Another significant factor is that with AC recordings, we can measure the endosomatic skin potential simultaneously with exosomatic measurement using the same pair of electrodes. On the safety imposed limitations, DC recordings are limited to 10μA/cm^2, while AC recordings can go as far as 100μA/cm^2. To conclude, in work done by Pabst and colleagues, their results showed that an AC circuit with 20 Hz has comparable results to DC measurement. DC methods raised the concern of a few experts in the field (e.g. Boucsein [2]), because the effects that DC stimulation may have on biological membrane are not sufficiently characterized. Overall, we can think of AC measurements as carrying more information than DC, since AC has into account the frequency-dependent part and the frequency-independent part, while DC measurements only have into account the frequency-independent part of the EDA.

3.4 Practical Considerations of Electrodermal Activity Measurement

3.4.1 Measurement Locations

Placement Considerations

The palms and the volar surfaces of the hand are commonly used as active sites for the electrodermal EDA measurement, since:

- Electrodes can be easily fixed and are less susceptible to disturbances caused by motion;
- Good size area;
- Usually, less scarring tissue is found;
- Palmar sites show good electrodermal activity.

The recommended sites are the medial phalanges of the index and middle fingers for bipolar recordings, as illustrated in Figure 3.7. However, recordings on the distal phalanges can yield comparable or better results.

Another good location to record electrodermal activity, are the thenar and hypothenar eminences. These sites are reported to even present a higher EDL and EDR amplitude than the fingers [59]. The non- dominant hand is preferred since it is less callous and less prone to motion (with the inherent artefacts), when compared to the dominant one.

The scalp area also reveals good signal quality but, unfortunately, in some cases it may, not be directly correlated with the EDA encountered at the palms as we will see in a later chapter.

The plantar sites, on the feet, are considered the second-best measurement locations, after the palmar sites, but since it is a location that is highly mobilized for walking, it may be inconvenient for the

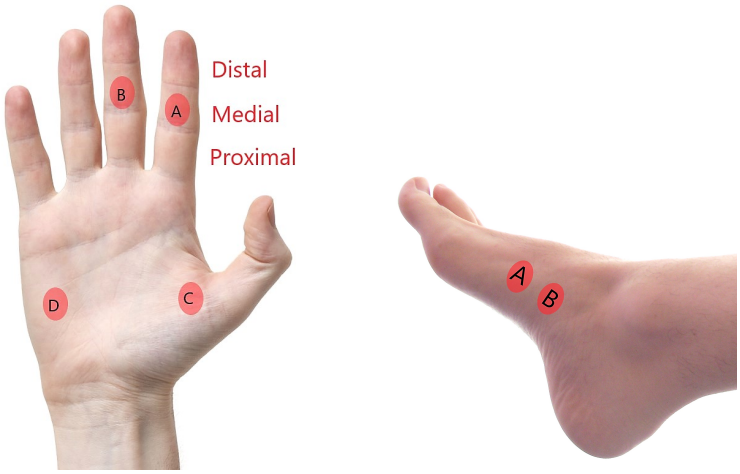

(a) Hand (b) Feet

Figure 3.7: Recommended EDA measurement locations [28]; the electrodes are placed between pairs A & B or C & D.

subject and it may be prone to pressure-induced artefacts by the user routine (as shown in Figure 3.7), nevertheless, it can provide higher amplitude EDRs in the foot area and comparable EDL as the plantar surface.

As previously mentioned, the use of an inactive electrode (needed for endosomatic recording), should be placed on a location that exhibits the smallest potential difference between the skin surface and the body core, ideally free of SPRs. A right place to attach the inactive electrode is on the volar surface of the forearm, approximately two-thirds of the distance from the wrist to the elbow, in case of measuring on the hand palms, and placed about 3 cm above the ankle if the recording is being done on the feet soles.

Generally, an electrodermal recording is performed using two electrodes, but there are exceptional cases where four electrodes are used [29]. Also, endosomatic measurement requires an active and an inactive site, while exosomatic recording uses two active sites. When placing electrodes on the skin, direct contact between the two electrodes must be avoided. According to [66] there are a other locations where it is possible to measure EDA, such as wrist, chest, forehead, abdomen and few more. Further information concerning the placement (e.g. optimal distance) can be found in [67].

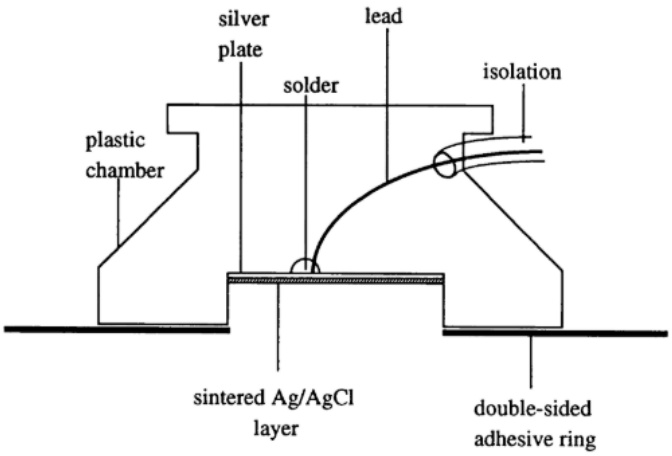

Figure 3.8: Cross-section of an Ag/AgCl electrode [2].

Pretreatment of Sites

It is known that the degree of hydration on the skin and electrolyte concentration affect the EDA. Moreover, the use of conductive paste to improve the interface with the skin , if allowed, will change the resistance over time as the paste dries. According to Bouscein [58], usually, there is no need for pretreatment of sites in case of exosomatic recording. If, for example, the skin is too oily and holding the electrodes in place becomes difficult as a result, cleaning the skin with alcohol is recommended. However, for endosomatic recordings, pretreatment for the inactive electrode must occur. Pretreatment encompasses the removal of the stratum corneum, without injuring the skin (otherwise another potential would appear), in order to diminish the potential difference between the site and the body core. If we do not pretreat the sites, reduced SPLs and SPR amplitudes will be obtained but, in contrast, unpleasant abrasion is not needed. If the subject is a child, no pretreatment is necessary, according to Venables and Christie [68].

3.4.2 Electrodes and Electrolytes

Electrode Types and their Attachment

The most commonly used EDA electrodes, are disc electrodes, with the electrode surface on the bottom of a cylindrical plastic chamber. They can use a conductive gel, containing the electrolyte, which acts as a media between the skin surface and the electrode.

As depicted in Figure 3.8, the electrode consists of a round silver plater about 6mm in diameter, on which a sintered silver/silver chloride (Ag/AgCl) layer is deposited. They are then attached to the skin by double-side adhesive collars providing a precisely defined area of contact between the skin and the electrolyte. Special attention must be given when applying the conductive paste, so that it does not gets between the adhesive collar and the skin. One method that minimises the problem caused by the conductive paste is using two adhesive collars; first attaching a single adhesive collar, and then attaching the electrode previously filled with conductive paste with the help of the other adhesive collar.

Nevertheless, this electrode fixed by means of an adhesive collar may detach quickly with heavy sweating. Using external support, like straps or adhesive around the electrode is discouraged because the pressure that they exert on the skin can affect the EDA, causing reduced EDR amplitude [59]. So, it is recommended that the electrode exerts the smallest pressure possible.

An alternative way to attach the electrode is using Histoacryl adhesive. First, an adhesive collar should be attached to the electrode, and then the electrode must be filled with conductive paste, without overflowing and afterwards fixed to the skin with the special glue. Collodium has a similar function as Histoacryl adhesive and can be applied in the same way. Acetone can be used to remove the electrodes. A more sturdy approach that can be used in more extreme environments is described in Boucsein [2] where they use Mastic Adhesive[2] to get a more durable electrode. In summary, full contact of the electrode to the skin and constant contact area must be ensured.

Choice or Assembling of Electrodes

The most common electrodes used for EDA are the sintered silver/silver chloride (Ag/AgCl), so-called reversible electrodes. They are made from metal in contact with a solution of Ag^+ ions that, overall, exhibit a minimal bias potential and are nonpolarizable to a high degree. There is an increasing number of studies [69] that analyse the potential use of e-textile electrodes with the EDA sensors. This type of electrodes has several advantages over the rigid Ag/AgCl, either dry or pre-gelled. In a study presented in Section 5.2, we conclude that there is a strong correlation between what is considered standard, the Ag/AgCl electrodes, and e-textiles materials, especially the conductive Lycra named "MedTex P130" by Statex. One of the advantages of e-textiles is their flexibility, which makes these type of electrodes adaptable to the shape of the skin and, in turn, can decrease artefacts induced by the variation of the contact area of the electrode with the skin.

Another factor is that they do not need any electrolyte media or adhesives, which can impose constraints in long-term recordings outside the laboratory environment and there is always a possibility of irritation caused by the electrolyte or the adhesive. They can also be reused several times before degrading and needing replacement, because they are lightweight, ductile and washable. Finally, they present advantageous breathability properties, which make them less prone to skin surface temperature variations and more suitable for long-term recordings when compared to non-breathable electrodes. The results described in [69, 70], confirm that indeed it is possible to use e-textiles to manufacture electrodes for EDA measurement; in these works, e-textiles electrodes appear to be the optimal material to detect EDR, with a Pearson correlation coefficient of 0.913 ± 0.041 comparatively with a measurement taken at the fingers. This kind of electrodes allied with, for example, flexible PCB technology, can reduce the volume of EDA sensors and their devices, while enabling a seamless integration of the sensors in a symbiosis form with more convenient form factor for human use, enabling the continuous monitoring of the sympathetic nervous system activity.

The contact surface area between the electrode and the skin should be around $1 cm^2$, in order to

[2] Also known as construction adhesive, it is a heavy-duty bonding agent that is extremely thick; additional information can be found at: http://www.usadhesive.com/mastics.aspx

reduce problems with possible seepage and linearity with the constant current method. However, most available commercial electrodes have a surface area of 0.6cm^2. There is some debate in this topic and further analysis must be done, as some studies have shown that that electrode/skin contact area has little effect [60], where others that experience with e-textile electrodes report the contrary [70]. As for maintenance of the electrodes, bias potentials and polarisation must be periodically checked (see Section 3.4.2) and, as long as they do not increase too much, the electrode will remain usable. As for e-textiles electrodes, one needs to regularly check the oxidation state of the electrodes (which can be caused by the sweating itself).

Electrolytes and Electrolyte Media

In the case of EDA signals, special care must be taken when choosing the type of electrolyte used. While other biosignals like EEG, ECG or EMG use hypertonic electrode gels, for the EDA it is not recommended because these gels have a higher conductivity than the epidermis, disturbing the measurements [58, 71]. During EDA measurement, disturbances to the electrolyte-skin system should be kept to the minimal.

A suitable type of conductive paste to be used in EDA measurement is one made of NaCl or/and KCl since these two appear as salts with monovalent ions in the stratum corneum. Between the two, NaCl is preferable, due to the fact that NaCl ions are predominant in sweat (NaCl concentration in sweat is around 0.015 to 0.06Mol depending on the amount of sweating). In light of this, studies show that a gel with a concentration of about 0.05Mol is suitable, and it is unlikely that sweat would infuse into the paste. Also, some studies recommend that a 0.05Mol NaCl paste is more suitable for exosomatic recordings and a 0.067Mol KCl for endosomatic EDA measurements [58, 68].

Tronstad in [72], experimented comparing four types of electrodes, with similar Ag/AgCl parts, but with distinct paste composition. Skin admittance was recorded using three electrodes in 18 participants (14 males); while at rest, two tasks were performed: a startling noise (breaking glass equivalent to 82 dB) and a thermal sweating elicitation task, in which the subject was asked to perform squats during two minutes. Depending on the water content and the viscosity of the paste, the author observed that the paste induced significant skin admittance level (SYL) changes over time. In the solid ones, SYL was able to recover better to the baseline 15 minutes after exercise. The author explained this phenomenon, arguing that the moister creams possibly penetrate the sweat glands. He also observed that SYL and SCL values were more affected than non-specific electrodermal response (NS.EDR) frequency. Baseline decay/adaptation can be expected at the initial phase of recording, so electrodes are recommended to be placed 15-20 minutes before the first measurement.

Bias Potentials and Polarization of Electrodes

There are two characteristics of the electrodes used in EDA measurement that require attention, these being:

- Electrodes with bias potential kept to a minimum;

- They should display, upon the passage of current, nearly no tendency toward polarisation.

The bias potential in this context is known as being the potential differences, deprived of voltage application, between two electrodes on the same environmental conditions. To measure it, the two electrodes filled with conductive paste must be joined together in full surface contact. Having a small bias potential is especially useful because it translates to a smaller drift over time and therefore reduces the number of times this needs to be checked in order to perform reliable measurements. Bias potential plays a significantly higher role in endosomatic recordings than in exosomatic. The reference bias potential for endosomatic measurements are under 1mV, and the electrode should be replaced when exhibiting a bias potential higher than 3mV. On the other hand, in exosomatic measurements, it is reasonable to have between 3 to 5mV potential difference across the electrodes.

As for the polarisation, it is more pronounced in exosomatic recordings, since when an external voltage is applied, a counter electromotive force appears in biological membranes and at the interface between the electrode and electrolyte. Polarisation is thought to influence SRL; to check for this phenomena, both in vitro and in vivo experiments can be done, as explained in [2]. Electrode polarisation effects are null in AC recordings.

3.4.3 Sources of Artifacts

Artefacts in this context, are unwanted signals that can be created by different sources, such as body movements, abnormal respiration, dialogue, mechanical interference on the skin-electrode interface, and ambient noise or unwanted stimuli, amongst others [58].

Electrical Artifacts

One of the most common artifacts encountered in biosignals, is the power line noise, which is a by-product from AC input power to the devices, or induced on the sensor by electromagnetic fields generated by powered devices operating in the vicinity. Shielding is one possible solution, but using a digital notch filter with a stopband between 50-60 Hz, depending on the country, can easily mitigate this kind of artifact.

Constant voltage recordings are more susceptible to noise, since they require more amplification than constant current and, since noise increases alongside amplification, this type of recording method is more prone to artefacts.

As for endosomatic recording and long-term recordings, drifts caused by bias potential may arise, therefore creating artefacts. These polarisation drift artefacts can be eliminated by changing the polarisation during recording.

Mechanical Artifacts

The most common types of artefacts are the ones caused by skin or muscle movements. Gross body motion should be avoided, especially on the limb in which electrodermal activity is being measured.

However, in ambulatory and long-term measurement use cases, it may be difficult to mitigate, therefore an computational methods to detect the artefacts should be deployed. Artefacts can result from merely stretching the skin or applying pressure, variation in skin blood flow or even electrodes wires being pulled.

Edelberg [59] highlights four primary sources of artefacts caused by movement. In general, the sources of artefacts can be characterised as follows:

- Disturbance of the electrolyte concentration due to degradation, evaporation or absorption of the conductive paste;
- Variations on the contact area between electrode and skin;
- Skin resistance changes caused by local pressure;
- The motion of the appendage across an electromagnetic field.

Burbank and Webster [73] studied the relation between skin stretching at the volar side of the forearm and elicited EDA artefacts. They concluded that skin potential continued to increase as the stretching increases. However, skin impedance measured with 10Hz AC did not show any change with the increased stretching.

Ödman [74] also studied the immediate consequence of a reduction of skin stretching in one individual, reaching the same conclusion as Burbank and Webster. These findings suggest that endosomatic recordings are more prone to stretching artefacts than exosomatic recordings.

It is worth mentioning that other factors may induce artefacts, such increased ambient and skin temperature, air humidity and special psychological and medical conditions (e.g. hypohidrosis and hyperhidrosis [75, 76]).

3.4.4 Ambulatory Monitoring of Electrodermal Activity

In ambulatory monitoring, the available storage space to record measurements, when available, the sampling rate and sampling resolution are correlated. As an example, sampling rates of around 20Hz are recommended for EDA [68], and if only the EDL data is to be stored, sampling rates as low as 1Hz can be enough. However, if phasic and tonic separation is needed, 4 to 8Hz is more appropriate. Another limiting factor for ambulatory monitoring, in particular for long-term recording, is the fact that problems with the conductive paste may arise and so, in some cases, dry electrodes would be preferrable preferred.

To address this issue, an experiment carried out by Poh, Swenson and Picard [46] was performed, in order to compare different kinds of electrodes, namely pre-gelled, dry or with conductive paste, attached to the volar side of the distal forearm and in palmar finger sites. This study had a base of 26 participants of both genders that were subjected to physical, cognitive and emotional tests consisting of a 10 minutes baseline, a 3 to 5 minutes task period and, finally, a 10 minute recovery period. Raw data was filtered using a low- pass filter with a cut-off frequency of 3 Hz and analysed. From these measurements, both recording devices from standard palmar sites revealed adequate correspondences. The

non-conventional electrode materials exhibit lower SCLs than other recording methods in 80% of the participants during the emotional and cognitive task, but recorded the highest SCLs towards the end of the physical test and during the recovery period in 46% of participants. A long-term measurement was also done in a 19-year-old male participant; an interesting finding was the existence of a consistent peak in the EDL component between midnight and 3 AM, supposedly during sleep. No SCL drift was recorded, and the measurements were relatively free of artefacts. However, when dry electrodes were used, instabilities had to be accountable for an unknown amount of time after their attachment.

Another experiment was conducted by Doberenz et al. [77], with a duration of 24 hours in 48 participants (32 females and 16 males), to study the influence of physical activity, ambient temperature, and corneal hydration. The experiment showed that all SC parameters yield higher values during physical activity when compared to sleep; temperature variations had little effect, but corneal hydration had a more pronounced result and had to be taken into account in long term measurement. Electrode sensitivity decreased by an average of 20% with the course of the experiment, as a result of corneal hydration.

The use of dry electrodes seems more convenient when performing ambulatory recordings or even long-term recordings, but further research is fundamental to better assess this method, as well as the possibility of using non-conventional electrode materials.

Chapter 4

Proposed System

The proposed system is an evolution of the original EDA sensor design for BITalino [31, 78]. Table 4.1 presents the main characteristics of this sensor and Figure 4.1 presents the two stages that compose it. The first stage is an operational transconductance amplifier, which fundamentally works with a differential input voltage, with electrodes attached to the subject skin on the negative feedback loop, producing an output current. The second stage is a low-pass second order Sallen-key filter with a cutoff frequency of 5 Hz and a gain of two. The main purpose is to attenuate noise above the 5 Hz, especially the power line noise.

The output at the first stage is given by Equation 4.1. The resistor value R_{23} imposes a limit to the maximum skin resistance value that this stage can sense without saturating, which in turn means that this sensor only can detect skin conductance levels of 1μS and above and not the entire skin resistance spectrum. It uses the AD8692 amplifier from Analog Devices, which operates on 3.3V single-supply (V_{cc}) and with differential inputs that have connected to the positive input V_{ref} =1.65V, affecting the amount of DC current that flows through the electrodes, Equation 4.3.

$$V_{out} = -\frac{R_{skin}}{R_{23}} \times V_{cc} + \frac{R_{23} + R_{skin}}{R_{23}} \tag{4.1}$$

The second stage applies a low-pass filter to the first stage output, eliminating noise present above the EDA frequency spectrum, and amplifying the denoised signal by a factor of 2. The output of the first stage fluctuates according to the skin resistance between 0V and 1.65V in a linear fashion, with the gain

Table 4.1: BITalino EDA sensor characteristics.

Characteristic	Value
Gain	2
Range	0-1MOhm
Bandwidth	0-3Hz
Consumption	2mA
Electrodes	2

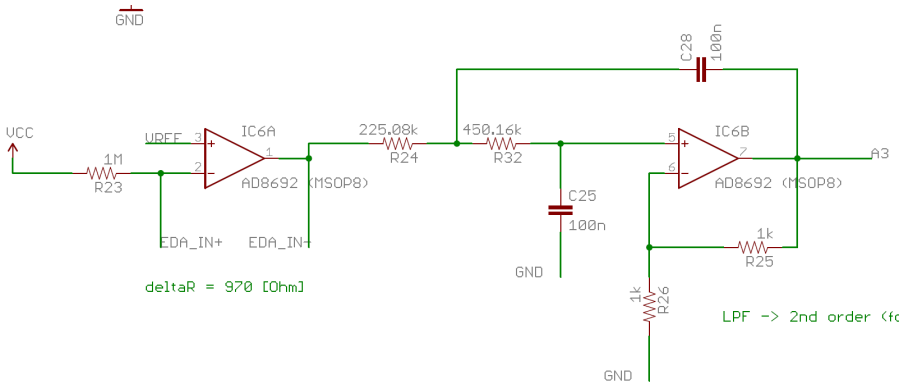

Figure 4.1: Schematics of the BITalino EDA sensor.

provided by the latter stage, the circuit manages to use the full dynamic range of the ADC. Equation 4.2 provides the output at the second stage.

$$V_{out} = (-\frac{R_{skin}}{R_{23}} \times V_{cc} + \frac{R_{23} + R_{skin}}{R_{23}} \times V_{ref}) \times (1 + \frac{R_{25}}{R_{26}}) \tag{4.2}$$

$$I_{skin} = (\frac{V_{cc} - V_{ref}}{R_{23}}) \tag{4.3}$$

This particular sensor provides an analog output, but it is generally used with a 10-bit ADC, supplied by a single supply 3.3V; when using the BITalino MCU, a total of six channels are available, with four of the channels streamed with 10-bit resolution and the remaining two with only 6-bit. According to Equation 4.4, it detects variations at the output of the EDA sensor equal or higher than 3.2mV, meaning that the resolution (Equation 4.5), either in conductance or resistance units, 1.03mS and 970Ω, respectively.

$$\Delta_v = \frac{V_{cc}}{2^{bits} - 1} = \frac{3.3V}{2^{10} - 1} \tag{4.4}$$

$$\Delta_G = G \times \frac{I_{skin}}{\Delta_v} \longrightarrow \Delta_R = (\Delta_g)^{-1} \tag{4.5}$$

4.1 Circuit Limitations

Although the average skin resistance in the general population ranges between 100kΩ and 1MΩ, there are still cases outside these assumptions. The recommended sites for sensing EDA are limited to the hand palm area and the foot area, since they present a higher density of sweat glands per cm^2, but these locations significantly reduce the freedom of movement of measured subjects, and constitute a constraint for the application to wearable devices that might otherwise integrate EDA sensors. A reason for the restricted number of recommended sites is attributed to properties of the skin and, characteristics of the sympathetic nervous system on those areas, and also to the higher density of sweat glands.

In the particular case of the BITalino EDA sensor, it is limited to skin resistance no higher than 1MΩ, in part because of the ADC used, which needs to have enough sensitivity to distinguish inter- and intra-

subject variability of the two components present in the EDA signal. This is the major challenge when designing an EDA sensor capable of being used in different body locations. It needs to detect a large range of the tonic component while still ensuring that it can detect the very small variations caused by the EDR.

In summary, the two main issues present with the previous configuration pinpoint to the limit ADC sensitivity that is not high enough to distinguish small variations, especially with high skin resistance and the maximum skin resistance that the sensor can measure. In Section 5.1, this limitation is experimentally characterized by means of real-world data, which demonstrates that in a number of subjects the EDA signal is either close to zero or saturated at full scale.

The following section presents a set of proposed solutions to mitigate these limitations.

4.2 Modified Circuit

4.2.1 Addressing the ADC Resolution Limitation

Although one can argue that to solve the limitations caused by the different behaviours of the tonic and phasic components, it would simply be necessary to increase the number of bits on the ADC, this has an impact on the complexity and cost of the final system. As such, one of the requirements that we proposed to consider, was to work with the internal ADC of the BITalino MCU. Additionally, this line of though also enables the new EDA sensor design to work with the less expensive ADCs found in other DiY platforms (e.g. the Arduino).

To address the ADC limitation, one desired feature if for the new sensor to have the ability to adapt to the target skin resistance. Decreasing the overall range of the skin resistance values that the sensor can measure would increase the sensitivity of the ADC since, according to Equation 4.5, we would have the dynamic range of the ADC (3.3V) spread along a much lower skin resistance range, meaning smaller μS per ADC step.

The proposed solution uses a N-MOSFET, namely the Nexperia PMV16XN, operating in the triode region, which means that it behaves like a voltage-controlled resistor. Figure 4.2 presents the three regions of operation that one can identify. When the applied voltage between gate and source (V_{GS}) is not enough to overcome the threshold voltage (V_{th}), the N-MOSFET is said to be in the cutoff region, where little to no current flows from the drain to the source. To be in the saturation region, two conditions must be met. First, the voltage from gate to source must be higher than the V_{th}, to induce a channel between the gate and source. Secondly, the voltage drain to source (V_{DS}) must be higher or equal than V_{GS} - V_{th}. In this region, I_d is modelled according to Equation 4.6 (k_n, W, and L are fabrication parameters of the N-MOSFET as established by the manufacturer), where V_{OV} is the overdrive voltage, which can be defined as V_{GS} - V_{th}. With an increase of V_{OV}, I_d will be higher, and vice-versa, and that is why in this region, the N-MOSFET is considered to behave as a voltage-controlled current source. Lastly, is the triode region (sometimes refered to as linear region), which is the region in which our N-MOSFET operates. To be in this region, V_{GS} must also overcome V_{th}, but now, V_{DS} must be lower than V_{OV}. In

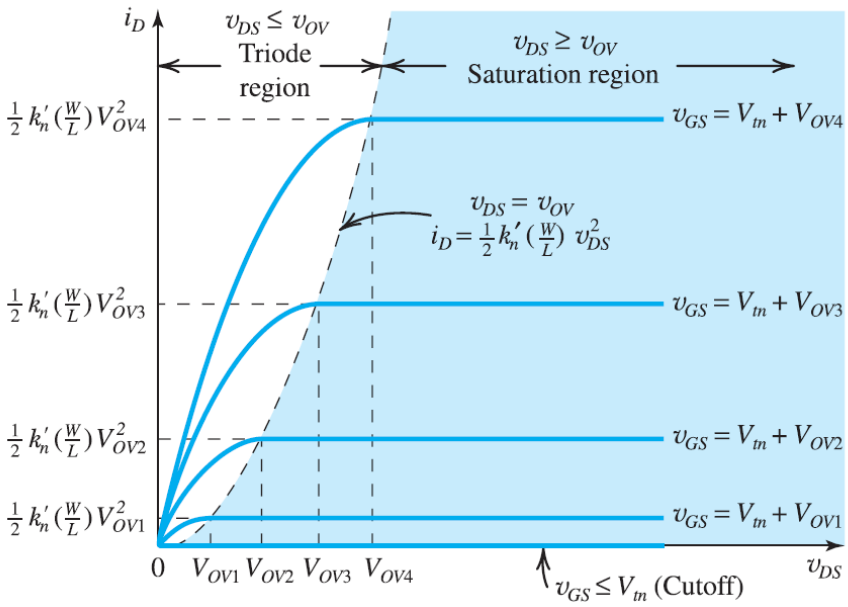

Figure 4.2: N-MOSFET operation regions [79].

the triode region, the N-MOSFET behaves as a voltage-controlled resistor where the slope between I_d and V_{DS}, Figure 4.2 triode region, gives us the inverse equivalent resistance of the N-MOSFET. I_d is then modeled by Equation 4.7.

$$I_D = \frac{1}{2}k_n\frac{W}{L}V_{OV}^2 \tag{4.6}$$

$$I_D = k_n\frac{W}{L}(V_{OV} - \frac{1}{2}V_{DS})V_{DS} \tag{4.7}$$

The proposed evolution of the base circuit is presented in Figure 4.3. Replacing the fixed resistor R_{23} by the N-MOSFET is the equivalent to implementing a voltage controlled potentiometer. This way, the system is no longer restrained to skin resistances lower than 1MΩ, and can now measure all skin resistance values provided that a correct control of the N-MOSFET gate voltage is performed. To control it, we take full advantage of the functionalities already available in BITalino (and analogous platforms). Namely, a software-controlled Pulse Width Modulation (PWM) signal can be generated by the MCU and used as input to an 8-bit Digital to Analog Converter (DAC) providing a 0-3.3V analog output. The output of the DAC is then connected to the N-MOSFET gate, controlling it. Being an 8-bit DAC, it means that the system has a finite resolution; Equation 4.8 shows the smallest possible step that the DAC can discriminate according to the provided input PWM wave. Figure 4.4 presents the relationship between the applied gate voltage and the current flowing at the drain. The red dots represent the points where the N-MOSFET has an equivalent resistance of 20MΩ, 10MΩ, 5MΩ, 1MΩ, 500kΩ, and 300kΩ, modelled according to Equation 4.9. As it can be seen, the current that flows through the skin, if the electrodes contact area is of $1cm^2$, does not exceed the maximum recommended current of 10μS/cm^2 allowed for DC techniques [58], ensuring that the sweat glands are not damaged. This is achieved thanks to the

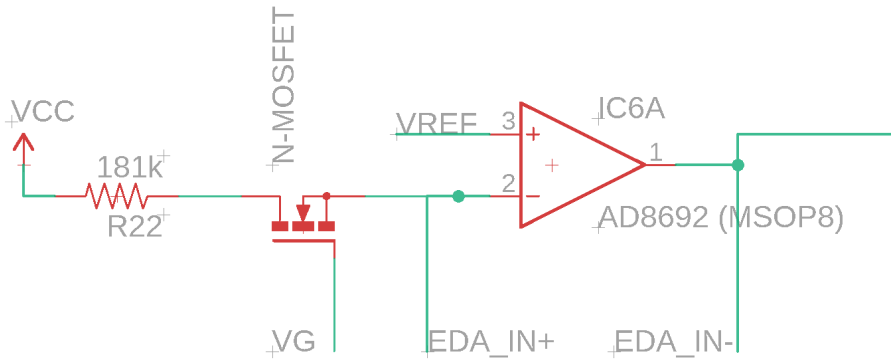

Figure 4.3: Proposed circuit for EDA measurement.

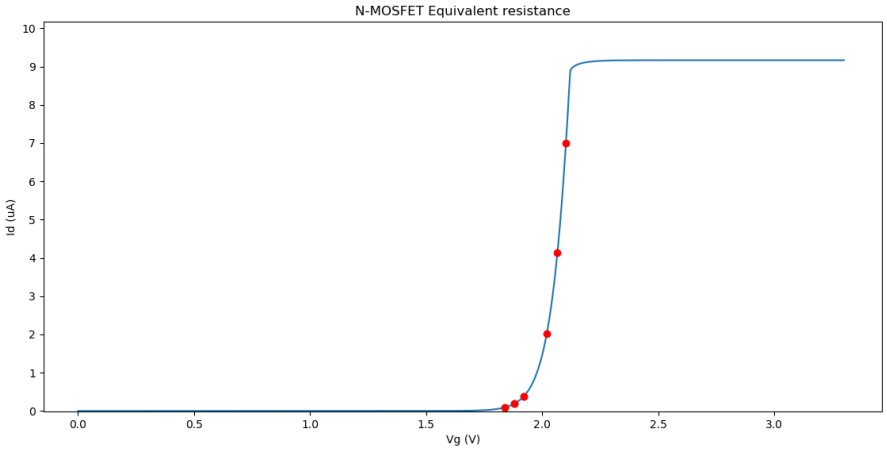

Figure 4.4: Relationship between V_g and I_d.

181kΩ resistor that is in series with the N-MOSFET.

$$\Delta_V = \frac{3.3}{2^8 - 1} = 12.9mV \tag{4.8}$$

$$MOSFETresistance = \frac{V_{REF}}{I_d} \tag{4.9}$$

With this implementation, the circuit now has an adaptive gain; depending on the situation, it can reduce is dynamic range from 1MΩ downwards, or it can increase it above the 1MΩ limit. According to Equation 4.10, we can conclude that if we reduce the measuring scale, the ADC sensibility goes up, meaning that we can detect smaller EDR events; on the other hand, if we increase it, the ADC sensitivity decreases, which means that the system would be less capable of detecting variations, especially those of EDR, imposing an additional limitation.

4.2.2 Addressing High Skin Resistance with High-Pass Filter

One possible way to get around the fact that with an increase of the N-MOSFET equivalent resistance value, the ADC sensitivity decreases, would be to also dynamically modify the gain of the second stage

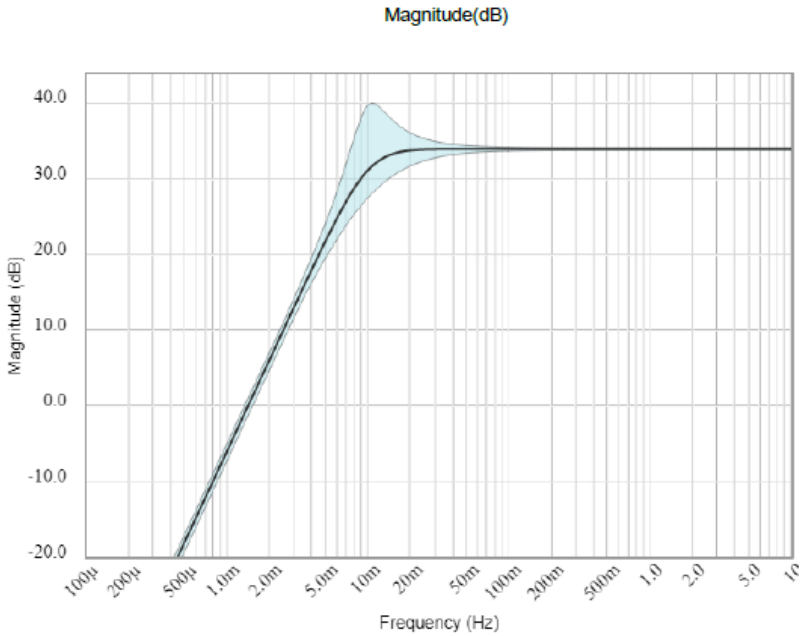

Figure 4.5: Frequency response of the high-pass filter.

(low-pass filter), but due to the low-pass configuration, which has capacitors on the positive feedback loop and connected to the ground, to change the gain while maintaining the desired frequency response, the capacitors would also need to change dynamically. Therefore, the proposed system applies a similar method as the one found in [5] to solve this limitation. A 2^{nd} order Sallen-key high-pass filter is implemented at the output of the previously known 2^{nd} stage, with a cutoff frequency of 10mHz and a stop-band frequency of 1mHz, Figure 4.5. Knowing the typical EDA frequency response (depicted in Figure 4.6), it is possible to implement the high-pass filter to separate the two components, leaving only the phasic one. Figure 4.7 presents the implemented circuitry with a gain of 34 dB, while Figure 4.8 presents the overall circuit implemented. Since the EDR are of much lower amplitude than EDL, separating the components allows to individually apply different gains. Although the high-pass filter system section does not have adaptive gain, contrary to the low-pass configuration, it can be easily modified since it only depends on resistors.

$$\Delta_r = \frac{R_{23}}{2^{10} - 1}\Omega \tag{4.10}$$

4.2.3 Proposed Configuration

As previously explained, the sensor in Figure 4.8 uses the BITalino MCU peripherals to control the N-MOSFET (R_{23}) according to software-controlled inputs. Three MCU input channels are used to acquire data from the sensor, one at the output of the low-pass filter (A3), which acquires the EDA waveform composed by both components, another MCU input acquires the output of the high-pass filter, which extracts the EDR data present in the EDA signal, and finally the applied gate voltage is monitored on the third input. The control logic consists firstly on reading the channel connected to the A3 node and, if

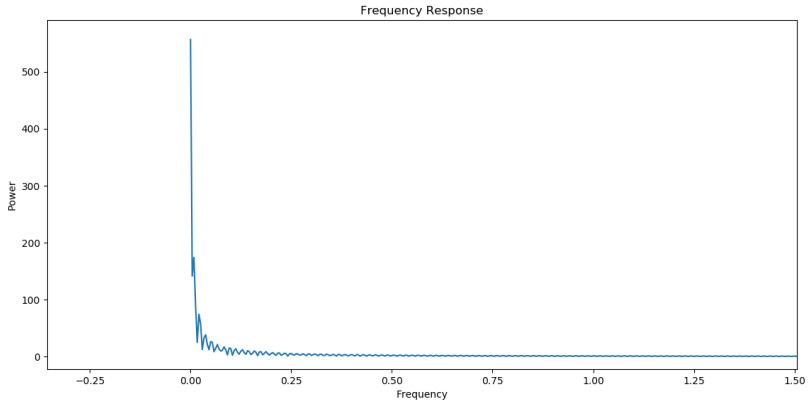

Figure 4.6: Frequency response of a representative EDA signal.

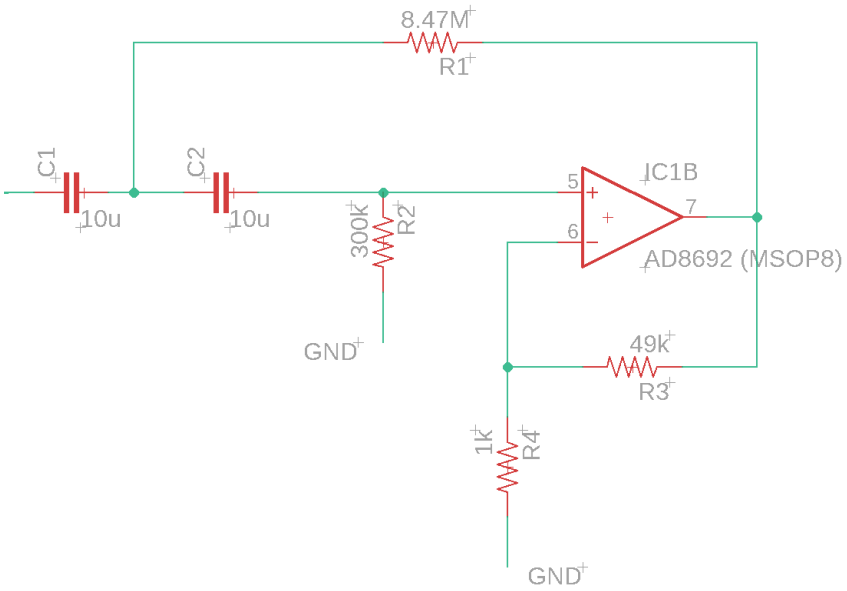

Figure 4.7: Second order high-pass Sallen Key filter with a cutoff frequency of 10mHz.

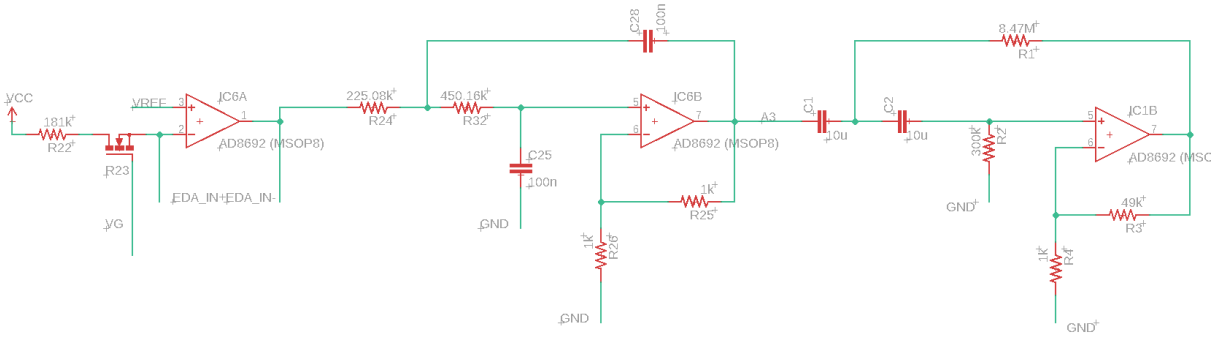

Figure 4.8: Overallproposed circuit with the N-MOSFET and high-pass filter.

the mean of the last 350 values is below a defined threshold (50 in ADC units, 0-1023), the PWM level will be decreased. On the other hand, if the mean value is higher than a defined threshold (950 in ADC units, 0-1023), the PWM level will be increased. This ensures that in both situations, saturation will be less likely.

The current sensitivity of the sensor varies with the gain of the sensor. When the equivalent N-MOSFET resistance is very high, it means that the sensitivity offered by the 10-bit ADC will still not be enough. According to Equation 4.10, if R_{23} has an equivalent resistance value of 5MΩ, each value of the ADC will represent a step of 4.9kΩ, which means that small EDR events cannot be detected; this effect continues to worsen as we increase the N-MOSFET equivalent resistance. This is one of the reasons for introducing the high-pass filter right after the low-pass filter. The high-pass filter will isolate those frequencies that carry EDR information, which represent a small amplitudes in comparison to the EDL, and applies a gain of 34 dB so that the EDR is noticeable.

Finally, the PWM level (N-MOSFET gate voltage) at any given stage is recorded so that the user can calculate the N-MOSFET equivalent resistance value (Equation 4.9), throughout the measurement session, and afterwards, apply the correct transfer function to convert the raw units to conductance units.

4.2.4 N-MOSFET Behaviour

The use of the N-MOSFET in the triode region to simulate the behaviour of a potentiomenter can be challenging at times, especially when using a PWM signal that is filtered through the use of a DAC.

When changing the gate voltage of the N-MOSFET, there is lag between the input and the output (e.g. V_D to V_S). This is important to consider when applying the transfer function, because what it is seen by the MCU input connected to the gate of the N-MOSFET will not correspond to the actual output of the N-MOSFET during a particular time frame. Simulating the real conditions that this sensor will encounter, we fed the N-MOSFET gate with a PWM level, made it oscillate following a square wave pattern, and monitored the input and output of the N-MOSFET. Figure 4.9 shows a mean delay of 9.393ms delay between input and output. According to Figure 4.10, the rise and fall time of the input was of 44ms and 47ms, respectively. Additionally it was possible to see that the N-MOSFET or the DAC have some variation at a particular level when a resistance of 1MΩ and 100kΩ are used to simulate a skin resistance (Figure 4.11).

We could calculate the individual equivalent resistance value of N-MOSFET at a particular level of PWM, but since the transition from one level to the other is not ideal, it is difficult to predict the equivalent resistance during the transition period from level to level.This further reinforces the importance of continuously monitoring the input gate voltage and taking into account the offset introduced by the delay between the input and output of the N-MOSFET.

4.2.5 Calibration Procedure and Dynamic Transfer Function

In order to calculate the correct equivalent N-MOSFET resistance, the circuit has implemented an additional segment on the first stage comprised of two resistances of 1MΩ and 100kΩ with 1% tolerance

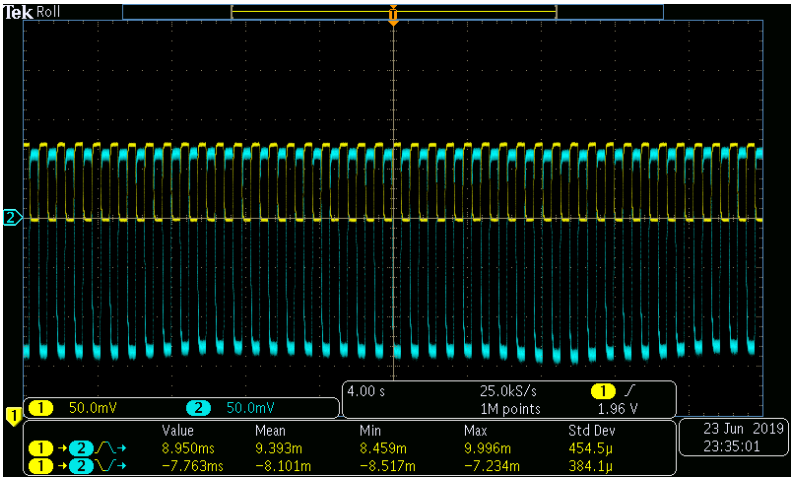

Figure 4.9: N-MOSFET response time.

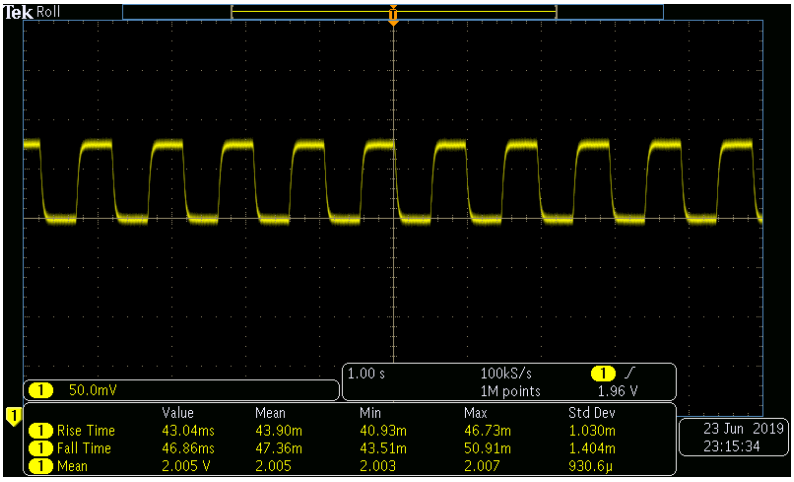

Figure 4.10: Characterization of the N-MOSFET output rise and fall times.

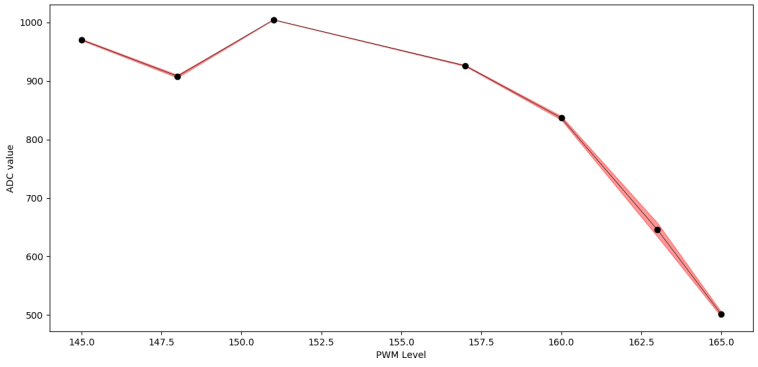

Figure 4.11: Circuit variation at different PWM levels.

and a dual 4-channel analog multiplexer/demultiplexer HEF4052B from NXP. The circuit uses the two digital outputs present in the BITalino acquisition board to select the input to output of the demultiplexer, which, according to Figure 4.3, has as inputs the EDA_IN-, a 100kΩ resistor in parallel between EDA_IN- and EDA_IN+, and another resistor of 1MΩ in parallel to the other 100kΩ resistor. The HEF4052B then connects only one resistor at the time to the second stage of the circuit, which, according to the selected combination of the HEF4052B, will allow a current flow across the electrodes either through the 100kΩ or through the 1MΩ resistor.

The calibration procedure involves calculating the equivalent resistance, R_{23}; rearranging Equation 4.2 and knowing the resistance value, we are left with :

$$R_{23} = \frac{R_{skin} - V_{ref}}{\frac{V_{out} \times V_{cc}}{(2^{ADCbits} - 1) \times Gain} - V_{ref}} \tag{4.11}$$

Simulating R_{skin} with resistances enables the calculation of R_{23} at a particular PWM level. The proposed circuit implements a very simple logic at the beginning of an acquisition; it first measures the skin resistance level of the user and then changes the current flow from the electrodes to the suitable resistance. If the target skin has a skin resistance higher than 1MΩ, the selection controls change the current flow so that the 1MΩ resistor is used; it then cycles through PWM levels around the target skin resistance and records the R_{23}, so the system later knows the corresponding R_{23} for a particular PWM level. The same procedure is used when the skin resistance is lower than 1MΩ. This process can be long since, as shown in Section 4.2.4, the N-MOSFET does not shift immediately and therefore the system has to wait for stabilization between changes of PWM levels applied to the gate N-MOSFET. To save time, we reduced the calibration procedure to take only 3 to 4 seconds, and measuring the R_{23} at reference points close to the user skin resistance, extrapolating the values in-between. After the calibration procedure the measurement of the subject EDA can start.

Chapter 5

Methodology and Results

In this section we present the main experimental results obtained for the different components of the work. Firstly, an experiment was conducted to verify the limitations reported in the literature related with EDA measurements, including a comparison between two recommended locations to obtain electrodermal activity. Secondly, we explore the use of non-conventional electrode materials and the possibility of extracting electrodermal activity from the forehead area. Thirdly, we present an experimental evaluation of the EDA signal performance in a dataset provided by BrainAnswer[1], consisting of a cognitive task, to provide evidence that the current BITalino EDA sensor may saturate in some cases. Finally, we present the results obtained with the proposed sensor circuit, to evaluate how the previously mentioned limitations are addressed. In all the experiments, the BITalino electrodermal activity sensor and MCU were used either directly or as the base for the proposed circuit.

5.1 Exploratory Study

The goal of this first experiment was to become familiar with the process of recording EDA, and to assess the difficulties that may appear if the EDA is recorded in a location that is more seamless for the user in comparison to the locations that are recommended in literature.

Data was collected from 4 volunteers, being two of the participants young adults with 20 and 27 years old (female and male) and the other two were adults with 57 and 59 years. Two sensors were used in turn, and the chosen locations for electrode placement were the medial phalanx, as the standard measurement, and the wrist volar side, on the non-dominant hand. The wrist area is of particular interest since it is a common area where wearables are used (e.g. smartwatch and fitness trackers) and, if we think in an office environment, can be used in the SNS assessment, incorporating an EDA sensor, for example, in a keyboard armrest. As for the electrodes used, they were pre-gelled polymer Ag/AgCl coated provided by Covidien [80].

The experiment consisted of 3 minutes baseline, where the participants were asked to remain still and not to talk; afterwards, the participants were asked to bite their tongue for 10 seconds following by

[1] http://brainanswer.pt/

Table 5.1: Summary of the exploratory study, expressed in μS.

Location	Mean	Median	Variance	Std. Deviation	Range	Max	Min	#Fullscale	#Zero
Medial Phalanx	3.195	3.380	0.573	0.528	1.746	4.114	2.368	0.000	0.000
Wrist Volar Side	0.369	0.358	0.004	0.049	0.241	0.511	0.270	0.000	3.000

a recovery period of 2 minutes.

5.1.1 Exploratory Study Results

Tables A.1 and A.2 presented in Appendix A show the results obtained from this experiment, and Table 5.1 presents an overview of the main results. The following metrics of the signal are presented: mean, median, variance, standard deviation, range, maximum, minimum, the number of signals with full-scale saturation or lack of response. Analysing Table 5.1, measurements done in the medial phalanx location presents no saturation or lack of response signals. The mean and median is approximately 3μS and the range, which in this context is the difference between the minimum and maximum value of a signal, is 1.75μS. The variance and standard deviation of the signals is approximately 0.57 and 0.53μS, respectively.

As for the results obtained in the wrist volar side location, no saturation is present, but this time there is a significant percentage of the signal with lack of response. From a pool of three recordings showing lack of response, two were 100% of the time at zero, and the other was at zero 28% of the time. The two signals that display constant lack of response are the ones acquired from the two adults, which is in agreement with the fact that skin dries and deteriorate along the years, therefore increasing skin impedance. Also, the young female adult presented lack of response moments, while the young male adult did not.

5.2 Non-Conventional Conductive Materials

With the increasing proliferation of physiological monitoring systems and new conductive materials, it is of utmost importance to study how this kind of novel materials perform in real-world conditions. In this experiment, the goal was to assess the performance of different electrodes with a known range of resistance values, in order to simulate the possible range of skin resistance. A performance comparison between e-textile electrodes, made of conductive leather and lycra, 3D printed electrodes and standard electrodes was performed. The breathability properties of e-textile electrodes make them less prone to skin surface temperature variations and more suitable for long-term recordings when compared to non-breathable electrodes [69]. The 3D printed electrodes are a low-cost and flexible form that can be easily customised to best suit the subject. To perform the assessment, a range of known resistors (50kΩ-3MΩ) was used between two electrodes. In order to ensure the same conditions across measurements, one lead electrode cable was soldered to each extremity of the resistors and fixed to a breadboard. Using the exosomatic constant current method to acquire EDA signal, a total of 10 measurements were done

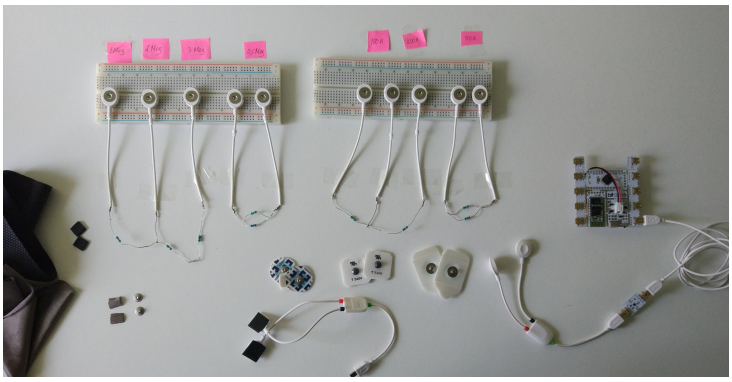

Figure 5.1: Experimental setup with the non-conventional electrode materials.

with each resistance and each electrode material to analyze the variability.

In this experiment, the goal was to assess the performance of different electrodes with a commonly used one (dry electrodes from Thought Technology). The chosen location for electrodes placement was the ring and index fingers; since two different EDA sensors were used, different setups of electrodes placements on the above locations were also study. To conclude our experiment, we compare the performance of the non-conventional electrodes with the standard ones, , as expressed by the Pearson correlation coefficient (p-coeff) as well as the Root Mean Square Error (RMSE). The two sensors were connected to independent systems and synchronised by means of optical synchronisation. Finally, with each setup, a cognitive test composed of a Stroop word-colour test and execution of Valsalva manoeuvre was conducted.

5.2.1 Materials

Figure 5.1 present the materials used in this experiment, which can be detailed as follows:

- 1x EDA sensor from BITalino (r)evolution (0-25 us)
- 1x 3MOhm, 2MOhm, 1MOhm, 0.5MOhm, 200kOhm, 100kOhm and 50kOhm resistor
- 2x Dry Ag/AgCl Thought Technology electrode
- 2x 1cm^2 conductive lycra (MedTex P-130)
- 2x 1cm^2 conductive leather (1 side conductive)
- 2x 1cm^2 3D printed dry electrode (PLA)

5.2.2 Non-Conventional Conductive Materials Results

After the creation of the prototype electrodes, and in order to correctly assess their performance, the resistance of each evaluated material was recorded several times (n=10) using a multimeter on a diagonal and horizontal direction while the material was laying flat, stretched or contracted. The conductive Lycra scored a mean resistivity of 4,2Ω/square, while the conductive leather and 3D printed electrodes present

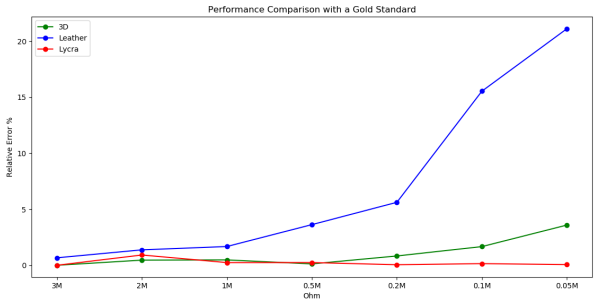

Figure 5.2: Relative error of the non-conventional electrodes comparatively to a gold standard.

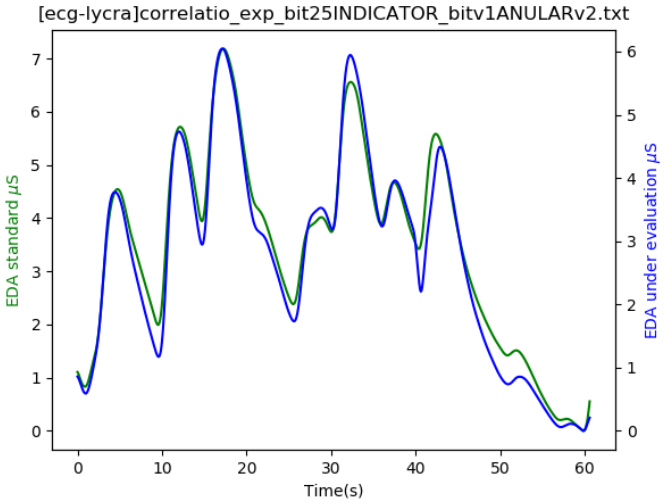

Figure 5.3: EDA recorded with Lycra material.

a resistivity value around 3.4kΩ/square. Figure 5.2 presents the relative error of the non-conventional conductive materials comparatively to a gold standard. The Lycra material (MedTex P130) scored the best, with a relative error below the 1% mark. The 3D printed electrodes come second, with an excellent performance until the resistance is 500kΩ and below. The leather material shows an increasingly worsen performance.

Figures 5.3 and 5.4 present the results obtained for an individual. Although this experiment only counts with one participant, it reveals that the conductive lycra obtained a Pearson correlation coefficient value of 0.798 with a standard deviation of 0.097 and a root mean square error of 0.909 with a standard deviation of 0.124, outperforming the other three materials, the Though Technology dry electrodes have shown a correlation value of 0.665 with standard deviation of 0.303 and a RMSE of 4.074 with standard deviation of 0.212, the conductive leather with a correlation value of 0.465 with standard deviation of 0.130 and a RMSE of 5.001 with standard deviation of 0.533, and the 3D printed electrodes, have shown promising results in previous work, but this time did not perform well in a real environment situation not enabling EDA recording. The potential cause can be a constraint imposed by the experience methodology because it was not long enough to check if there was any EDA when in the presence of build-up of sweat under the electrode and consequently a decrease in the skin resistance.

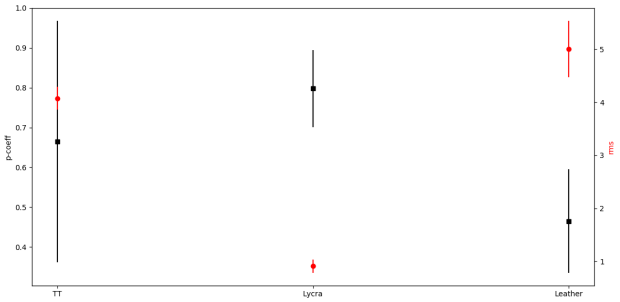

Figure 5.4: Pearson and RMSE values for the non-conventional electrode materials.

(a) Fingers placement

(b) Forehead placement

Figure 5.5: EDA sensors attached to the fingers and forehead.

5.3 Forehead EDA Measurement

In an effort two study the potential integration of EDA sensors in head mounted devices and the hypothesis of having EDA sensors working in symbiosis with technologies such as augmented and virtual reality, we evaluated the potential application of an EDA sensor on the forehead. Empirically the sweat occurring at this location is typically associated with thermoregulation phenomena, nevertheless, and having in mind the results obtained in [66], we tested EDA measurement on the forehead. Data was collected from two participants, both male, with one sensor placed on the index and ring fingers, and a second sensor placed on the forehead, centred with 5 cm approximately of inter-electrode spacing (Figure 5.5). Pre-gelled self-adhesive Ag/AgCl electrodes were used with both sensors. In order to guarantee electrical isolation between both sensors, two separate acquisition units were used (one for each sensor), and synchronisation was performed optically employing a LED turned on/off on one of the units and a light sensor (LUX) on the other. In post-processing, the time series were aligned by detecting the onset on the LED trigger channel and on the LUX sensor output, removing afterwards the period until those points in each of the recorded files.

Given that the LUX sensor only changes its output when the LED is turned on, and that both signals are synchronously acquired with the EDA data channels, this procedure guarantees that the data is synchronised. For better visual observation, in post-processing, EDA signals were low-pass filtered and normalised in amplitude. To promote phasic changes in the signal, the experimental protocol involved the Valsalva manoeuvre in some of the experiments and having one subject with closed eyes and exposed to unexpected stimuli (i.e. clapping the hand once).

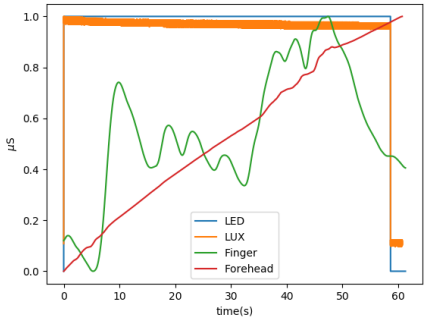

(a) Older Subject.

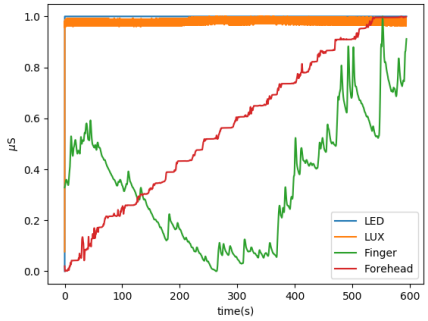

(b) Older Subject 2^{nd} attempt.

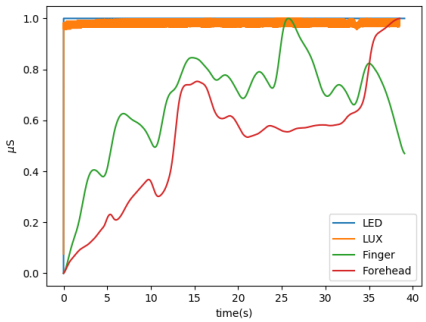

(c) Younger Subject

Figure 5.6: Preliminary evaluation of the possibility of recording EDA on the forehead.

5.3.1 EDA Forehead Results

From the performed tests, the experimental sensor on the forehead does not seem to present phasic changes in agreement with the standard location sensor application within the older subject, Figure 5.6. However, the data acquired in the younger subject shows more convincing results, with phasic changes that follow the trends identified in the measurements performed with the sensor applied in the standard location. The size of the sample extracted from this experiment is too small to find any firm conclusion regarding the fact that we were able to record a signal that was in agreement with the gold standard in the younger subject than that of the older one. Nevertheless, this experiment says that it may be possible to record EDA on the forehead, which in turn if further validated, can mean the integration of EDA sensors on head mounted devices, enabling the seamless measurement of the SNS.

5.4 Standard Sensor Characterization

To characterize the performance of the standard sensor, we analyzed a real world dataset collected by neuroscience company BrainAnswer, containing, amongst other modalities, EDA data collected from 99 participants during a cognitive elicitation experiment. The objective of this experiment was to address the need for an EDA sensor with adaptive gain. From the 99 recordings, we quantify the signal, extracting temporal metrics (e.g. mean value, max value, range, and others), in order to empirically characterize the performance of the sensors, namely by evaluating how many subjects exhibit full scale saturation,

lack of response (e.g. due to high skin impedance), among other factors.

The chosen locations were the distal phalanx, and the electrodes were the same pre-gelled polymer Ag/AgCl coated [80], but this time, applied with tape. It consisted of a cognitive task, with an initial baseline recording; afterwards participants were asked to do a Stroop word-colour matching test and a geometric combination game.

5.4.1 Standard Sensor Characterization Results

An example of a normal EDA signal randomly selected from the BrainAnswer database is presented in Figure 5.7, and examples of EDA signals with full-scale saturation and lack of response (extracted from the same database) are presented in Figure 5.8.

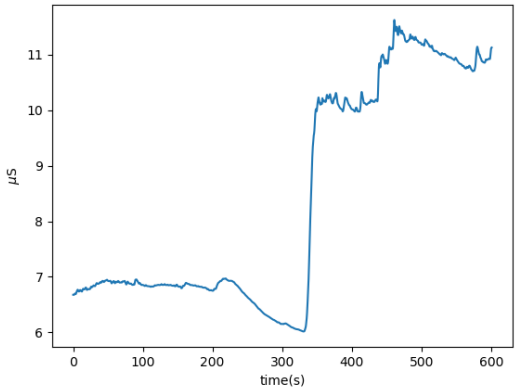

Figure 5.7: Example of a normal EDA signal.

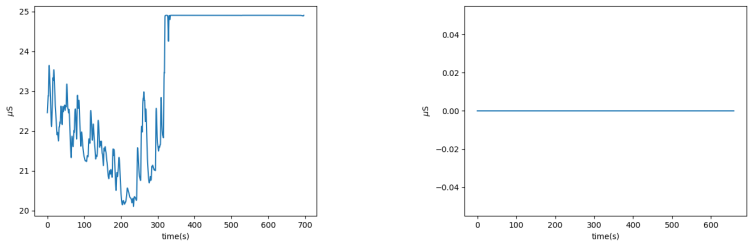

(a) Saturated EDA signal.

(b) EDA signal showing lack of response.

Figure 5.8: Example EDA signals showing saturation (a) and lack of response (b).

Table 5.2 presents the same metrics shown in the initial experiment to characterize the database. From all the recordings, six signals present full-scale saturation while one presents a lack of response. From those six saturated signals, four present saturation over 80% of the acquired signal, while the signal that presented lack of response, does not present variations throughout the session. The mean and median of all 99 signals is approximately 10.56μS, and the range is approximately 4.5μS. As for the variance and standard deviation of the signals, it is approximately 1.5 and 1μS. All this information leads us to conclude that an electrodermal activity sensor with an adaptive gain is beneficial. Table A.3

Table 5.2: Standard sensor characterization summary, expressed in μS.

Mean	Median	Variance	Std. Deviation	Range	Max	Min	#Fullscale	#Zero
10.563	10.555	1.408	1.002	4.534	13.092	8.558	6.000	1.000

in Appendix A presents all the metrics obtained from each record on the database.

5.5 Proposed Circuit Evaluation

The goal of this experiment was to evaluate the proposed sensor through the comparison with an unmodified EDA BITalino sensor, providing evidence that the identified limitations were solved. The new sensor should be capable of adjusting itself so it cannot saturate or being insensitive to high skin resistance levels ($\geq$1MΩ), and is expected to record smaller variations in comparison to the unmodified sensor.

5.5.1 Participants

Data was collected from 16 participants, 5 Females and 11 Males, with ages comprised between 23 and 39 years during a 4-minute protocol consisting of a baseline, a reflex elicitation task, and a recovery period. The objective was to stimulate the SNS in a reflex manner; according to [81], there are several possibilities to achieve that, namely through the elicitation of cardiovascular reflexes induced by tasks such isometric exercises, mental arithmetic, cold pressor test, Valsalva manoeuvre, and/or others. In this experiment, the chosen task was the isometric handgrip exercise, due to the simplicity of deployment [82]; the participant had to apply one-third achieved in the strength of the maximum voluntary contraction, during 3 to 5 minute, causing an increase in the diastolic blood pressure that originates from the heart rate acceleration. An interesting fact is the possibility of the patient performing the Valsalva manoeuvre simultaneously, during the task, which can alter the final results. Nevertheless, since we are focused on comparing the two sensors under evaluation, the possibility of existing a Valsalva manoeuvre is not critical, since its effects will be recorded in both devices. Informed consent was obtained from all participants before the beginning of the experiment. In 8 of the 16 participants, the EDR acquisition was not possible through the implemented high-pass filter due to hardware error (unstable connection). All participants declared not to have any physiologically related condition, nor being on medication that could alter their autonomic nervous system at the time of the recording.

5.5.2 Materials

The EDA was recorded as skin conductance changes with both sensors used in the experiment (the proposed and reference sensor) at the middle and proximal phalanges of the index and ring fingers, on the non-dominant hand. The base sensor was attached to the index finger while the proposed sensor to the ring finger.Dry Ag/AgCl electrodes from Thought Technologies with embedded velcro straps were used

Figure 5.9: Custom force measuring device.

to ensure that the $1cm^2$ area of the electrodes was in contact with the skin at all time. No skin pretreatment nor conductive paste was used. Each sensor was separately attached to an independent BITalino board and data was acquired with a 1000Hz sampling frequency. The devices were synchronised using the same method explained in Section 5.3.

5.5.3 Isometric Handgrip Test

To ensure that the experiment could be replicated on several participants, a graphical software application was developed, as shown in Appendix A.4. The first screen introduced the content of the experiment and what kind of personal data was going to be extracted. The second screen was consisted on the calibration procedures. In this stage, the proposed sensor adapts the gain to the participant skin resistance, choosing the optimal gain. We ask the participant to apply is maximum voluntary contraction so that in the following screen, the software can correctly calculate the current force that the participant is applying. Figure 5.9 presents the custom force measuring device built with 3D technology and with a load cell sensor connected to one of the two MCUs [82]. The final screen presents a gauge with the instant force percentage and the target one-third maximum contraction strength, as well as a clock with the time left to the end of the experience and some guidance of the current stage (baseline, test, or recovering).

5.5.4 Data Analysis

All data was acquired through a Python API developed by Pedro Gonçalves & Carlos Azevedo from PLUX - Wireless Biosignals, S.A., which enables Bluetooth communication between the MCU and a laptop. The data was then analysed using custom software routines written in Python. Several metrics were computed to compare the two sensors, namely: number of onsets; statistical data such as mean, variance, and range; Pearsons correlation coefficients between the two signals; and finally a close

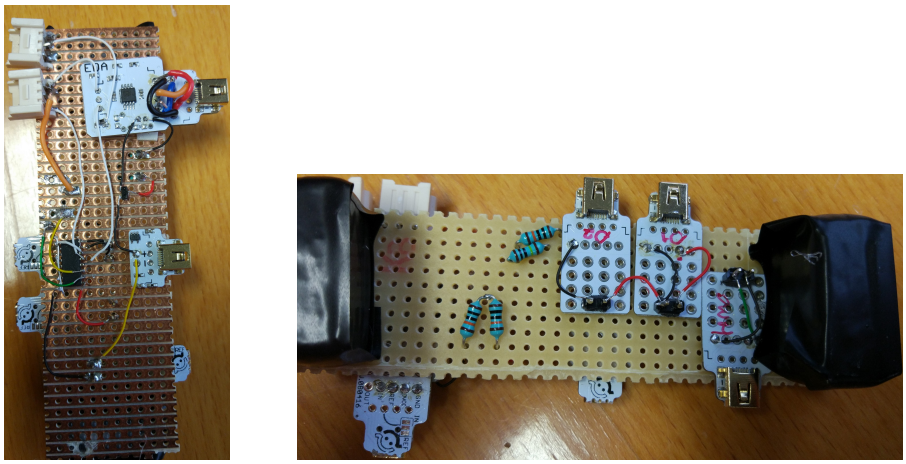

(a) Top view. (b) Back view .

Figure 5.10: Prototype circuit using a N-MOSFET for dynamic gain adaptation. .

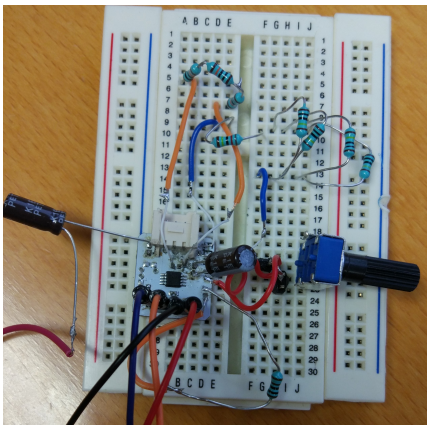

Figure 5.11: High-pass filter prototype.

comparison of each individually marked onset on both sensors.

5.5.5 Proposed Circuit Evaluation

The implementation of the proposed circuit design is presented in Figure 5.10, with the prototype high-pass filter depicted in Figure 5.11. The raw signals obtained from the 16 participants with both sensors is presented in Figure 5.12. To compare them, we extracted eight signal properties, summarised in Table 5.3, where the new sensor values are presented at the first row out of the two of each subject. In this first assessment, we focused on two particular properties, namely, the Pearson correlation coefficient and the RMSE, which implies that the signals are normalised, Figure 5.13 (extended results in in Appendix A.3 in Figure A.1). Excluding the two cases where some sort of artefact induced by saturation is present, the mean Pearson coefficient was 0.967 with a mean RMSE of 0.238, which can be translated as a highly strong correlation with good accuracy signal.

Subject 4 and 12 both present saturation artefactsin the measurements performed with the standard sensor, illustrating how the new sensor is able measure a wider range of EDA signals. In subject four, the EDA is slowly decreasingly with time until the base sensor is no longer capable of measuring it, which in

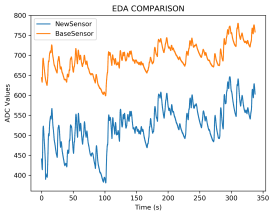

(a) Subject 1

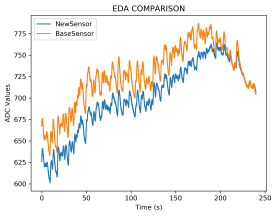

(b) Subject 2

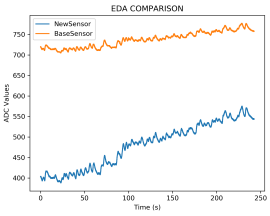

(c) Subject 3

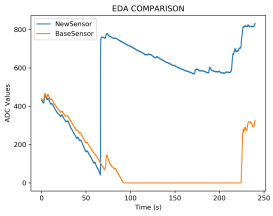

(d) Subject 4

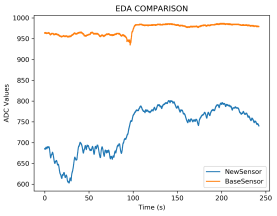

(e) Subject 5

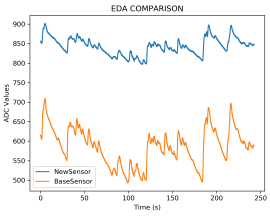

(f) Subject 6

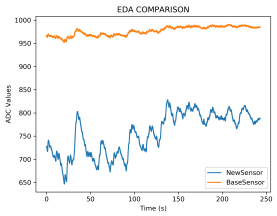

(g) Subject 7

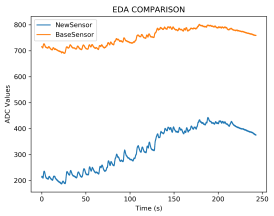

(h) Subject 8

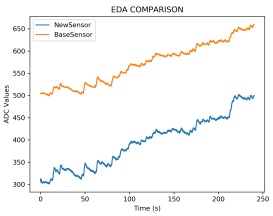

(i) Subject 9

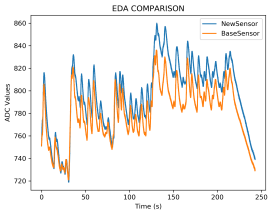

(j) Subject 10

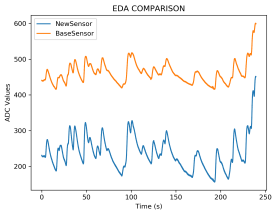

(k) Subject 11

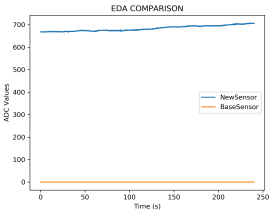

(l) Subject 12

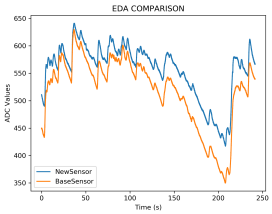

(m) Subject 13

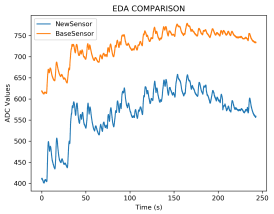

(n) Subject 14

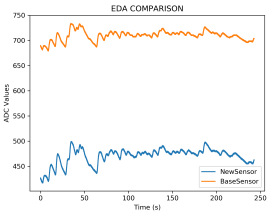

(o) Subject 15

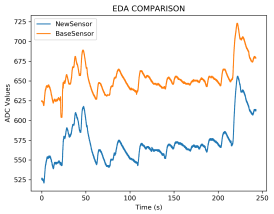

(p) Subject 16

Figure 5.12: Raw EDA signals collected using the reference and proposed sensors for the 16 participants.

Table 5.3: Extracted signal properties, expressed in ADC unit (0-1023). For each subject the top line corresponds to the reference sensor and the bottom line to the proposed circuit.

Subject	Mean	Median	Max	Variance	Std. Deviation	Onsets	P-Coeff	RMSE
Subject 1	522.881 694.034	524.000 693.000	141.881 95.034	2849.777 1222.731	53.383 34.968	44.000 47.000	0.981 –	0.193 –
Subject 2	700.649 726.555	703.000 728.000	99.649 93.555	1597.493 1210.280	39.969 34.789	53.000 55.000	0.956 –	0.298 –
Subject 3	479.530 737.529	490.000 739.000	95.470 39.471	2965.529 343.029	54.457 18.521	52.000 52.000	0.986 –	0.165 –
Subject 4	556.742 111.042	594.000 0.000	515.742 355.958	38671.901 22860.485	196.652 151.197	1.000 5.000	-0.475 –	1.718 –
Subject 5	733.669 973.043	756.000 980.000	130.669 38.043	3030.999 146.333	55.055 12.097	52.000 8.000	0.891 –	0.468 –
Subject 6	843.369 586.524	844.000 591.000	58.631 122.476	477.825 2190.088	21.859 46.798	27.000 26.000	0.985 –	0.174 –
Subject 7	756.034 976.873	769.000 978.000	109.034 24.873	1976.509 88.442	44.458 9.404	46.000 61.000	0.967 –	0.257 –
Subject 8	324.660 752.630	327.000 759.000	137.660 62.630	6664.945 1097.607	81.639 33.130	38.000 42.000	0.985 –	0.171 –
Subject 9	395.185 572.059	404.000 577.000	106.815 87.941	3219.526 2197.239	56.741 46.875	36.000 34.000	0.996 –	0.089 –
Subject 10	795.788 780.638	801.000 784.000	76.788 59.638	905.291 592.679	30.088 24.345	32.000 33.000	0.973 –	0.232 –
Subject 11	238.309 461.630	233.000 458.000	213.691 139.370	2160.283 871.567	46.479 29.522	25.000 22.000	0.967 –	0.258 –
Subject 12	683.726 0.000	680.000 0.000	23.274 0.000	141.270 0.000	11.886 0.000	43.000 0.000	– –	– –
Subject 13	556.449 518.140	571.000 536.000	139.449 168.140	2462.090 4110.590	49.619 64.114	24.000 20.000	0.989 –	0.146 –
Subject 14	570.587 727.865	579.000 742.000	169.587 115.865	3136.935 1397.818	56.008 37.387	41.000 39.000	0.972 –	0.236 –
Subject 15	470.395 709.718	475.000 711.000	53.395 30.718	242.992 94.414	15.588 9.717	25.000 28.000	0.941 –	0.344 –
Subject 16	572.156 653.329	567.000 650.000	83.844 69.671	601.608 363.811	24.528 19.074	20.000 14.000	0.955 –	0.302 –

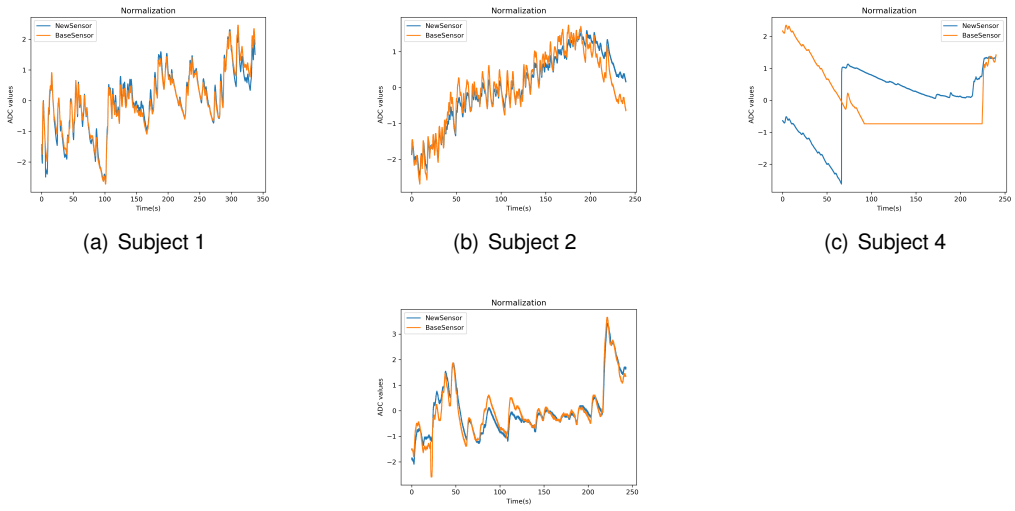

(a) Subject 1 (b) Subject 2 (c) Subject 4

(d) Subject 16

Figure 5.13: Normalized EDA signals collected using the reference and proposed sensors for 4 participants.

turn means losing information between time instants 90 and 225 seconds. On the other hand, the control logic for the new sensor detects that the EDA signal is decreasing and close to reaching saturation, increasing the equivalent resistance of the N-MOSFET. This dynamically changes the transfer function of the sensor, hence the abrupt change on the EDA signal obtained with the new sensor between 65 and 75 of the recording. If we then manage to record the equivalent N-MOSFET resistor value continuously, we can determine the actual transfer function that should be applied, and this way, the artefact induced by changing the level of the N-MOSFET can be eliminated.

In subject 12, the base sensor could not read the actual EDA of the participant. The reason for this is that this participant has a skin resistance higher than 1MΩ. Once again, the control logic of the new sensor will take advantage of its adaptable characteristics, changing the N-MOSFET resistor equivalent to a more adequate value, which enables the recording of the EDA. However, at a certain level, especially above the 3MΩ N-MOSFET equivalent resistor value, the 10-bit ADC does not enable the distinction of the EDR component of the EDA signal. In this case, the implemented third stage, namely the high-pass filter with a 34 dB gain, separates the two components and solely amplifies the EDR component. Analysing the EDR obtained from subject 12 (Figure 5.15), we see that although very small, there are a few peaks that correspond to an EDR (extended results in Appendix A.3 in Figure A.2). Ultimately, the obtained EDR can be superimposed to the EDA obtained in the above mention conditions to recreate the signal that one would obtain using an ADC with higher resolution.

Looking at the overall obtained signals of the 3^{rd} stage, we see that there are cases of data corruption induced by saturation, cases where no saturation occurs, and cases where almost no fluctuation exists (Figure 5.14). In the first case, we have the same limitations that the base sensor has, where it can not adapt its measurement range to the target skin. As an example, on subject 10, we see multiple variations meaning the existence of an EDR component, but the gain of this section is too high for the EDR that this subject experiences, inducing saturation at times. This is a limitation that can be solved

in future work, by applying the same principle used in the first section of the new sensor design. The topology of the Sallen-key high-pass filter enables the use of the N-MOSFET as resistance, which, in turn, enables the control of the gain as well its frequency response. The second possible finding with these results is where we can successfully record suitable EDR data, as exemplified by the subject 2 recording. Finally, the cases where we did not manage to record the EDR signal, can be justified by a loose connection problem identified during the recordings. When implemented in a PCB, and since the filtering is performed at the hardware level, the EDR can be superimposed to the original EDA signal that could not be correctly sampled by limitations on the ADC resolution, and recreate the original signal. Another benefit of using a filtering stage for the EDR, is the more accurate identification of onsets and peaks, and the corresponding derived metrics, presented in Table 2.1, that can be extracted from the EDA signal.

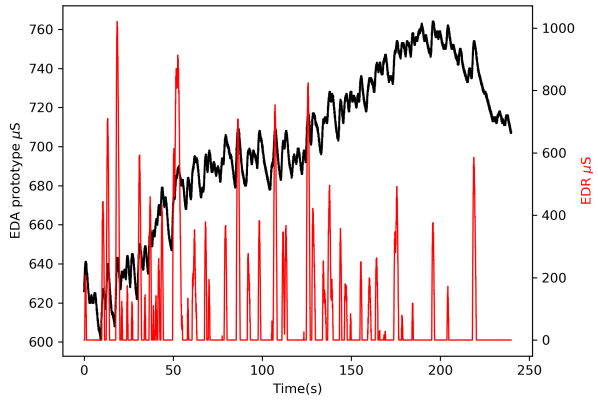

(a) Subject 2

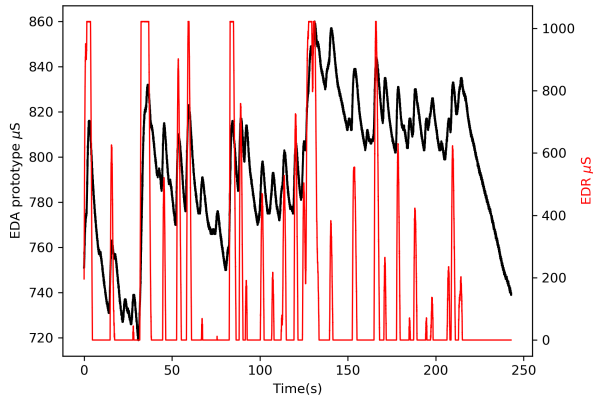

(b) Subject 10

Figure 5.14: Measured EDA signal and EDR events isolated using the implemented high pass filter.

Figure 5.16 presents a portion of the EDA signals after applying the correct transfer function (extended results in Appendix A.3 in Figure A.3). As observed in subject 4, there is a small artefact induced by the modification of the N-MOSFET equivalent resistance value. This is caused by the current method previously discussed in Section 4.2.3.

From Table 5.3 the overall mean for the proposed sensor was 575 compared to 624 of the base

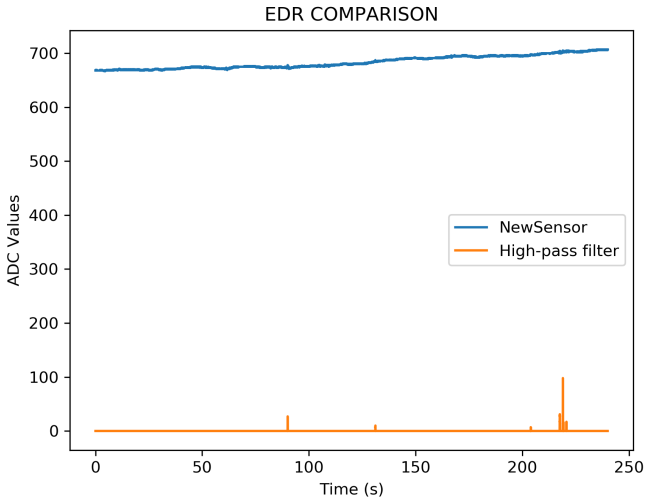

Figure 5.15: EDR signals extracted with the high-pass filter in subject 12.

sensor. This means that the EDA is more centred around the reference voltage in the proposed sensor, which in turns can be interpreted as using a wider dynamic range of the ADC. The median value also re-enforces this fact, with 582 on the proposed sensor against 620 on the standard sensor. A significant comparison factor is the information presented in column 3 of Table 5.3, which gives us the maximum amplitude to the mean value. The proposed sensor scored a maximum amplitude of 135, while the reference sensor scored 94. Having more noticeable variations is generally better, since the same possible EDR will be expanded across a larger set of ADC codes, reducing the probability of not detecting EDR events due to limitations on ADC resolution. Finally, and using the same classification of minimum amplitude to classify an onset of a response, the proposed sensor had a comparable result to the base sensor, but in cases where saturation occurs, obviously, from the data measured using base sensor it is not possible to detect EDR onsets, while with the proposed sensor it is still possible to detect EDR events to some extent.

In order to do a more thorough analysis, we examine each onset in detail. As an example, Figure 5.17 presents the subject 13 onsets. Table A.4 in AppendixA.3 presents the Pearson correlation coefficient and RMSE. In general there is a strong correlation in almost all detected onsets, but good to weak correlation in a minority of the onsets occur.

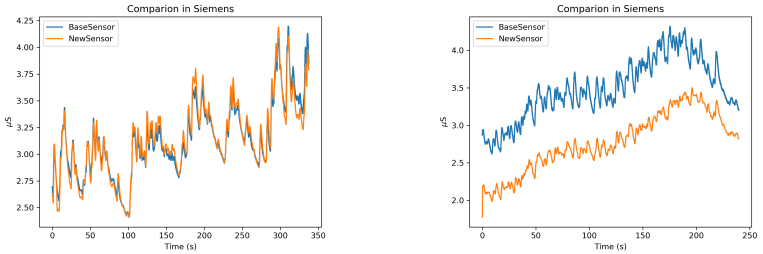

(a) Subject 1

(b) Subject 2

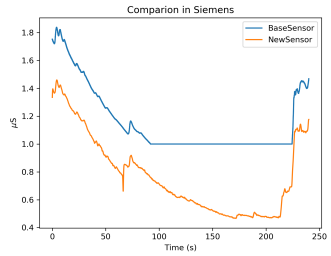

(c) Subject 4

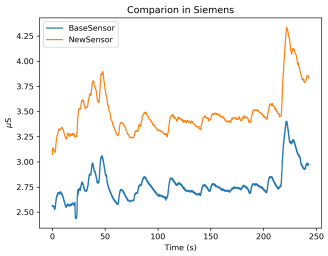

(d) Subject 16

Figure 5.16: Reconstructed EDA, in conductivity units (μS), comparing the reference and proposed sensors.

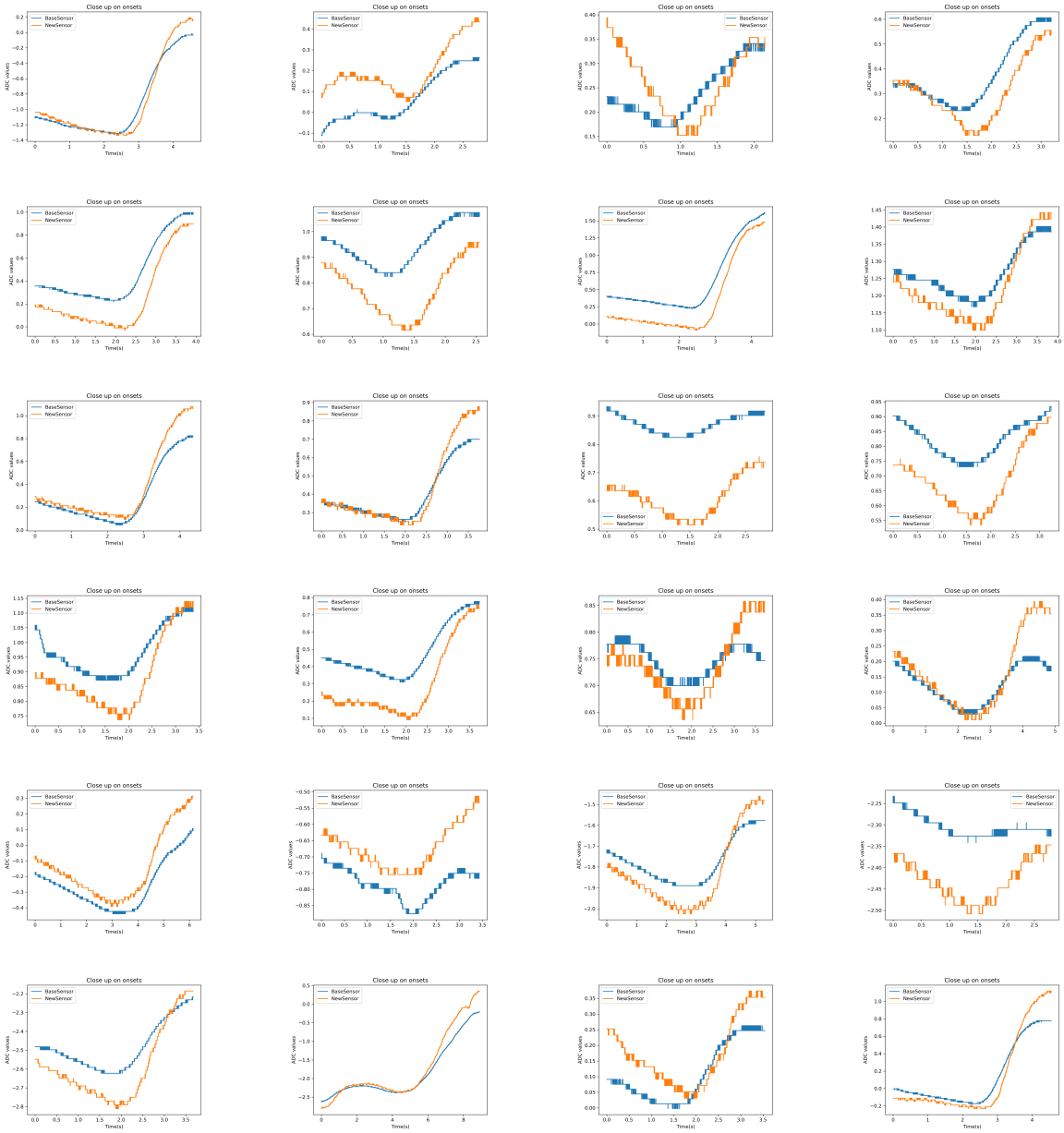

Figure 5.17: Detected EDA onsets for Subject 13.

Chapter 6

Conclusions and Future Work

The EDA contains useful information related with the sympathetic nervous system, which are at the core of several psychophysiological research areas such as epilepsy and autism. Its most significant advantage is the smaller footprint and ease of use comparatively to other biosignal modalities, however, at the instrumentation level a few limiting factors still exist. This work has contributed to further extend the potential of EDA signals, by addressing multiple outstanding issues.

There is a wide range of devices that implement EDA technology, but they lacked a few essential characteristics. The exploratory work, the EDA forehead experiment, and the cognitive experiment lead us to the conclusion that it is possible to acquire a comparable signal in different locations, other than the hands, and secondly and more importantly, that there is a clear need for a sensor that can adapt to a broad spectrum of individuals and hopefully even all of the entire population.

On the forehead experiment, due to small gathered data, the results are merely indicative. Overall it seems that it is viable to study EDA on the forehead, and further studies should address what the optimal position is, the size of electrodes and distance between them.

This work contributes to the study of non-conventional electrode materials, highlighting the MEDTEX P130 material, which showed excellent performance in a control situation and good performance on a real-life subject. Further testing should be done to validate the results obtained, especially on real subjects, since the provided results only used one person and therefore are merely indicating that it can be used as electrode material. Also, there is the possibility that this material suffers oxidation, but if correctly validated and if proved that the lifetime of this type of electrodes is long enough to be viable in practise, it would be possible to have a more seamless integration of EDA sensors. This way, it solves the issue of interference with everyday tasks that most of current EDA devices impose to the user when using the hand palms and feet soles as sensor application locations.

The 3D printed electrodes showed good performance when simulating the skin resistance with physical resistor components, however, they did not perform so well in a real subject. This is unfortunate since the success of these type of electrodes could mean the possibility of printing them on-demand, and use a more environmentally conscious electrode since it quickly dissolves thanks to the biodegradable compound, serving as a big advantage compared to the pre-gelled electrodes that generally are

disposed of after used. One possible cause can be related with the duration of the experiment in the real subject which was under one minute and a half. With the existence of a build-up of sweat under the electrode, it could provoke an offset, lowering the impedance of the skin. Future work should not fully discard the use of 3D electrodes since it presents excellent opportunities, and also the validation of the fabrication of these 3D electrodes should be done through the analysis of its microscopic properties. Additionally, new studies should explore other, more convenient, conductive materials and improve the methods to validate them as viable electrodes materials.

This work further contributes to address outstanding issues in EDA measurement, especially when using low-cost and DiY hardware platforms, by devising a sensor design with adaptive gain. The proposed circuit has shown adequate results, and in cases where saturation occurred in the reference sensor, it still managed to acquire EDA signal. The dynamically adjustable gain enables the circuit to acquire an EDA signal in all conditions, although there is still room for improvement. For example, it would be preferred if there was no need for external processing of data, and consequently have the control on the sensor itself. The optimal condition would be one where through an onboard control logic, the sensor could adjust itself. Nonetheless, the current circuit offers the user a more flexible solution, particularly advantageous for research, since it enables the control of the PWM output through software. Regarding the transformation to conductivity units, which is directly related with the control logic, the procedure used to calibrate the sensor can be further improved to eliminate the overall offset experienced in the sensor validation experiment, dictating a better N-MOSFET equivalent resistor value to be applied dynamically to the transfer function.

Moreover, this new sensor implements a new stage that separates the two EDA components. This can enable a better study of the EDA itself, and can potentially give better insights into EDRs. However, this stage suffers from multiple limitations, namely, it still has fixed gain settings, it saturates on some users, although as previously explained, due to the properties of this stage, a similar control as that implemented in the proposed can be applied and therefore provide adaptability functions. Further validation regarding the optimal cutoff frequency versus the complexity of the filter should be studied as well as delivering adaptable gain to this stage.

Future work should continue to explore the hardware aspect of the presented electrode materials and sensor, especially improving the calibration procedure and the control logic used, focus on the developing of algorithms to mitigate artefacts, and finally, explore different areas to measure electrodermal activity signals.

The ultimate goal of wearable devices is to gather information 24/7 in a seamless and unobtrusive fashion to the user. Most of the present work focused on further affirming the EDA as an added-value biosignal modality for everyday use scenarios.

Bibliography

[1] H. Critchley. Electrodermal responses: What happens in the brain. *The Neuroscientist*, 8(2):132–142, 2002.

[2] W. Boucsein. *Electrodermal Activity*. Springer, 2^{nd} edition, 2012. ISBN:978-1-4614-1125-3.

[3] M. Taj-Eldin, C. Ryan, B. O'Flynn, and P. Galvin. A review of wearable solutions for physiological and emotional monitoring for use by people with autism spectrum disorder and their caregivers. *Sensors (Basel, Switzerland)*, 18(12), Dec. 2018. ISSN 1424-8220. doi: 10.3390/s18124271.

[4] A. Hasanbasic, M. Spahic, D. Bosnjic, H. H adzic, V. Mesic, and O. Jahic. Recognition of stress levels among students with wearable sensors. pages 1–4, Mar. 2019. doi: 10.1109/INFOTEH.2019.8717754.

[5] M. Schmidt, D. Penner, A. Burkl, R. Stojanovic, T. Schürmann, and P. Beckerle. Implementation and evaluation of a low-cost and compact electrodermal activity measurement system. *Measurement*, 92, 06 2016.

[6] U. Birgersson, E. Birgersson, P. Åberg, I. Nicander, and S. Ollmar. Non-invasive bioimpedance of intact skin: mathematical modeling and experiments. *Physiological Measurement*, 32(1):1–18, 2010.

[7] J. Malmivuo and R. Plonsey. The electrodermal response. In *Bioelectromagnetism*, pages 568–574. Oxford University Press, 1995.

[8] K. Sato, W. Kang, K. Saga, and K. Sato. Biology of sweat glands and their disorders. I. Normal sweat gland function. *Journal of the American Academy of Dermatology*, 20(4):537–563, 1989.

[9] P. Millington and R. Wilkinson. *Skin, Biological structure and function*. Cambridge University Press, 1^{st} edition, 1983.

[10] K. Kurosumi, S. Shibasaki, and T. Ito. Cytology of the secretion in mammalian sweat glands. *International Review of Cytology*, 87:253–329, 1984.

[11] K. Wilke, A. Martin, L. Terstegen, and S. Biel. A short history of sweat gland biology. *International Journal of Cosmetic Science*, 29(3):169–179, 2007.

[12] V. Sokolov, S. Shabadash, and T. Zelikina. Innervation of eccrine sweat glands. *Biology bulletin of the Academy of Sciences of the USSR*, 7(5):331–346, 1980.

[13] N. Taylor, J. Caldwell, and I. Mekjavic. The sweating foot: Local differences in sweat secretion during exercise-induced hyperthermia. *Aviation, space, and environmental medicine*, 77:1020–1027, 2006.

[14] Y. Dancik, O. Jepps, and M. Roberts. Beyond stratum corneum. In *Dermal Absorption and Toxicity Assessment*, pages 209–250. CRC Press, 2008.

[15] Blausen.Staff. Medical gallery of blausen medical. *WikiJournal of Medicine*, 1(2), 2014.

[16] J. Grant. An atlas of anatomy. `https://commons.wikimedia.org/wiki/File:Grant_1962_663.png`. (last accessed on 24 December 2018).

[17] R. Salvesen. Innervation of sweat glands in the forehead: A study in patients with Horner's syndrome. *Journal of the neurological sciences*, 183:39–42, 2001.

[18] S. Nicolaidis and J. Sivadjian. High-frequency pulsatile discharge of human sweat glands: Myoepithelial mechanism. *Journal of Applied Physiology*, 32(1):86–90, 1972.

[19] H. Schliack and R. Schiffter. Neurophysiologie und pathophysiologie der schweißsekretion. In *Handbuch der Haut- und Geschlechtskrankheiten Ergänzungswerk book series (HAUT, volume 1 / 4 / a)*, pages 349–458. Springer, 1979.

[20] J. Allen, J. Armstrong, and I. Roddie. The regional distribution of emotional sweating in man. *The Journal of Physiology*, 235:749–759, 1973.

[21] R. W. Picard. *Affective Computing*. The MIT Press, Cambridge, Mass, second edition 1998 edition edition, Sept. 1997. ISBN 978-0-262-16170-1.

[22] R. Edelberg. Biophysical properties of the skin. In *Electrical properties of skin*, volume 1, pages 519–551. John Wiley & Sons, 1971.

[23] R. Edelberg. Biopotentials from the skin surface: The hydration effect. *Annals of the New York Academy of Science*, 148:252–262, 1968.

[24] R. Edelberg. Electrical activity of the skin: Its measurement and uses in psychophysiology. In *Handbook of psychophysiology*, pages 367–418. Holt, Rinehart, & Winston, 1972.

[25] D. Fowles. Mechanisms of electrodermal activity. In *Methods in physiological psychology*, volume 1, pages 231—271. New York: Academic, 1974.

[26] R. Edelberg. Electrodermal mechanisms: A critique of the two-effector hypothesis and a proposed replacement. In *Progress in electrodermal research*, pages 7–30. Plenum, 1993.

[27] L. Johnson and A. Lubin. Spontaneous Electrodermal Activity during Waking and Sleeping. In *Psychophysiology*, volume 3, pages 8–17. John Wiley and Sons, 1966.

[28] iMotions. GSR Pocket Guide, 2016. URL https://imotions.com/gsr-guide-ebook/. last accessed on 24 December 2018.

[29] H. Silva, A. Fred, and A. Lourenço. Electrodermal response propagation time as a potential psychophysiological marker. In *2012 Annual International Conference of the IEEE Engineering in Medicine and Biology Society*, pages 6756–6759, Aug. 2012. doi: 10.1109/EMBC.2012.6347545.

[30] H. P. da Silva. Physiological Sensing Now Open to the World: New Resources Are Allowing Us to Learn, Experiment, and Create Imaginative Solutions for Biomedical Applications. *IEEE Pulse*, 9 (2):9–11, Mar. 2018. ISSN 2154-2287, 2154-2317. doi: 10.1109/MPUL.2018.2790903.

[31] H. P. da Silva, A. Fred, and R. Martins. Biosignals for Everyone. *IEEE Pervasive Computing*, 13(4): 64–71, Oct. 2014. ISSN 1536-1268, 1558-2590. doi: 10.1109/MPRV.2014.61.

[32] D. Batista, H. P. da Silva, and A. Fred. Experimental characterization and analysis of the BITalino platforms against a reference device. In *Proc. of the IEEE Engineering in Medicine and Biology Society Annual Int'l Conf. (EMBC)*, pages 2418–2421, 2017.

[33] D. Batista, H. P. da Silva, A. Fred, C. Moreira, M. Reis, and H. Ferreira. Benchmarking of the BITalino biomedical toolkit against an established gold standard. *Healthcare Technology Letters*, 6 (2):32–36, May 2019.

[34] K. Kutt, W. Binek, P. Misiak, G. Nalepa, and S. Bobek. Towards the development of sensor platform for processing physiological data from wearable sensors. pages 168–178, 06 2018.

[35] Libelium Comunicaciones Distribuidas S.L. MySignals SW eHealth and Medical IoT Development Platform Technical Guide. http://www.libelium.com/downloads/documentation/mysignals_technical_guide.pdf. (last accessed on 04 January 2019).

[36] C. McCarthy, N. Pradhan, C. Redpath, and A. Adler. Validation of the Empatica E4 wristband. In *2016 IEEE EMBS International Student Conference (ISC)*, pages 1–4, May 2016. doi: 10.1109/EMBSISC.2016.7508621.

[37] A. Borrego, J. Latorre, M. Alcañiz, and R. Llorens. Reliability of the Empatica E4 wristband to measure electrodermal activity to emotional stimuli. *Proc. 13th Int'l Conf. on Virtual Rehab*, pages 21–24, 2019.

[38] Thought Technology Ltd. Gsr 2 - t2001m. https://thoughttechnology.com/index.php/hardware/gsr-2.html, . (last accessed on 19 January 2019).

[39] Thought Technology Ltd. eVu TPS Package - T4500. https://thoughttechnology.com/index.php/hardware/tps-evu-package-t4500.html, . (last accessed on 19 January 2019).

[40] Thought Technology Ltd. Skin conductance sensor - SA9309M. https://thoughttechnology.com/index.php/sensors-116/skin-conductance-sensor.html, . (last accessed on 19 January 2019).

[41] Biopac Systems, INC. EDA100C Electrodermal Activity Amplifier. https://www.biopac.com/product/eda-electrodermal-activity-amplifier/, . (last accessed on 19 January 2019).

[42] Biopac Systems, INC. Wireless Photo Plethysmogram (PPG) and Electrodermal Activity (EDA/GSR) BioNomadix Transmitter. https://www.biopac.com/product/bionomadix-wireless-ppg-and-eda-transmitter/, . (last accessed on 19 January 2019).

[43] Shimmer Realtime Technologies, Ltd. GSR+ User Guide. http://www.shimmersensing.com/images/uploads/docs/GSR%2B_User_Guide_rev1.13.pdf. (last accessed on 04 January 2019).

[44] Mind Media. Skin conductance sensor. https://www.mindmedia.com/en/products/sensors/skin-conductance-sensor/. (last accessed on 19 January 2019).

[45] M. Poh, T. Loddenkemper, C. Reinsberger, N. Swenson, S. Goyal, J. Madsen, and R. Picard. Autonomic changes with seizures correlate with postictal EEG suppression. *Neurology*, 78(5): 1868–1876, 2012.

[46] M. Poh, N. Swenson, and R. Picard. A wearable sensor for unobtrusive, long-term assessment of electrodermal activity. *IEEE Transactions on Biomedical Engineering*, 57:1243–1252, 2010.

[47] G. Pope, V. Mishra, S. Lewia, B. Lowens, D. Kotz, S. Lord, and R. Halter. An ultra-low resource wearable EDA sensor using wavelet compression. In Proc. of the Int'l Conf. on Wearable and Implantable Body Sensor Networks (BSN), 2018.

[48] R. Picard and J. Scheirer. The galvactivator: A glove that senses and communicates skin conductivity. Technical Report, MIT Media Laboratory, 2001.

[49] Y. Lee, S. Yoon, C. Lee, and M.-H. Lee. Wearable EDA sensor gloves using conducting fabric and embedded system. *Proc. of the Annual Int'l Conf. of the IEEE Engineering in Medicine and Biology Society.*, pages 6785–6788, 2006.

[50] R. Fletcher, K. Dobson, M. Goodwin, H. Eydgahi, O. Wilder-Smith, D. Fernholz, Y. Kuboyama, E. Hedman, M.-Z. Poh, and R. Picard. iCalm: Wearable Sensor and Network Architecture for Wirelessly Communicating and Logging Autonomic Activity. *IEEE Transactions of Information Technology in Biomedicine*, 14(2):215–223, 2010.

[51] J. Sousa, H. da Silva, N. Santos, and P. Aires. Smart wearable sensors for biomedical data monitoring in the treatment of depression. *Proc. of the Int'l eHealth, Telemedicine and Health ICT Forum (Med-e-Tel)*, page 12, 2012.

[52] The Pip. URL https://thepip.com/en-eu/. (last accessed on 10 October 2019).

[53] J. Jussila, N. Venho, H. Salonius, J. Moilanen, J. Liukkonen, and M. Rinnetmäki. Towards Ecosystem for Research and Development of Electrodermal Activity Applications. In *Proceedings of the 22nd International Academic Mindtrek Conference*, Mindtrek '18, pages 79–87, New York, NY, USA, 2018. ACM. ISBN 978-1-4503-6589-5.

[54] R. Picard, G. Regalia, C. Caborni, M. Migliorini, and F. Onorati. Embrace, a wearable convulsive seizure detection and alert system: First performance report of a case study in real-life settings. Dec. 2016.

[55] M.-Z. Poh, T. Loddenkemper, C. Reinsberger, N. C. Swenson, S. Goyal, J. R. Madsen, and R. W. Picard. Autonomic changes with seizures correlate with postictal EEG suppression. *Neurology*, 78 (23):1868–1876, June 2012. ISSN 1526-632X. doi: 10.1212/WNL.0b013e318258f7f1.

[56] A. Herlan, J. Ottenbacher, J. Schneider, D. Riemann, and B. Feige. Electrodermal activity patterns in sleep stages and their utility for sleep versus wake classification. *Journal of Sleep Research*, 28 (2):e12694, Apr. 2019. ISSN 1365-2869. doi: 10.1111/jsr.12694.

[57] U. Cambra, L. Martinez Martinez, and J. Niño. A case study in neuromarketing: analysis of the influence of music on advertising effectivenes through eye-tracking, facial emotion and GSR. *European Journal of Social Science Education and Research*, 5:84, July 2018. doi: 10.26417/ejser.v5i2.p84-92.

[58] W. Boucsein, D. Fowles, S. Grimnes, G. Ben-Shakhar, W. Roth, M. Dawson, and D. Filion. Publication recommendations for electrodermal measurements. *Psychophysiology*, 49(8):1017–1034, 2012.

[59] R. Edelberg. Electrical properties of the skin. In *Methods in psychophysiology*, pages 1–53. Williams & Wilkins, 1967.

[60] D. Mitchell and P. Venables. The relationship of EDA to electrode size. *Psychophysiology*, 17: 408–412, 1980.

[61] J. Montagu and E. Coles. Mechanisms and measurement of the galvanic skin response. *Physiological Bulletin*, 69:74–76, 1968.

[62] Ørjan Martinsen, O. Pabst, C. Tronstad, and S. Grimnes. Sources of error in AC measurement of skin conductance. *Journal of Electrical Bioimpedance*, 6:49–53, 2015.

[63] D. Salter. Alternating current electrical properties of human skin measured in vivo. In *Bioengineering and the skin*, pages 267–274. Lancaster: MTP Press, 1981.

[64] F. Schaefer and W. Boucsein. Comparison of electrodermal constant voltage and constant current recording techniques using phase angle between alternating voltage and current. *Psychophysiology*, 37:85–91, 2000.

[65] O. Pabst, C. Tronstad, S. Grimnes, D. Fowles, and O. G. Martinsen. Comparison between the AC and DC measurement of electrodermal activity. *Psychophysiology*, 54(3):374–385, 2017. ISSN 1540-5958.

[66] M. V. Dooren, J. Vries, and J. Janssen. Emotional sweating across the body: Comparing 16 different skin conductance measurement locations. *Physiology & Behavior*, 106:298–304, 2012.

[67] E. Vavrinsky, V. Stopjakova, M. Donoval, M. Daricek, H. Svobodova, J. Mihalov, M. Hanic, and V. Tvarozek. Design of sensor systems for long time electrodermal activity monitoring. *Advances in Electrical and Electronic Engineering*, 15:184–191, 2017.

[68] P. Venables and M. Christie. Electrodermal activity. In *Techniques in psychophysiology*. Wiley, 1980.

[69] P. A. Haddad, A. Servati, S. Soltanian, F. Ko, and P. Servati. Breathable Dry Silver/Silver Chloride Electronic Textile Electrodes for Electrodermal Activity Monitoring. *Biosensors*, 8(3):79, Sept. 2018. doi: 10.3390/bios8030079. URL `https://www.mdpi.com/2079-6374/8/3/79`.

[70] P. A. Haddad, A. Servati, S. Soltanian, F. Ko, and P. Servati. Effects of Flexible Dry Electrode Design on Electrodermal Activity Stimulus Response Detection. *IEEE transactions on biomedical engineering*, 64(12):2979–2987, 2017. ISSN 1558-2531. doi: 10.1109/TBME.2017.2754220.

[71] R. Barry. Comparability of EDA effects obtained with constant-current skin resistance and constant-voltage skin conductance methods. *Physiological Psychology*, 9:325–328, 1981.

[72] C. Tronstad, G. Johnsen, S. Grimnes, and O. Martinsen. A study on electrode gels for skin conductance measurements. *Physiological Measurement*, 31:1395–1410, 2010.

[73] D. Burbank and J. Webster. Reducing skin potential motion artifact by skin abrasion. *Medical & Biological Engineering & Computing*, 16:31–38, 1978.

[74] S. Ödman. Potential and impedance variations following skin deformation. *Medical & Biological Engineering & Computing*, 19:271–278, 1981.

[75] H. Tey and B. Chia. Approach to hypohidrosis. *Journal of the European Academy of Dermatology and Venereology*, 27:799–804, 2013.

[76] British Association of Dermatologists. Hyperhidrosis. `http://www.bad.org.uk/library-media/documents/Hyperhidrosis%20Update%20Apr%202014%20-%20lay%20reviewed%20Mar%202013.pdf`. (last accessed on 07 January 2019).

[77] S. Doberenz, W. Roth, E. Wollburg, N. Maslowski, and S. Kim. Methodological considerations in ambulatory skin conductance monitoring. *International Journal of Psychophysiology*, 80:87–95, 2011.

[78] J. Guerreiro, R. Martins, H. P. da Silva, A. Lourenço, and A. Fred. BITalino: A multimodal platform for physiological computing. In *Proc. Int'l Conf. on Informatics in Control, Automation and Robotics (ICINCO)*, pages 500–506, 2013.

[79] A. S. Sedra and K. C. Smith. *Microelectronic Circuits*. Oxford University Press, seventh edition edition, Nov. 2014. ISBN 978-0-19-933913-6.

[80] Covidien (UK) Commercial Ltd. Kendall ECG Electrodes Product Data Sheet. https://cdn.sparkfun.com/datasheets/Sensors/Biometric/H124SG.pdf. (last accessed on 29 December 2018).

[81] A. Zygmunt and J. Stanczyk. Methods of evaluation of autonomic nervous system function. *Archives of Medical Science : AMS*, 6(1):11–18, Mar. 2010. ISSN 1734-1922. URL https://www.ncbi.nlm.nih.gov/pmc/articles/PMC3278937/.

[82] P. Costa, M. Rocha, R. Batista, and H. P. da Silva. GripIT: A mobile isometric handgrip test for evaluation of autonomic cardiovascular reflexes in non-clinical applications. In *Proc. of the IEEE Engineering in Medicine and Biology Society Annual Int'l Conf. (EMBC)*, pages –, 2019.

Appendix A

Experimental Results

A.1 Exploratory Study Table

Table A.1 and A.2, present the following metrics of the signal related with the exploratory study presented in Chapter 5: mean, median, variance, standard deviation, range, the maximum, the minimum, the percentage of saturation and of zero signal.

A.2 Standard Sensor Characterization Table

Table A.3, presents the following metrics of the signal related to the standard sensor characterization presented in Section 5.4: mean, median, variance, standard deviation, range, the maximum, the minimum, the percentage of saturation and of zero signal.

Table A.1: Results from medial phalanx, expressed in μS units.

Participant	Mean	Median	Variance	Std. Deviation	Range	Max	Min	Fullscale%	Zero%
Young Female	2.234	2.222	0.041	0.204	0.787	2.643	1.856	0.000	0.000
Adult Female	3.377	4.203	2.142	1.464	4.094	5.356	1.262	0.000	0.000
Young Male	5.486	5.470	0.087	0.295	1.521	6.411	4.890	0.000	0.000
Adult Male	1.682	1.627	0.023	0.151	0.583	2.048	1.465	0.000	0.000

Table A.2: Results from wrist volar side, expressed in μS units.

Participant	Mean	Median	Variance	Std. Deviation	Range	Max	Min	Fullscale%	Zero%
Young Female	0.276	0.276	0.001	0.034	0.195	0.359	0.164	0.000	28.000
Adult Female	0.106	0.090	0.001	0.037	0.138	0.208	0.071	0.000	100.000
Young Male	0.861	0.833	0.013	0.115	0.502	1.208	0.706	0.000	0.000
Adult Male	0.231	0.232	0.000	0.009	0.128	0.267	0.139	0.000	100.000

A.3 Proposed Circuit Evaluation

The Following section presents the outputs of the experiment conducted on the 16 participants. Figure A.1 presents the normalized raw EDA data extracted from both sensors, Figure A.2 presents the raw EDR data extracted from both sensors, and finally, Figure A.3 presents the EDA data converted to conductive units (Siemens).

A.4 Graphical Interface

In order to standardize as much as possible the experimental protocol, in an attempt to reduce external variables, make it comparable with other experiments, and reusable, a graphical interface was developed (GUI). A total of 5 screens constitute the GUI, Figure A.4shows the first screen, where the participant is informed about the experiment, receive the instructions, as well as his informed consent. On the second screen the participant is asked to fill his personal data. On the third screen the electrodes are attached to the body, and a calibration procedure of the newly designed sensor as well as the force measuring device is conducted. On the fourth screen, the participant receives brief instructions during the isometric task and a force gauge is present with the current applied force reading. At the end of the experiment, in a last screen we acknowledge the contribution provided to this work by the participant.

Table A.3: Metrics extracted from the BrainAnswer database, expressed in μS units. Each line corresponds to one record.

Mean	Median	Variance	Std. Deviation	Range	Max	Min	Fullscale%	Zero%
6.979	6.806	1.302	1.141	3.895	9.005	5.110	0.000	0.000
13.708	14.151	1.361	1.166	5.001	16.092	11.091	0.000	0.000
10.497	10.540	1.564	1.250	4.295	12.790	8.495	0.000	0.000
8.772	8.750	0.578	0.760	2.557	10.151	7.594	0.000	0.000
8.423	6.918	4.062	2.015	5.606	11.623	6.016	0.000	0.000
14.832	14.988	0.443	0.666	3.601	16.372	12.772	0.000	0.000
12.282	12.118	1.113	1.055	6.713	16.738	10.024	0.000	0.000
13.963	13.973	1.498	1.224	6.767	17.188	10.421	0.000	0.000
24.862	24.902	0.027	0.165	1.073	24.902	23.830	94.000	0.000
16.663	16.482	5.280	2.298	12.267	21.993	9.726	0.000	0.000
13.121	13.074	0.208	0.456	2.858	15.105	12.248	0.000	0.000
24.902	24.902	0.000	0.000	0.000	24.902	24.902	100.000	0.000
19.759	20.226	2.366	1.538	8.666	24.902	16.236	1.000	0.000
12.842	13.189	1.065	1.032	4.653	15.913	11.260	0.000	0.000
16.352	16.007	0.892	0.944	5.384	20.463	15.078	0.000	0.000
10.978	10.883	0.254	0.504	2.246	12.118	9.872	0.000	0.000
8.692	8.743	0.248	0.498	2.366	10.229	7.863	0.000	0.000
19.337	19.514	0.965	0.982	3.911	21.677	17.766	0.000	0.000
15.168	15.296	2.826	1.681	4.962	18.116	13.154	0.000	0.000
4.630	4.650	0.174	0.417	1.816	5.574	3.757	0.000	0.000
5.845	5.983	0.477	0.691	2.463	7.079	4.616	0.000	0.000
4.636	4.600	0.219	0.467	2.391	6.093	3.702	0.000	0.000
7.440	7.286	0.606	0.779	2.897	9.130	6.233	0.000	0.000
7.944	8.127	1.247	1.117	3.686	9.751	6.066	0.000	0.000
2.832	2.787	0.115	0.339	1.637	3.678	2.040	0.000	0.000
20.219	20.151	0.593	0.770	4.646	23.459	18.813	0.000	0.000
11.468	11.487	0.312	0.558	2.593	12.827	10.234	0.000	0.000
5.150	5.164	0.216	0.465	2.167	6.320	4.154	0.000	0.000
13.968	14.180	2.210	1.486	7.631	18.293	10.662	0.000	0.000
4.399	4.362	0.394	0.628	3.463	6.188	2.726	0.000	0.000
1.854	1.820	0.067	0.259	1.229	2.677	1.448	0.000	0.000
1.255	1.353	0.068	0.260	1.039	1.864	0.826	0.000	0.000
2.556	2.534	0.027	0.166	0.930	3.177	2.247	0.000	0.000
3.937	4.403	2.331	1.527	6.687	7.592	0.904	0.000	0.000
0.000	0.000	0.000	0.000	0.000	0.000	0.000	0.000	100.000
5.129	5.082	0.204	0.451	2.370	6.434	4.064	0.000	0.000
16.327	16.392	3.506	1.872	8.036	19.661	11.625	0.000	0.000
4.243	4.233	0.070	0.265	1.198	5.046	3.848	0.000	0.000
7.291	6.662	1.949	1.396	4.536	9.984	5.447	0.000	0.000
8.844	7.327	6.813	2.610	8.571	14.275	5.704	0.000	0.000
7.181	7.178	0.072	0.268	1.172	7.787	6.616	0.000	0.000
6.375	6.400	0.057	0.238	1.625	7.073	5.448	0.000	0.000
8.138	8.183	0.893	0.945	4.483	10.731	6.248	0.000	0.000
9.822	9.687	1.545	1.243	6.513	13.983	7.469	0.000	0.000
11.260	11.409	0.242	0.492	2.303	12.466	10.163	0.000	0.000
9.624	9.530	0.432	0.657	3.009	11.430	8.422	0.000	0.000
13.229	13.641	3.779	1.944	7.917	17.463	9.546	0.000	0.000
9.972	9.916	1.424	1.193	4.645	12.438	7.793	0.000	0.000
23.395	24.902	2.999	1.732	4.800	24.902	20.102	54.000	0.000
7.791	7.686	0.801	0.895	4.000	10.630	6.629	0.000	0.000
16.943	16.792	5.512	2.348	10.732	22.247	11.515	0.000	0.000
4.422	4.333	0.225	0.475	1.984	5.688	3.704	0.000	0.000
3.943	3.973	0.183	0.428	1.771	4.903	3.133	0.000	0.000
9.677	9.606	0.446	0.668	2.959	11.485	8.526	0.000	0.000
5.617	5.653	0.751	0.867	10.166	14.727	4.561	0.000	0.000
12.618	12.464	0.588	0.767	4.698	16.046	11.347	0.000	0.000
24.115	24.229	0.341	0.584	2.346	24.894	22.548	12.000	0.000
9.017	9.009	0.805	0.897	3.592	11.215	7.623	0.000	0.000
9.156	8.883	1.747	1.322	5.227	11.667	6.440	0.000	0.000
7.878	7.028	4.212	2.052	6.498	11.222	4.724	0.000	0.000
11.230	10.966	2.737	1.654	9.185	17.692	8.507	0.000	0.000
20.562	20.359	1.788	1.337	7.154	24.854	17.700	0.000	0.000

4.866	5.023	0.354	0.595	2.625	5.933	3.309	0.000	0.000
20.077	19.921	1.230	1.109	5.309	23.211	17.902	0.000	0.000
6.367	6.406	1.355	1.164	5.309	9.260	3.951	0.000	0.000
12.535	12.637	1.650	1.285	6.218	15.867	9.649	0.000	0.000
6.662	6.628	0.191	0.437	2.453	8.457	6.004	0.000	0.000
4.679	4.632	0.315	0.561	1.984	5.629	3.644	0.000	0.000
17.002	15.901	4.765	2.183	6.573	20.591	14.018	0.000	0.000
19.492	19.572	0.834	0.913	3.840	21.362	17.522	0.000	0.000
5.828	5.814	0.158	0.397	1.907	7.204	5.297	0.000	0.000
4.558	4.450	0.348	0.590	2.047	5.795	3.748	0.000	0.000
8.648	8.650	0.875	0.935	4.584	11.315	6.732	0.000	0.000
10.799	10.830	1.326	1.152	5.480	14.097	8.616	0.000	0.000
24.670	24.902	0.401	0.633	3.001	24.902	21.902	85.000	0.000
16.084	16.689	3.193	1.787	6.420	18.513	12.093	0.000	0.000
24.262	24.902	3.140	1.772	8.149	24.902	16.754	81.000	0.000
13.361	12.841	4.642	2.155	10.361	19.615	9.253	0.000	0.000
10.567	10.592	0.204	0.452	2.449	12.079	9.629	0.000	0.000
4.814	4.621	0.694	0.833	3.344	6.676	3.332	0.000	0.000
8.325	8.320	1.021	1.010	3.748	10.165	6.418	0.000	0.000
18.287	18.573	2.359	1.536	9.124	23.000	13.875	0.000	0.000
12.897	13.157	2.408	1.552	6.759	16.382	9.623	0.000	0.000
7.369	7.403	0.349	0.591	3.106	8.887	5.781	0.000	0.000
8.989	8.833	1.219	1.104	6.445	13.843	7.398	0.000	0.000
4.819	4.828	0.075	0.274	8.530	13.043	4.513	0.000	0.000
4.420	4.450	0.054	0.232	1.102	4.912	3.810	0.000	0.000
8.938	8.891	0.060	0.245	1.451	9.979	8.528	0.000	0.000
6.728	6.675	0.206	0.454	1.939	7.844	5.905	0.000	0.000
10.003	10.814	2.605	1.614	5.818	12.309	6.492	0.000	0.000
6.013	6.397	5.400	2.324	8.821	10.767	1.946	0.000	0.000
12.650	13.431	10.678	3.268	12.500	17.491	4.991	0.000	0.000
3.523	3.349	0.122	0.350	1.367	4.448	3.081	0.000	0.000
4.749	4.743	0.658	0.811	3.420	6.776	3.356	0.000	0.000
4.407	4.091	1.889	1.374	5.163	7.117	1.954	0.000	0.000
8.694	8.671	1.077	1.038	7.220	13.807	6.587	0.000	0.000
14.782	14.809	2.437	1.561	7.542	18.517	10.976	0.000	0.000
14.132	13.997	0.924	0.961	4.442	16.843	12.401	0.000	0.000
16.684	16.668	0.989	0.994	4.705	19.649	14.944	0.000	0.000

Table A.4: Subject 13 onsets analysis.

Onset#	P-coeff	RMSE
0	0,986	0,101
1	0,853	0,145
2	0,494	0,066
3	0,89	0,091
4	0,982	0,222
5	0,83	0,184
6	0,995	0,288
7	0,989	0,054
8	0,996	0,109
9	0,991	0,067
10	0,882	0,262
11	0,922	0,143
12	0,956	0,096
13	0,982	0,194
14	0,712	0,045
15	0,925	0,077
16	0,991	0,128
17	0,724	0,119
18	0,991	0,088
19	0,574	0,131
20	0,989	0,122
21	0,997	0,234
22	0,828	0,088
23	0,985	0,134

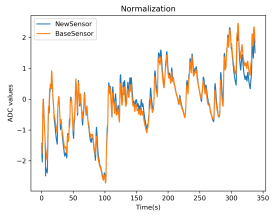

(a) Subject 1

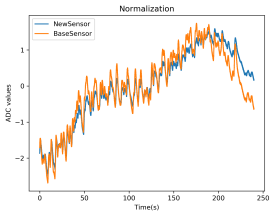

(b) Subject 2

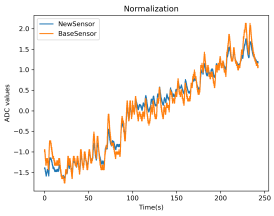

(c) Subject 3

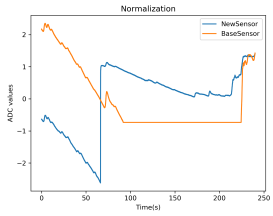

(d) Subject 4

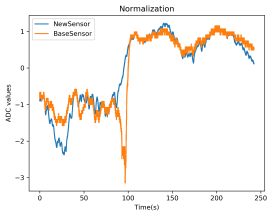

(e) Subject 5

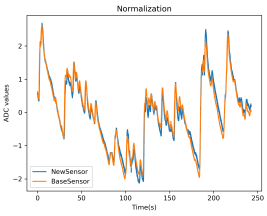

(f) Subject 6

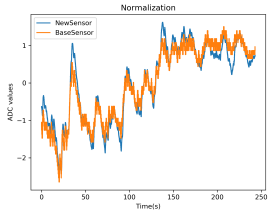

(g) Subject 7

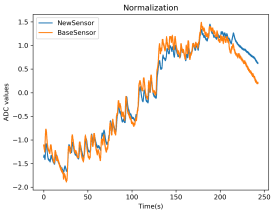

(h) Subject 8

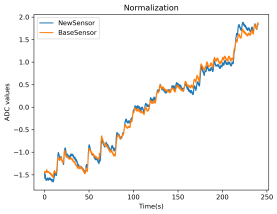

(i) Subject 9

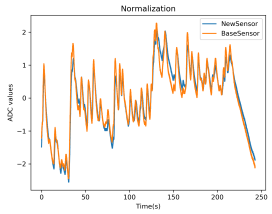

(j) Subject 10

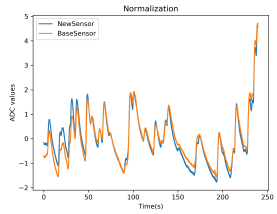

(k) Subject 11

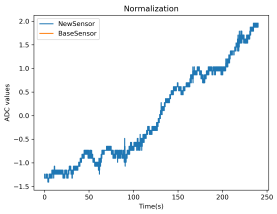

(l) Subject 12

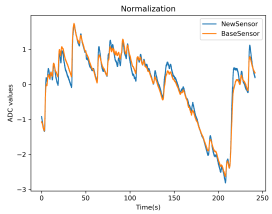

(m) Subject 13

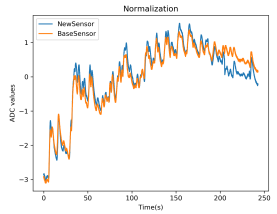

(n) Subject 14

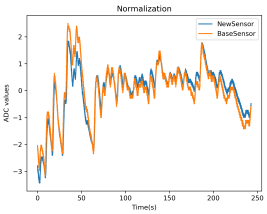

(o) Subject 15

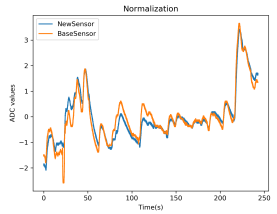

(p) Subject 16

Figure A.1: Normalized EDA signals extracted from the reference and proposed sensor of the 16 participants.

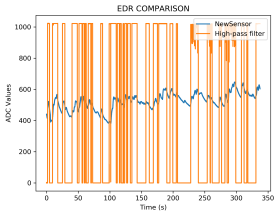

(a) Subject 1

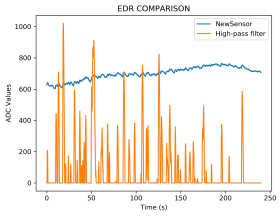

(b) Subject 2

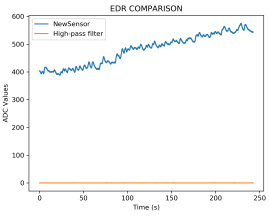

(c) Subject 3

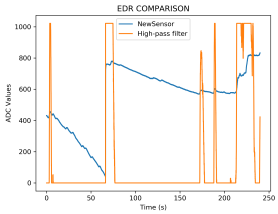

(d) Subject 4

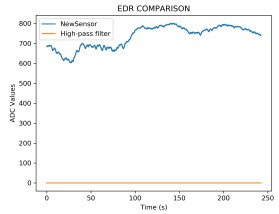

(e) Subject 5

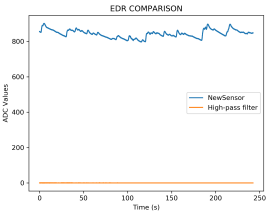

(f) Subject 6

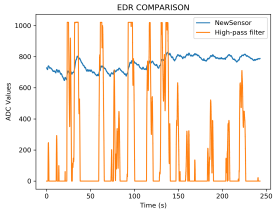

(g) Subject 7

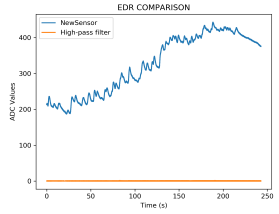

(h) Subject 8

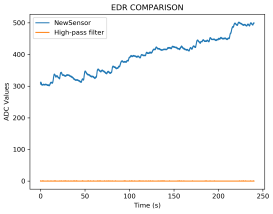

(i) Subject 9

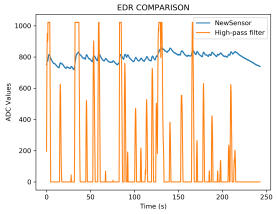

(j) Subject 10

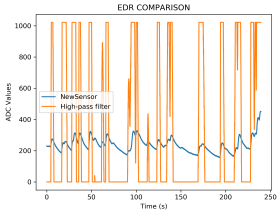

(k) Subject 11

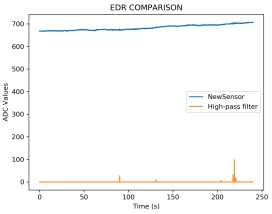

(l) Subject 12

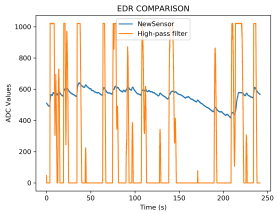

(m) Subject 13

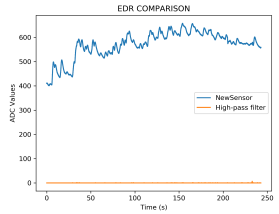

(n) Subject 14

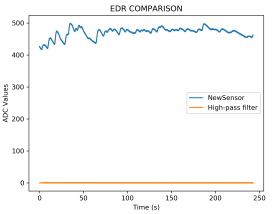

(o) Subject 15

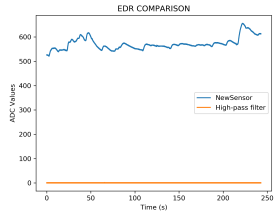

(p) Subject 16

Figure A.2: EDR signals extracted with highpass-filter stage of the proposed sensor of 16 participants.

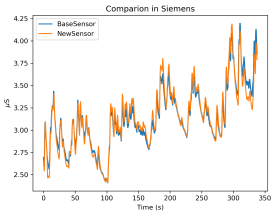

(a) Subject 1

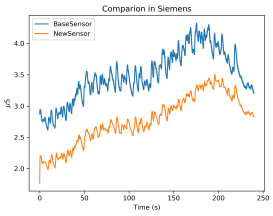

(b) Subject 2

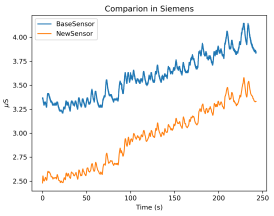

(c) Subject 3

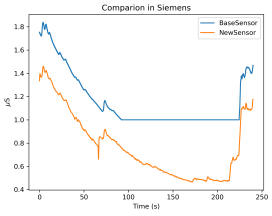

(d) Subject 4

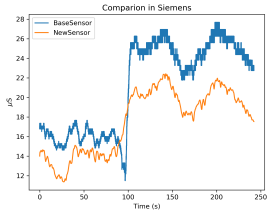

(e) Subject 5

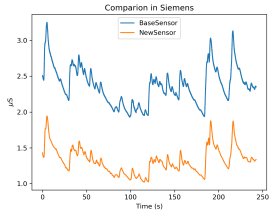

(f) Subject 6

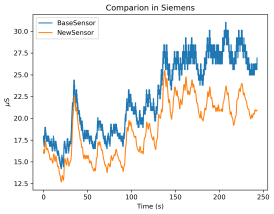

(g) Subject 7

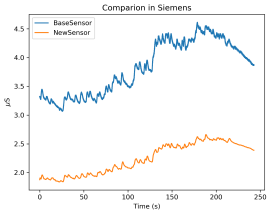

(h) Subject 8

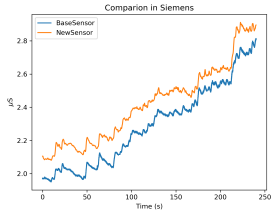

(i) Subject 9

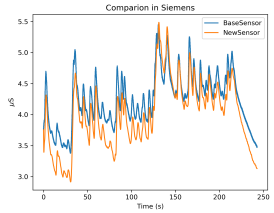

(j) Subject 10

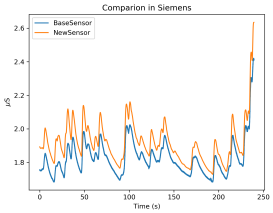

(k) Subject 11

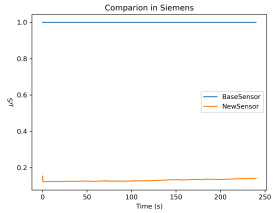

(l) Subject 12

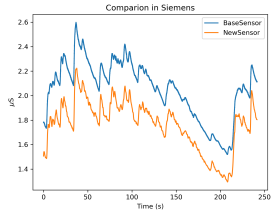

(m) Subject 13

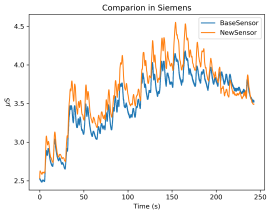

(n) Subject 14

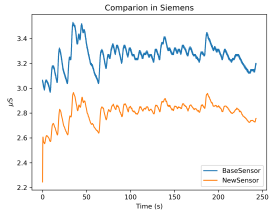

(o) Subject 15

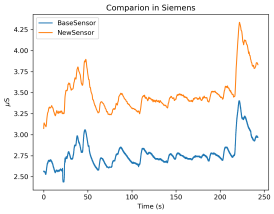

(p) Subject 16

Figure A.3: EDA signals collected with the reference and proposed sensors, converted from ADC to Siemens units.

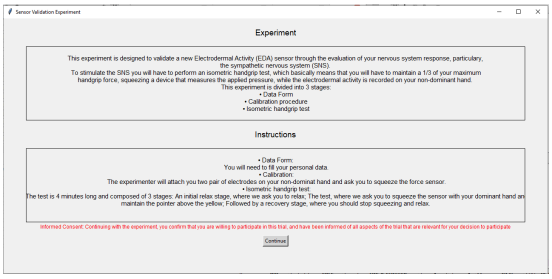

(a) Experiment Information screen

(b) Participant Data screen

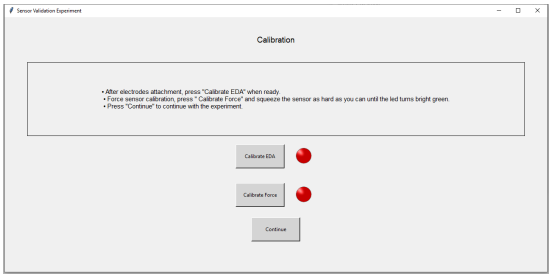

(c) Calibration screen

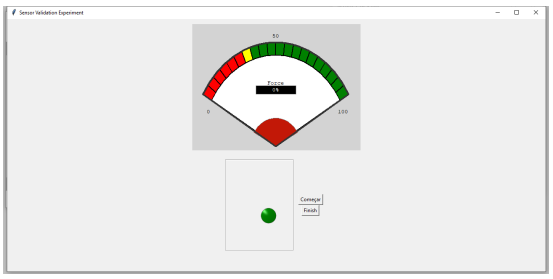

(d) Isometric handgrip task screen

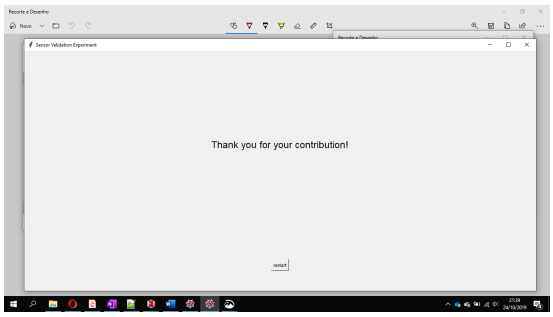

(e) Acknowledgements screen

Figure A.4: Graphical User Interface (GUI) developed to support the experimental protocol.

Appendix B

Contributions

B.1 Abstract Accepted at Physioma 2019

Id: 13690
Key: 0001313BAE
Theme: By way of the Skin
Presentation: Oral communication

Title: Preliminary Evaluation of Non-Conventional Conductive Materials for Electrodermal Activity Data Acquisition

Author's: António Banganho[1,2]; Hugo Silva[1]; Marcelino Santos[2,3]
Affiliaton's: 1 - IT – Instituto de Telecomunicações, Lisboa, Portugal; 2 - Instituto Superior Técnico, Lisboa, Portugal; 3 - INESC-ID, Lisboa, Portugal
Keyword's: Electrodermal Activity, Physiology, Electrodes, E-textiles

Abstract

Introduction: Electrodermal activity (EDA) signal carries useful information about the sympathetic nervous system. Normally, it is recorded using non-polarizable Ag/AgCl electrodes, on the palm of the hand or the sole of the foot, which, in turn, can impose a hard constraint. More convenient locations and sensor setups are needed. A solution may pass by the use of e-textiles or 3D printed materials as electrodes since they can be integrated in a seamless manner and present advantageous proprieties useful for long-term recordings.

Methods: Conductive leather (GMLC), Lycra (MedTexP-130), and PLA (3D) materials were tested as electrodes, compared with dry Ag/AgCl electrodes from Thought Technology, considered as the gold standard. We used several know resistances, each at a time, ranging from 50kΩ to 3MΩ with tolerances of 1%, and connected them to a BITalino EDA sensor and acquisition board, via the electrodes. Each electrode had a 1 cm^2 contact area, and exosomatic DC technique was the chosen method for EDA recording. A total of 10 measurements were taken with each resistance and each electrode material to and the Pearson correlation coefficients were computed in regard to the gold standard.

Results: The conductive lycra showed high correlation (r=0.999±0.000) as well as a very low resistivity of 4.27Ω.cm^2. The 3D electrodes presented a resistivity of 3.3kΩ.cm^2 and high correlation (r=0.950±0.005), although having an increased deviation under the 100kΩ mark. The conductive leather performed the worst, nonetheless, with good correlation (r=0.718±0.041) and resistivity of 3.5kΩ.cm^2, while suffering as well of an increased deviation under 0.5MΩ.

Conclusions: Conductive lycra is the most promising material, opening the possibility to integrate EDA sensors in a more seamless fashion. Further studies should focus on testing the different electrode materials on live subjects to further validate our results and also study other possible locations to extract the EDA.

Presenting author profile

Biography: António Banganho received the B.S. degree in Biomedical Engineering from the Instituto Superior de Engenharia de Coimbra - Instituto Politécnico de Coimbra, Portugal, and currently pursuing the M.S. degree in Electrical and Computer Engineering from Instituto Superior Técnico – Universidade de Lisboa, Portugal, with the thesis "Electrodermal Activity Sensor (EDA) with Adaptive Gain Control" with the support of Instituto de Telecomunicações (IT) and INESC-ID.

B.2 Submitted article to the IEEE Potentials Magazine ”Medical Technology Breakthroughs, March 2020”

Electrodermal Activity: Fundamental Principles, Measurement and Application

António Banganho, *Researcher, IT - Instituto de Telecomunicações,* Marcelino Santos, *IEEE Senior Member, INESC-ID,* and Hugo Plácido da Silva, *IEEE Senior Member, IT - Instituto de Telecomunicações*

I. Introduction

RECENTLY there have been significant developments in the field of wearable devices, low-cost embedded systems and Internet of Things (IoT) for biomedical applications. These technologies provide new opportunities to simplify health care and assessment processes, as well as to solve problems in unprecedented ways due to the increased periodicity and diversity of data collected from the patients. Electrodermal Activity (EDA) sensing devices present themselves as a low-cost and non-intrusive tool to monitor the emotional state of a subject, and a viable gateway to study the Sympathetic Nervous System (SNS), which is responsible for the so-called fight-or-flight responses happening at the unconsciousness level.

It is a frequently used modality in psychophysiology, because of its ability to obtain a distinct Electrodermal Response (EDR) in response to a stimulus. The possible uses of EDA are well documented; examples include the integration in polygraph machines, research on epilepsy, autism, post-traumatic stress disorder, schizophrenia, depression or, in medical applications, to detect hyper/hypo-hidrosis cases, as an indicator of stress and anxiety, and for emotion assessment, just to name a few. However, challenges still exist at multiple levels. One is the high variability of physiological and non-physiological factors that influence the dynamic range of the measurement, as well as its susceptibleness to artefacts.

The term EDA is strongly correlated with measuring the activity of sudoriferous glands, and it is used to describe all the electrical phenomena of the skin. These include active and passive electrical properties that could be traced back to the integumentary system and its related organs. The EDA is composed of two main components: the tonic and the phasic. The tonic component is known as the electrodermal level (EDL) and can be considered as the baseline of the signal, presenting a slowly varying behaviour. Factors related to the external environment, physiological conditions or autonomic regulation will contribute to a changing rising or declining of the EDL within an individual. The phasic component is known as the electrodermal response (EDR), depicted in Figure 1, and it is characterised by having higher frequency short-term variations, which superimposes to the baseline level. It normally appears as a response to specific stimuli, expressing sensitivity to emotional arousal, but can also be classified as non-specific or spontaneous when are not related to any stimuli.

Throughout the following sections, we provide an overview of fundamental principles, measurement considerations and current applications of EDA sensing, with emphasis on what are the current devices, and typical practical constraints that should be taken into account.

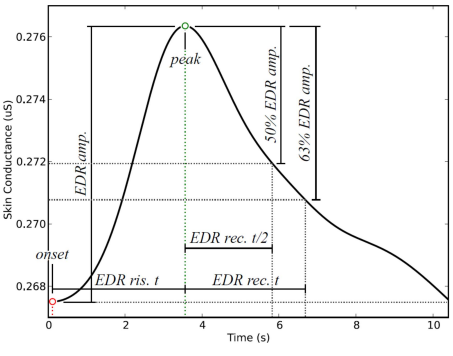

Fig. 1. Typical electrodermal response waveform and extracted features. Reprinted with permission from Silva et al, 2012.

II. Background

A. Skin Structure

The skin is the largest organ in the human body with several responsibilities, namely: preventing the body from drying out; enabling a controlled emission of bodily fluids for thermal regulation, and offering protection from the external environment. It houses different types of nerve cells, which provide afferent information related to touch (mechanoreceptors), pain (nociceptors), and temperature (thermoreceptors). It is stratified in layers, namely, the cutis, composed by the epidermis and dermis layer, and the subcutis composed by the hypodermis layer.

The epidermis is the skin outermost layer and consists of epithelial tissue, which becomes progressively tougher and dryer closer to the surface. The stratum corneum, which makes part of the epidermis, is the toughest and driest of all skin layers and is noticeably thicker at locations where the sympathetic regulation of sweat glands is higher. The dermis is composed of taut and fibrous connective tissue, separated in two major layers, the papillary and the reticular layer, distinguished by their arrangement of the collagen fibres, which concedes the skin its strength and elasticity.